

Understanding the Surface of Hemozoin and its Synthetic Analogue Hematin Anhydride

Elizabeth Danae Guerra, M. Sc.

Doctor of Philosophy

Department of Mining and Materials Engineering

McGill University, Montreal, Canada



A thesis submitted to the Faculty of Graduate and Postdoctoral Studies of McGill University in
partial fulfillment of the degree of Doctor of Philosophy

Copyright © E. D. Guerra, 2019

Abstract

Hemozoin is a biocrystal widely studied due to its relevance as an antimalarial target, potential diagnosis biomarker, and immune modulator during malaria infection. Many investigations are carried out using the crystals isolated from *in vitro* or *in vivo* models, or by producing a synthetic analogue called hematin anhydride. Although most of the structural and morphological properties of both hemozoin and hematin anhydride are understood, little is known about their surface. Studying the surface of the crystals is critical for gaining insight into the physical and chemical interactions involved during hemozoin formation, the mechanism of action of current antimalarials, and its role as immune modulator and biomarker for diagnosis. For this reason, this work aimed to develop a critical understanding of some physicochemical properties of the surface of hemozoin and hematin anhydride.

In our first study, we investigated the surface of hematin anhydride produced by two different synthesis methods, one in an aqueous medium and another under anhydrous conditions. We demonstrated that the synthesis selected to produce the crystals impacts their surface properties. The products obtained from both syntheses are non-porous and show different values of the specific surface area, elemental composition and amount of water adsorbed on the surface. We also confirmed the presence of carboxylate groups on the surface of all crystals; their amount also differs depending on sample preparations.

In our next study, we collected hemozoin from *in vitro* cultures of *Plasmodium falciparum*. We cleaned the surface of the crystals from its organic contaminants by two purification procedures, one involving two additional steps than the other. The crystals showed differing surface properties in terms of composition and amount of organic contaminants adsorbed on the crystals surface. We showed that the surface of hemozoin may never be free of contaminants,

either because they are part of the crystalline structure of hemozoin or because the cleaning methods introduced them. Additionally, we demonstrated that carboxylate groups play a crucial role in the interaction between hemozoin or hematin anhydride and biomolecules.

In our final investigation, we isolated hemozoin from *in vitro* and *in vivo* models of *Plasmodium* to investigate the composition of the organic layer adhered onto the crystals surface. We demonstrated that the elemental composition of the organic layer does not vary among the crystals sources. We reported for the first time the presence of inorganic species of silicon, calcium and phosphorous associated with hemozoin. By assessing the surface speciation and possible origin of these inorganic species, we showed that silicon could be related to an unknown mechanism exploited by the parasite for defense and survival, while calcium and phosphorus may be related to Ca^{2+} -dependent proteins and phosphorylated proteins, respectively. Finally, we proposed that the inorganic elements could be involved in hemozoin biomineralization, may influence the mode of action of some antimalarials and could play a role in the immunomodulatory properties attributed to hemozoin.

Résumé

L'hémozoïne est un biocristal largement étudié en raison de sa pertinence en tant que cible antipaludique, biomarqueur de diagnostic potentiel et modulateur immunitaire lors d'une infection paludéenne. De nombreuses études sont effectuées à l'aide de cristaux isolés à partir de modèles *in vitro* ou *in vivo*, ou en produisant un analogue synthétique appelé anhydride d'hématine. Bien que la plupart des propriétés structurelles et morphologiques de l'hémozoïne et de l'anhydride d'hématine soient bien comprises, on en sait peu sur leurs surfaces. L'étude de la surface des cristaux est essentielle afin de mieux comprendre les interactions physiques et chimiques intervenant lors de la formation de l'hémozoïne, le mécanisme d'action des antipaludéens actuels, et le rôle de l'hémozoïne en tant que modulateur immunitaire et biomarqueur pour le diagnostic. Pour cette raison, ce travail visait à développer une compréhension critique de certaines propriétés physico-chimiques de la surface de l'hémozoïne et de l'anhydride d'hématine.

Dans notre première étude, nous avons étudié la surface de l'anhydride d'hématine produite par deux méthodes de synthèse différentes, l'une en milieu aqueux et l'autre en conditions anhydres. Nous avons montré que la synthèse choisie pour produire les cristaux avait un impact sur leurs propriétés de surface. Les produits issus des deux synthèses sont non-poreux et présentent des valeurs différentes de surface spécifique, composition élémentaire, et quantité d'eau adsorbée à la surface. Nous avons également confirmé la présence de groupes carboxylates à la surface des tous les cristaux; leur quantité diffère également en fonction de la méthode de synthèse utilisée.

Dans l'étude suivante, nous avons recueilli l'hémozoïne à partir de cultures de *Plasmodium falciparum* *in vitro*. Nous avons éliminé les contaminants organiques de la surface des cristaux en utilisant deux méthodes différentes, l'une impliquant deux étapes de plus que l'autre. Les cristaux présentaient des propriétés de surface différentes en termes de composition et de quantité de

contaminants organiques adsorbés à la surface des cristaux. Nous avons montré que la surface de l'hémozoïne peut ne jamais être exempte de contaminants, soit parce qu'ils font partie de la structure cristalline de l'hémozoïne, soit parce que les méthodes de nettoyage les ont introduits. De plus, nous avons montré que les groupes carboxylates jouent un rôle crucial dans l'interaction entre l'hémozoïne ou l'anhydride d'hématine et les biomolécules.

Lors de notre dernière étude, nous avons isolé l'hémozoïne à partir de modèles de *plasmodium* in vitro et in vivo afin d'étudier la composition de la couche organique adhérente à la surface des cristaux. Nous avons montré que la composition élémentaire de la couche organique ne varie pas entre les sources de cristaux. Nous avons reporté pour la première fois la présence d'espèces inorganiques de silicium, calcium et phosphore associées à l'hémozoïne. En évaluant la spéciation de surface et l'origine possible de ces espèces inorganiques, nous avons montré que le silicium pourrait être lié à un mécanisme inconnu exploité par le parasite pour sa défense et sa survie, tandis que le calcium et le phosphore pourraient être liés à des protéines dépendantes du Ca^{2+} et à des protéines phosphorylées, respectivement. Enfin, nous avons proposé que les éléments inorganiques puissent être impliqués dans la biominéralisation de l'hémozoïne, influencer sur le mode d'action de certains antipaludéens, et jouer un rôle dans les propriétés immunomodulatrices attribuées à l'hémozoïne.

Acknowledgments

First of all, I would like to express my deepest gratitude and appreciation to both my supervisors, Prof. Marta Cerruti and Prof. Scott Bohle, for giving me the opportunity to be part of their group to work in such a fascinating project. Thank you for your unlimited guidance and patience throughout my PhD journey; for being my mentors, for continually encouraging me to excellence and giving me the confidence to pursue my ideas.

My thanks also go to our collaborators: Prof. Mary Stevenson and Prof. Elias Georges for providing the facilities to perform the *in vitro* and *in vivo* experiments, and for sharing ideas and discussions for my project. Special thanks go to Fadi Baakdah and Mifong Tam for carrying out the experiments despite their own work, thanks for putting a lot of effort in this collaboration and for helping me with your insightful discussions. I would also like to thank Dr. Nadim Saadeh for his help and patience in the MALDI-ToF experiments.

I also thank all the Biointerface Lab and Bohle's lab members, past and present, it was an honor sharing my days and experiment time with you. Special thanks go to my dearest friends at McGill: my labmates Ophélie Gourgas, Emily Buck, Sophia Smith and Yiwen Chen, and to my office mates Marianna Uceda and Yang Liu. Thank you for your support, advice and help throughout the darkest days; you definitively made my PhD experience more fun and valuable, you're the best!

I would like to acknowledge the financial sources that made this project possible: McGill Excellence Doctoral Award (MEDA), Consejo Nacional de Ciencia y Tecnología de México (CONACyT), Secretaría de Educación Pública de México (SEP) and the GREAT travel award.

I would like to send my deepest gratitude to my husband and best friend, Rafael Castiello. Thank you for supporting me with love all the time, for believing in me regardless of circumstances, and for inspiring me to become better. You were my sun in the brightest days and my rock when I was drowning. Thank you for not letting me fail.

Last but not least, I would like to thank my parents and my families for always believing in me and encouraging me to keep going. Your love and support were worth more than I can express.

To God, without you, nothing would be.

Table of contents

Abstract.....	i
Résumé.....	iii
Acknowledgments	v
Table of contents	vii
List of figures.....	x
List of tables.....	xviii
Glossary of abbreviations and symbols.....	xx
Contributions of authors	xxiii
Thesis outline.....	xxv
Chapter 1. General Introduction.....	1
Chapter 2. Hypothesis and Objectives	4
Chapter 3. Literature review.....	7
3.1. Malaria.....	7
3.2. Hemozoin.....	9
3.3. Synthetic analogues of Hemozoin	13
3.4. Hemozoin biomineralization	16
3.4.1. The role of lipids in hemozoin biomineralization process.....	18
3.4.2. The role of proteins in hemozoin biomineralization.....	20
3.5. Hemozoin surface	22
3.6. Understanding Hz biomineralization based on the characterization of HA surface.....	24
3.7. Antimalarial drugs that interfere with hemozoin formation	26
3.7.1. Quinoline-based antimalarial drugs	26
3.7.2. Artemisinin and its derivatives as antimalarials	29
3.8. Relevance of Hz as tool in diagnosis and as immune modulator during malaria infection	33
3.8.1. Hz as a tool for detection in malaria diagnosis.....	33
3.8.2. Hemozoin as immune modulator	37
Chapter 4. Surface characterization of hematin anhydride: a comparison between two different synthesis methods.....	41

4.1. Abstract.....	42
4.2. Introduction	42
4.3. Experimental.....	44
4.3.1. Synthesis of hematin anhydride through the anhydrous non-coordinated-base (NB) method and aqueous acid-catalyzed (AC) method	44
4.3.2. Chemical derivatization of carboxyl groups with 2,2,2-Trifluoroethanol (TFE) ...	44
4.3.3. Characterization techniques	45
4.3.4. Statistical analysis	46
4.4. Results and Discussion	46
4.5. Outlook	54
4.6. Acknowledgments	56
4.7. Abbreviations.....	56
4.8. Supporting information.....	56
4.8.1. Synthesis of hematin-anhydride through the anhydrous non-coordinated-base method (NB)	56
4.8.2. Synthesis of hematin anhydride by the aqueous acid-catalyzed method (ACM) ...	57
4.8.3. Chemical derivatization of carboxylate groups with 2,2,2-Trifluoroethanol (TFE)...	57
4.8.4. Characterization with X-Ray Diffraction (XRD)	59
4.8.5. Theoretical Specific Surface Area (SSA) calculation.....	60
4.8.6. Details relative to high-resolution XPS spectra collected after TFE functionalization of HA	62
Chapter 5. What is pure hemozoin? A close look at the surface of the malaria pigment	63
5.1. Abstract.....	64
5.2. Introduction	65
5.3. Experimental.....	67
5.3.1. Materials	67
5.3.2. Methods.....	68
5.4. Results	72
5.4.1. The cleaning method impacts the composition and amount of residual biomolecules on Hz surface	72
5.4.2. Residual biomolecules adsorbed on Hz surface are related to protein fragments or amino acids	77
5.4.3. Surface carboxylate groups act as main adsorption sites on Hz	81
5.4.4. The cleaning procedure introduces partial contamination on Hz surface.....	82

5.5. Discussion.....	84
5.6. Conclusions and Outlook.....	86
5.7. Associated content.....	87
5.8. Author information.....	88
5.9. Author Contributions.....	88
5.10. Acknowledgments.....	88
5.11. Supporting information.....	89
5.11.1. Materials.....	89
5.11.2. Methods.....	89
Chapter 6. Inorganic ions on hemozoin surface provide a glimpse into <i>Plasmodium</i> biology.	99
6.1. Abstract.....	100
6.2. Introduction.....	101
6.3. Results and Discussion.....	104
6.4. Conclusions and Outlook.....	117
6.5. Experimental.....	119
6.5.1. Materials.....	119
6.5.2. Methods.....	120
6.6. Supporting Information.....	124
6.6.1. Materials.....	124
6.6.2. Methods.....	125
6.6.3. Characterization techniques.....	130
Chapter 7. Original contributions.....	137
Chapter 8. Conclusions and future perspectives.....	140
References.....	143
Appendix: Copyright waivers.....	161

List of figures

Figure 3.2.1. The life cycle of Plasmodium starts in the sexual stage inside a female Anopheles mosquito. During a blood meal, the mosquito transmits sporozoites into a human host, which infect liver cells where the parasite will mature for 10-14 days, followed by their release as merozoites into the bloodstream to invade red blood cells. In the blood stage, the schizont will feed on hemoglobin and proceed throughout various stages of asexual multiplication, consisting of rings, trophozoites, and schizonts. After schizont rupture, Hz crystals and merozoites are released into the bloodstream and reinvade healthy red blood cells and start a new asexual cycle (Reproduced from ref. [25] with permission from Springer Nature).....	10
Figure 3.2.2. Schematic of the conversion of heme into HA. Free heme is oxidized into α -hematin at low pH, the hydroxyl group on the iron of α -hematin protonates and is replaced by the coordination with the propionate group of the neighboring hematin with loss of water, resulting in the crystallization of HA.	12
Figure 3.3.1. Molecular structure of hemin, the chloride equivalent of α -hematin. Hemin is formed when the central iron of a heme group coordinates with a chloride ligand.....	14
Figure 3.3.2. Scanning electron micrographs of A) HA produced by the acidic-annealing method at high temperature and B) HA crystallized in anhydrous conditions using DMSO, methanol and the base 2,6-lutidine and C) Hz obtained from P. falciparum.	16
Figure 3.4.1. Schematic of a Plasmodium-infected RBC and Hb catabolism within the DV of the parasite (inset). It is proposed that after the proteolysis of hemoglobin, heme is released in the DV, and the parasite forms Hz crystals assisted by lipids in four possible ways: A) inside lipid droplets, B) at the water-lipid interface of lipid droplets, C) at the water-lipid interface of the DV membrane or D) in a complex of lipids and proteins.....	19
Figure 3.4.2. Hypothesized mechanism of Hz formation assisted by HDP, where histidine-residues in the protein interact with heme to allow the proper positioning of the heme monomers to initiate the nucleation of Hz (Reproduced from ref. [63] with permission from Springer Nature).	21

Figure 3.6.1. Illustration of the biomimetic synthesis of HA crystals. A) The crystals are produced at the interface between the wet octanol and the citric acid buffer. B) After 4-6 days HA is formed and is found in the aqueous phase; the crystals are removed and used as seeds in a second step. C) The seeds are suspended in a fresh citric buffer and this solution is incubated with an octanol phase saturated with hematin. After 2-4 days the crystals grew to an estimated size of 35-50 μm and migrate to the organic phase. D) SEM images of material collected from the preparation of HA seeds after 30 min of growth. The upward arrow indicates the presumably crystalline phase while the downward arrow is indicative of amorphous phases. E) AFM images of microcrystals isolated after 1.5 h of reaction, showing several faceted microcrystals of around 600 nm in length and not much amorphous material. F) AFM image of HA crystals of 3-5 μm in length obtained after 1.5 h of the second-step process involving saturated hematin. G) AFM image of a 28 μm HA crystal grown in the hematin-saturated octanol-citric acid buffer after 16 days. (Printed from ref. [68] with permission from American Chemical Society).....	25
Figure 3.7.1. Chemical structure of quinine and its related antimalarial chloroquine, showing their protonation sites. The quinoline group is marked in blue in both molecules.	27
Figure 3.7.2. Structure proposed for the μ -oxo-dimer, a complex stabilized by the interaction between CQ and hematin.	28
Figure 3.7.3. Structure of the most important artemisinins; the endoperoxide bridge is colored in red.	30
Figure 3.7.4. Heme-artemisinin adduct resulting from the alkylation of heme. (Printed from ref. [105] with permission of American Society for Microbiology).....	32
Figure 3.8.1. A) Vapor nanobubbles induced by short-laser pulses directed at Hz (H-VNB) inside infected RBCs. B) Optical detection (OD) scattering signals emitted by the vapor nanobubble and C) detection of pressure pulses of the vapor nanobubble via ultrasound transducer (UT) (Printed from ref. [124] with permission from Proceedings of the National Academy of Sciences of the United States of America).....	35
Figure 3.8.2. (a) Schematic illustration of the diagnostic concept of malaria-infected cells carried out through a microvasculature microscope. The crystals are typically	

circulating free in the bloodstream, or within the parasite's organelles, RBC membranes or phagocytized by blood cells. (b) Unstained blood smears showing Hz crystals within infected RBCs, the crystals are visualized under bright field and (c) cross-polarized illumination. (Printed from ref. [125] with permission from Journal of Biomedical Optics Express)..... 36

Figure 3.8.3. Schematic illustration of the interaction of Hz with blood cells after its release from a lysed schizont. The surface of Hz is prone to adsorb various components from the cells such as proteins or peptides, fatty acids, carbohydrates, and DNA. 39

Figure 4.4.1. SEM images of HA obtained by the NB (A) and AC (B) methods showing different size and morphology of crystals. (C) N₂ adsorption-desorption isotherms measured at 77 K for NB (blue line) and AC (red line) crystals. 47

Figure 4.4.2: XPS high-resolution spectra of C_{1s} (A and E), O_{1s} (B and F), N_{1s} (C and G); and Fe_{2p} (D and H) core levels, collected for HA synthesized by NB (first row) and AC (second row) methods. Experimental data are shown in gray, peak fits in red or blue, and the overall fit in black. 52

Figure 4.4.3: XPS high-resolution spectra of C_{1s} (A and D), O_{1s} (B and E) and F_{1s} (C and F) levels collected for HA synthesized with NB (first row) and AC (second row) method after TFE functionalization. Experimental data are shown in gray, peak fits in red or blue, and the overall fit in black. 54

Figure 5.4.1. (A) Flow chart of the methodologies used to treat Hz to produce pwHz and ewHz. (B) Elemental composition of pwHz (blue bars) and ewHz (red bars) evaluated by XPS and compared with HA (gray bars). Values represent mean \pm SD calculated for three independent experiments and three different spots analyzed along the same sample. *Significant differences between area ratios, with *P<0.0004, **P<0.003 and ***P<0.002. 74

Figure 5.4.2. XPS high-resolution spectra of the O_{1s} level collected for (A) pwHz (B) ewHz, and (C) HA. Experimental data are shown in dark gray dotted line, peak fits in continuous blue, red or light gray (A, B, or C, respectively), and the overall fit in black. (D) Area ratios of the 533.3 eV/531.5 eV peaks for the O_{1s} core level measured for pwHz (blue bar), ewHz (red bar), and HA (gray bar). Values represent mean \pm SD calculated for three independent samples and three different spots analyzed along the

same sample. *Significant differences between area ratios, with $*P<0.0003$ and $**P<0.006$ 75

Figure 5.4.3. XPS high-resolution spectra of the N_{1s} core level collected for (A) pwHz (B) ewHz and (C) HA. The dashed blue line in pwHz distinguishes the contribution from the π - π^* delocalization. Experimental data are shown in dark gray dotted line, peak fits in blue, red or light gray, and the overall fit in black. (D) Area ratios of the XPS N_{1s} 401.0 eV/398.2 eV and 399.7 eV/398.2 eV peaks acquired for pwHz (blue bars), ewHz (red bars), and HA (gray bars). Values represent mean \pm SD calculated for three independent experiments and three different spots analyzed along the same sample. *Significant differences between area ratios, with $*P<9\times 10^{-7}$, $**P<5\times 10^{-8}$ and $***P<1\times 10^{-6}$ 76

Figure 5.4.4. XPS high resolution of the N_{1s} core level acquired for purified HA after suspension in (A) dead parasites of *P. falciparum* of the clone 3D7, (B) RBC membranes, (C) enzymes and detergents used to prepare ewHz. Experimental data are shown in dark gray dotted line, peak fits in blue and the overall fit in black. (D) N_{1s} 399.7 eV/398.2 eV peak area ratio calculated for the spectra shown in A, B, and C. *Significant differences between area ratios, with $*P<0.006$. Values represent mean \pm SD calculated for three independent experiments and three different spots analyzed along the same sample. 78

Figure 5.4.5. XPS high resolution of the N_{1s} core level acquired for (A) HA after interacting with amino acids, (B) fluorinated HA crystals after interacting with amino acids. Experimental data are shown in dark gray dotted line, peak fits in blue and the overall fit in black. All data are representative of three independent experiments and three different spots analyzed along the same sample. 82

Figure 5.4.6. Representative MALDI-ToF mass spectra of positive ions in reflectron mode collected in the m/z region of (A) 150-350 and (B) 465-625 for HA (green), pwHz (blue), ewHz (red) and HA treated with the extensive washes (black). All experiments were repeated three independent times with similar results. The intensity was normalized with respect to the intensity of the peak at 616 Da. The peaks related to the matrix are marked with an asterisk (*). The peaks arising after the washing procedure are marked with an inverted triangle (\blacktriangledown). 83

Figure 6.3.1. A) XPS survey collected for nHz samples obtained from CQS *P. chabaudi* AS infected-macrophages (blue) and *P. falciparum* of the strains 3D7-H (CQS, green) and 7G8 (CQR, red), (no significant differences were found among samples). Data represent mean \pm s.d. of 3 independent samples and three different spots analyzed along the same sample. One-way ANOVA test was used for statistical analysis, followed by Bonferroni's test correction to evaluate the statistical difference of multiple samples, where $P < 0.01$ was considered a significant difference. All data are expressed as mean \pm standard deviation (SD). *Significant differences between atomic percentage, with * $P < 0.01$, ** $P < 0.001$, *** $P < 1 \times 10^{-5}$ and **** $P < 1 \times 10^{-6}$. SEM images of B) nHz crystals rinsed with hexane and dichloromethane. The red arrows indicate the crystals devoid of most of the cell components, while the yellow arrows note the crystals still coated with biological residues. C) Clean sample of Hz showing individual crystals lacking most of the organic residues as a result of treatment for proteins precipitation, enzymatic hydrolysis, and rinses with detergents and water, as reported in [192]. Data represent mean \pm SD of 3 independent experiments. 105

Figure 6.3.2. A) Scanning electron microscopy (SEM) images of nHz obtained from *P. falciparum* strain 3D7-H and energy-dispersive x-ray spectroscopy elemental (EDS) mapping for B) Fe, C) C, D) Ca, E) P, F) Si and G) Na. 107

Figure 6.3.3. XPS high-resolution spectra of Si_{2p} collected for A) Hz extracted from *P. falciparum* of the strain 3D7-H, B) *P. falciparum* parasites of the strain 3D7-H, C) HA suspended in silicic acid, D) cucumber skin (*Cucumis sativus*), E) horsetail (*Equisetum hyemale*) and F) HA suspended in PDMS (Mn~550). Experimental data is shown in green, peaks fit in gray, and the overall fit in black. 109

Figure 6.3.4. XPS high-resolution spectra of Ca_{2p} collected for A) Hz extracted from *P. falciparum* of the strain 3D7-H, B) HA suspended in calcium acetate, C) dried cucumber skin (*Cucumis sativus*) and D) HA and calcium pyrophosphate suspended in cholesterol. Experimental data is shown in blue, peaks fit in gray, and the overall fit in black. 113

Figure 6.3.5. High-resolution P_{2p} XPS spectra collected for A) Hz extracted from *P. falciparum* of the strain 3D7-H, B) HA suspended in RBC membranes, C) HA mixed with PC, D) reference sample of ortho-DL-phosphoserine, E) sodium polyphosphate,

and F) calcium pyrophosphate. Experimental data is shown in red, peaks fit in gray, and the overall fit in black. 116

Figure S.4.8.1. Schematic of HA derivatization with TFE. The -COOH groups susceptible to TFE labeling are marked with red..... 58

Figure S.4.8.2. XPS survey spectra of HA after TFE derivatization. (A) Samples of HA synthesized with NB method. (B) HA crystals obtained AC via and (C) Hemin chloride. All samples show an F1s signal at around 689 eV, confirming the incorporation of fluorine into the -COOH termination groups of HA and Hemin. 58

Figure S.4.8.3. XRD patterns showing the characteristic peaks of HA seen at 7°, 21° and 24° 2θ for HA (C₆₈H₆₀Fe₂N₈O₈) produced by the (i) AC and (ii) NB methods. The XRD spectrum of hemin (C₃₄H₃₂ClFeN₄O₄) is shown in (iii) for comparison..... 62

Figure S.5.11.1. Experimental atomic percent measured from XPS surveys for dead parasites of *P. falciparum* 3D7 washed with hexane and dichloromethane..... 94

Figure S.5.11.2. XPS high resolution of C_{1s} collected for (A) pwHz and (C) ewHz. XPS Fe_{2p} obtained for (B) pwHz and (C) ewHz. Experimental data is presented in gray dotted line, peaks fit in gray continuous line, and the overall fit in black. The C_{1s} spectra of both samples show a signal at 284.5 eV corresponding to C-C/C=C from the porphyrin ring and side chains; while the peaks at 286.5 and 288.4 eV are assigned to C-O and C=O, respectively from the carboxylates. These peaks also have contributions from C-N and C=N from the porphyrin ring [164]. The Fe_{2p} spectra show the characteristic peaks of the spin-orbit splitting of Fe. The Fe_{2p3/2} and Fe_{2p1/2} doubles at 711.2 and 725 eV, respectively, are representative of Fe in oxidative state III.[164] 94

Figure S.5.11.3. Area ratios of the XPS N_{1s} 401 eV/398.2 eV peak acquired for HA suspended in: (A) dead parasites of *P. falciparum* of the clone 3D7 (turquoise bar), (B) RBC membranes (yellow bar), (C) enzymes and detergents used to prepare ewHz (pink bar), (D) mixture of amino acids (green bar) and (E) mixture of amino acids after derivatization of HA surface carboxylate groups (orange bar)..... 95

Figure S.5.11.4. XPS data of (A) high resolution of C_{1s} and (B) survey of HA after a surface esterification of the -COOH groups by TFE. The new peak around 292 eV in

the C _{1s} spectra (inset in panel A) and the new signal at 688.4 eV in the survey evidence the successful functionalization of HA surface.	95
Figure S.5.11.5. Mass spectrum of sinapinic acid used as matrix for the analysis with MALDI-ToF showing the molecular masses at m/z 206, 224 and 246, also found in HA, ewHz, and HA washed with a thorough procedure. The matrix was mixed with trifluoroacetic acid and the spectrum acquired as described in Experimental Section 5.3.2.4 of the main manuscript.	96
Figure S.5.11.6. Representative MALDI-ToF mass spectra of positive ions in reflectron mode collected in the m/z region of 100-1000 for HA (green), pwHz (blue), ewHz (red) and HA treated with the extensive washes (black). The intensity was normalized with respect to the intensity of the peak at 616 Da.	96
Figure S.5.11.7. (A) XRD spectrum obtained for HA synthesized by the acid-annealing method and used for all the controls presented in this work. The spectrum shows the characteristic peaks of HA at 7.5°, 21°, and 24°.[14] (B) FT-IR spectrum of HA showing the peaks of at 1664 and 1209 cm ⁻¹ , representative of the coordination between the iron in heme and a propionate group. The peak located at 1712 cm ⁻¹ is characteristic of the hydrogen-bonded carboxylate group that links the heme dimers to extend the crystalline array.[32, 190]	97
Figure S.6.6.1. XPS surveys measured on dead parasites of <i>P. falciparum</i> strain 3D7-H washed with hexane and dichloromethane.....	132
Figure S.6.6.2. XPS high-resolution Si _{2p} spectra collected on nHz isolated from A) <i>P. falciparum</i> strain 7G8 (CQ-resistant), and B) <i>P. chabaudi</i> AS (CQ-sensitive). Experimental data is presented in green, peak fitting in gray, and the overall fit in black.....	132
Figure S.6.6.3. Elemental composition obtained from XPS surveys collected from control samples consisting of HA suspended in blood serum (purple), red blood cell ghosts (RBCg, green) and the buffer used to extract Hz (CHAPS, orange).	133
Figure S.6.6.4. XPS high-resolution Ca _{2p} spectra acquired on A) a reference sample of CaHPO ₄ and B) nHz isolated from macrophages derived from <i>P. chabaudi</i> AS infected mice. Experimental data is presented in blue, peak fitting in gray, and the overall fit in black.	133

Figure S.6.6.5. XPS survey collected for HA suspended in a solution of Ca pyroP. The data show the signals of C _{1s} , O _{1s} , N _{1s} , and Fe _{2p} , characteristic of HA. The lack of a P _{2p} signal at 133 eV and Ca _{2p} at 348 eV indicates that Ca pyroP did not adsorb on HA crystals due to the absence of an adherent intermediate, e.g. lipids or proteins.	134
Figure S.6.6.6. Representative Ca K-edge NEXAFS reference spectra of nHz collected from <i>P. falciparum</i> strain 3D7-H, dead parasites <i>P. falciparum</i> strain 3D7-H and calcium acetate (Ca(CH ₃ COO) ₂).	134
Figure S.6.6.7. XPS high resolution of P _{2p} collected for A) a reference sample of CaHPO ₄ , B) nHz isolated from <i>P. falciparum</i> strain 7G8 (CQ-resistant) and C) <i>P. chabaudi</i> AS (CQ-sensitive). Experimental data is presented in red, peak fitting in gray, and the overall fit in black.	135
Figure S.6.6.8. A) XRD spectrum obtained for HA synthesized by slow acidification with propionic acid and used for all the control samples carried out in this work. The characteristic diffraction patterns of HA at 7.5°, 21°, and 24° are marked with an asterisk (*) [14]. B) The FT-IR spectrum of HA shows the peaks of at 1664 and 1209 cm ⁻¹ , representative of the coordination between the iron in heme and a propionate group. Whereas the peak located at 1712 cm ⁻¹ is characteristic of the hydrogen-bonded carboxylate group that links the heme dimers to extend the crystalline array [32, 190], these peaks are indicated with a diamond symbol (♦).	135

List of tables

Table 4.1. Experimental SSA, pore size distribution and pore volume estimated with BET and BJH models from N ₂ adsorption-desorption measurements at 77 K for HA produced by the NB and AC methods. Each value represents the average of four measurements on different samples. Experimental SSA is compared with theoretical SSA evaluated based on crystal size. The crystal size is measured based on SEM image analysis (eight crystals analyzed per sample).	48
Table 4.2: Elemental composition evaluated by XPS, compared with theoretical values (See SI 4.8.5 for details).	49
Table 4.3: Atomic percentage measured with XPS survey scans of HA samples after TFE functionalization.	53
Table S.4.1. Atomic percentage measured with XPS survey scans of HA samples after TFE functionalization.	59
Table S.4.2. Experimental domain sizes of HA samples calculated from XRD data.	60
Table S.4.3. XPS peak positions, and area ratios for the components fitted to the high-resolution C, O, N and Fe spectra measured for HA synthesized by NB and AC methods. Standard deviations are based on the measurements of at least three points on three different samples. The area ratios are standardized, for each element, to the most intense component. No statistically significant differences are found between any of the values reported for the NB and AC samples relative to either peak positions or area ratios.	62
Table S.5.1 XPS binding energies and area ratios of O _{1s} obtained for HA, pwHz, and ewHz. The peaks at 531.5 and 533.3 eV for all the samples were fitted according to the experimental FWHM obtained for HA.	97
Table S.5.2. XPS binding energies and area ratios of N _{1s} obtained for HA, pwHz, ewHz and all the controls used, in which HA was suspended in different solutions. The peaks at 398.2 and 401.1 eV for all the samples were fitted according to the experimental FWHM obtained for HA; whereas the peak at 399.7 eV was fitted according to the FWHM obtained for ewHz.....	98

Table S.6.1. Percentages of $\text{Ca}(\text{CH}_3\text{COO})_2$, CHA and DCPD obtained from Hz cultured from <i>P. falciparum</i> of the strains 3D7-H, determined by LCF using NEXAFS spectra of reference samples, and R-factors of the LCF.....	136
---	-----

Glossary of abbreviations and symbols

AC	Aqueous acid-catalyzed method
ACTs	Artemisinin combination therapy
AFM	Atomic force microscopy
Ala	Alanine
Arg	Arginine
BET	Brunauer-Emmett-Teller
BJH	Barrett-Joyner-Halenda method
Ca pyroP	Calcium pyrophosphate
CCL5	Chemokine C-C motif ligand 5
CDPK	Ca ²⁺ -dependent protein kinases
CQ	Chloroquine
CQR	Chloroquine-resistant
CXL8	Chemokine (C-X-C motif) ligand 8
DC	Dendritic cells
DCM	Dichloromethane
DCPD	Dicalcium phosphate dihydrate
DNA	Deoxyribonucleic acid
DV	Digestive vacuole
EDS	Energy-dispersive x-ray spectroscopy
ewHz	Extensively washed hemozoin
FT-IR	Fourier Transform – Infrared spectroscopy

GAP45	Glideosome-associated protein 45
HA	Hematin anhydride
Hb	Hemoglobin
HDP	Heme detoxification protein
HEPES	<i>N</i> -2-hydroxyethylpiperazine- <i>N'</i> -2-ethanesulfonic acid
His	Histidine
HRP	Histidine-rich proteins
Hz	Hemozoin
ITNs	Insecticide-treated mosquito nets
LCF	Linear combination fitting
Leu	Leucine
MACS	Magnetic-activated cell sorting
MALDI-ToF	Matrix-assisted laser desorption/ionization time of flight
MPG	Monopalmitic glycerol
MSG	Monostearic glycerol
MTIP	Myosin A tail domain-interacting protein
Mφ	Macrophage
Na polyP	Sodium polyphosphate
NB	Anhydrous non-coordinated-base method
NEXAFS	Near-edge X-ray absorption fine structure
nHz	Native hemozoin
PBS	Phosphate buffer saline
PC	Phosphatidylcholine

PDMS	Poly(dimethylsilane)
PfATP6	<i>Plasmodium falciparum</i> ATPase-6
pwHz	Partially washed Hz
RBC	Red blood cell
RDTs	Rapid diagnostic tests
RNA	Ribonucleic acid
RPMI 1640	Roswell Park Memorial Institute 1640 medium
SA	Sinapinic acid
SEM	Scanning electron microscopy
Ser	Serine
SERCA	Sarco endoplasmic reticulum Ca ²⁺ ATPase
sp²-N	sp ² -hybridized nitrogen components
sp³-N	sp ³ -hybridized nitrogen components
SSA	Specific surface area
TEM	Transmission electron microscopy
TFA	Trifluoroacetic acid
TFE	2,2,2-Trifluoroethanol
TSA	Theoretical surface area
XPS	X-ray photoelectron spectroscopy
XRD	X-Ray Diffraction
β-TCP	β-tricalcium phosphate

Contributions of authors

This thesis is presented as a collection of manuscripts written by the candidate under the supervision of **Prof. Marta Cerruti** and **Prof. Scott Bohle**. These papers are presented in **Chapter 4, 5** and **6** of this thesis.

As first author of all manuscripts, I envisioned and developed all the experiments, including the acquisition and analysis of the data collected. I was responsible for the synthesis of the materials, their physicochemical characterization and conducting the tests, as well as writing the three manuscripts. Both supervisors directed me throughout my research and revised the manuscripts.

Given the highly interdisciplinary nature of this research, extensive collaboration was necessary for the successful completion of this work. The role of each collaborator is explained below.

Chapter 4 and 5

Mr. Fadi Baakdah is a PhD candidate at Prof. George Elias' lab at McGill University. His contribution involved performing the *in vitro* cultures of *Plasmodium falciparum*, extraction of hemozoin and writing the respective experimental section of the manuscripts.

Prof. George Elias is a professor at the Institute of Parasitology at McGill University. He helped by providing the facilities for the parasite cultures and revising the manuscript.

Chapter 6

Dr. Mifong Tam is a research associate at Prof. Mary M. Stevenson's lab at McGill University. She performed the *in vivo* experiments and hemozoin extraction.

Prof. Mary M. Stevenson is a professor in the Faculty of Medicine at McGill University. Her contributions to the paper included proposing some experiments, providing animal-related facilities, offering discussions and recommendations and revising the manuscript.

Ophélie Gourgas is a PhD candidate at Prof. Marta Cerruti's lab in McGill University. Her contribution included data acquisition and analysis.

Thesis outline

This thesis is written in a manuscript-based format. The chapters are divided as follows:

Chapter 1 presents a brief description of the problem related to malaria in the context of hemozoin research and the rationale behind studying the surface of hemozoin and its synthetic counterpart, hematin anhydride. **Chapter 2** introduces the research hypothesis and objectives.

Chapter 3 reviews the literature relative to this investigation, including malaria, hemozoin and hematin anhydride, methods to produce synthetic hemozoin, hemozoin biomineralization, and relevance of Hz in antimalarials mode of action, as a tool for malaria diagnosis and as modulator of host response during malarial infection.

Chapter 4, Chapter 5 and **Chapter 6** present the three manuscripts showing the findings of the objectives established in this work. **Chapter 7** summarizes the contributions of this research to advance the knowledge in the field of malaria. **Chapter 8** discusses general conclusions of this work and future perspectives. Finally, the **Appendix** includes the copyrights waivers.

Chapter 1. General Introduction

Malaria is a blood infection caused by parasites of the *Plasmodium* genus that are transmitted to humans and vertebrates by the bite of a female *Anopheles* mosquito [1]. In 2017, there were about 219 million cases of infection, resulting in 435,000 deaths among the global population, mostly in poor areas of the tropical and sub-tropical regions [2]. The distribution of sprayed bed nets, the use of insecticides, a prompt diagnosis and improved antimalarial treatments have decreased the risk of infection by 50% since 2000; however, no significant reduction in mortality rates has been reported in recent years [2]. Moreover, socio-economic factors, changes in land use, and resistance to drugs and ineffective insecticides doom the efforts made in controlling the risk of infection in areas where the disease is not prevalent [3, 4]. For this reason, the search for accurate diagnostic methods, new antimalarial drugs, and an effective vaccine are urgently needed to reduce malaria morbidity and mortality [1].

After the transmission of the parasites by the bite of the *Anopheles* mosquito, *Plasmodium* invades the host liver, where it matures and multiplies over several days to months, depending on the species of *Plasmodium*. Then, the invaded liver cells burst releasing the parasites back into the bloodstream to invade the red blood cells and continue asexual reproduction. The parasite feeds on hemoglobin present inside the red blood cell as a source for nutrients to sustain growth and multiplication [1]. The proteolysis of hemoglobin is carried out inside an acidic organelle known as the digestive vacuole (or food vacuole), found within the parasite. During this process, all the heme present in hemoglobin is released inside the digestive vacuole of the parasite [5]. The structure of heme comprises an iron atom bound to four nitrogen atoms in a protoporphyrin ring [6]. Free heme is highly toxic to the parasite as it can disrupt parasitic membranes and cell functions; therefore, its rapid detoxification is crucial for *Plasmodium* survival [6]. For this reason,

the parasite crystallizes heme into inert hemozoin, also known as the “malaria pigment” due to its characteristic dark brown color [5]. Hemozoin is a crystalline biomineral, consisting of dimers of heme linked reciprocally by iron-carboxylate bonds; the dimers are further arranged in chains linked by hydrogen bonds to produce brick-shaped crystals [7]. Many biological components are thought to play a role in hemozoin (Hz) formation *in vivo*, such as lipids, proteins, and the acidic pH of the digestive vacuole; however, the exact process inside the parasite is still under debate [8]. The role of these components has been extensively investigated through *in vitro* formation assays of synthetic Hz, also known as hematin anhydride (HA) or β -hematin, the synthetic isostructural phase of Hz. HA is produced from the crystallization of heme using one of the several protocols reported in the literature [8]; although their biochemistry does not mimic what happens *in vivo* and, in fact, many preparations result in poorly crystalline or amorphous phases [9].

Hz is also the target of some of the primary line of antimalarials in current use that act by blocking Hz biomineralization, either by complexing with heme or by adsorbing onto the surface of the crystals [10]; further experimental evidence is necessary to establish their mechanism of action. Additionally, there are reports of some *Plasmodium* species becoming resistant to these drugs [1]. Therefore, information about the process of Hz formation and the mode of action of the current antimalarials could open avenues for the design of more efficacious treatments [10].

On the other hand, Hz is also used as a biomarker for novel diagnosis methods. The high spin of the Fe^{3+} ion together with the protoporphyrin ring provides Hz with paramagnetic and optical properties that are exploited to produce accurate and sensitive diagnostic platforms [11]. The current methods involve the use of light microscopy or rapid test for diagnosis, which present some challenges related either to their operation, cost and stability under field conditions [12].

Hz is also involved in the pathogenesis of malaria. The role of Hz is studied using crystals isolated from the parasite or by cultivating the synthetic crystals with diverse cells, or injecting them in *in vivo* models using mice [13]. The results of these experiments indicate that after Hz is released in the bloodstream, the crystals interact with several cells and biomolecules that ultimately adsorb on Hz surface [8]. Thus, it is not clear whether these adsorbed molecules or the crystals themselves are responsible for the immunomodulating properties of Hz [8]. In addition, different preparations of HA or the protocols used to wash Hz after its extraction give rise to contradictory and conflicting results [14].

To clarify the issues, the surface of Hz should be analyzed; however, despite numerous investigations on the morphology, crystal habit and overall bulk properties of Hz, there is still no knowledge about the surface of Hz or HA. These studies are limited due to the poor quantities of Hz obtained after its extraction and the lack of a standardized method to remove the biological impurities adsorbed onto the crystals surface [15].

Chapter 2. Hypothesis and Objectives

We hypothesize that surface-sensitive techniques can be used to study the physicochemical properties of Hz and HA to clarify their impact on Hz's role as an immune modulator in malaria pathogenesis, in antimalarial drugs mode of action, and to provide insights into Hz biomineralization.

To test this hypothesis, we established three main objectives:

- (i) Investigate the physicochemical properties of the surface of HA prepared by two different methods of synthesis**

HA is commonly used as isostructural synthetic substitute of hemozoin. However, there are various protocols to produce the crystals, which result in materials with large variations in size, morphology, and crystallinity that in turn impact their surface properties. We synthesized HA following two of the most widely used methods reported in the literature. We then studied some physicochemical properties of the surface of these materials and compared our findings to theoretical values. Additionally, we performed a chemical derivatization to label and semi-quantify the active carboxylate groups on HA surface produced by the two methods as an indirect means to understand differences in their biological activity.

(ii) Compare the impact of two washing protocols on the surface of Hz in terms of composition and amount of contaminants, and assess their possible source(s) and adsorption sites using a model of HA suspended in biomimetic solutions

The next objective is to study the surface composition of Hz from *in vitro* cultures of the human-malaria specie *Plasmodium falciparum*. Typically, the freshly-extracted crystals present organic contamination adhered onto the crystals surface; therefore, the crystals are washed to remove this coating as much as possible. However, due to the lack of a standardized protocol to clean Hz, in this study we assessed the impact of the washing method on the composition of Hz surface. We used two methods to clean extracted Hz, one of them more exhaustive than the other. Then, we used HA crystals suspended in solutions that mimic its biological environment as models to assess the origin of the organic contaminants adsorbed on Hz and their main adsorption sites. From these experiments, we proposed that the surface of Hz is never free of contaminants despite the method selected to clean the crystals since the contamination may be part of the crystalline structure of Hz.

(iii) Characterize the composition of the organic material adhered onto native hemozoin isolated from *in vitro* and *in vivo* models and evaluate their possible source using a model of hematin anhydride suspended in biomimetic solutions

Based on the results obtained for Hz washed with a short protocol from Objective (ii), we extended our work to deepen our understanding of the composition of the surface contaminants adhered to Hz. In this investigation, we extracted Hz from *P. falciparum*-infected red blood cells cultivated *in vitro*, and Hz collected from murine macrophages infected from *P. chabaudi*

from an *in vivo* model. We rinsed the crystals using organic solvents to remove the organic contaminants weakly adhered onto the crystals surface. We then compared Hz isolated from the different models to determine if their surface composition varies according to the model used to obtain Hz (*in vitro* vs *in vivo*). We found that the organic contaminants associated to Hz surface contained unexpected inorganic species of Na, Cl, Si, Ca and P in all Hz collected from *in vitro* and *in vivo* models. We then proposed the possible origin of these elements by using a model consisting of HA suspended in solutions containing the element of interest that may adhere to Hz during its formation or ejection from the RBC. Based on these results, we hypothesized the biological function of these elements in *Plasmodium*.

Chapter 3. Literature review

3.1. Malaria

Malaria is a blood disease caused by parasites of the *Plasmodium* genus that are transmitted to human and vertebrates by the bite of infected female *Anopheles* mosquitoes. The species of *Plasmodium* that cause malaria in humans are *P. vivax*, *P. malariae*, *P. ovale*, *P. knowlesi*, and *P. falciparum*, the latter being the most common and deadly [16]. According to the World Health Organization, there were about 219 million cases of malaria and an estimated 435,000 deaths in 2017, mostly in Africa and South-East Asia [2]. Although malaria mortality rates have fallen by almost 50% since 2000, data from 2015-2017 indicate no substantial progress in reducing malaria cases worldwide in this time frame [2]. Moreover, poverty, human migration, the decrease of financial support, changes in land use and fast spreading of drug resistance threaten to increase the transmittance of the disease in areas where malaria was under control, such as the East African highlands [3, 4, 17].

Malaria is a curable disease if diagnosed early and accurately [2]. Microscopic images of blood smears and rapid diagnostic tests are the most common methods to diagnose malaria in individuals [16]. After a parasitological confirmation, the patient is treated with antimalarial agents. The current recommended therapy for malaria includes artemisinin combination therapy (ACTs) as first-line treatment [2], which consists of an artemisinin derivative combined with another structurally unrelated antimalarial, typically more slowly cleared from the body [18]. ACTs are effective and fast acting; however, the widespread resistance to artemisinin drugs threatens the efficacy of the ACTs. Hence, while the current antimalarial therapies are threatened

by parasitic resistance, preventing high-risk populations from potential infections is crucial to reduce the malaria burden [2].

The transmission of malaria is mainly prevented through vector control methods to avoid the bite of infected mosquitoes. The most important and widely used method is the deployment of insecticide-treated mosquito nets (ITNs), and in a lesser extent, indoor residual spraying with insecticides [2]. The most commonly used insecticides include pyrethroids, organochlorines, carbamates and organophosphates [2]; whereas bed nets are sprayed with pyrethroids only [1]. However, resistance to at least one class of insecticides has been detected in 68 out of the 80 countries affected by malaria. Meanwhile, resistance to pyrethroids, the only insecticide in current use to treat ITNs, was reported in more than two-thirds of the areas tested and is quickly spreading [2].

In African regions, malaria is also prevented in pregnant women and children by prophylaxis with an intermittent treatment with the antimalarial drug sulfadoxine-pyrimethamine, which is used for chloroquine-resistant strains of *P. falciparum* [2]. Prophylaxis is also recommended for travelers from non-endemic malaria areas, along with personal protective measures, such as the use of insect repellent, and wearing of long-sleeved garments and trousers [19]. Overall, these preventive measures are decreasing the risk of malaria infection in highly afflicted-malaria areas; however, they involve the use of chemical agents, such as insecticides and chemotherapies that are susceptible to mosquito and parasitic resistance, respectively. Therefore, the progress achieved in controlling malaria is at substantial risk [20], and the search for prevention is still a major concern.

Recently, GlaxoSmithKline Biologicals developed the first malaria vaccine, RTS,S/AS01, also known as RTS,S. The vaccine acts on *Plasmodium falciparum*, the most prevalent and deadly

malaria parasite [21]. A phase 3 trial conducted for RTS,S on infants and young children in 7 sub-Saharan African regions showed 18-36% efficacious protection against malaria [21], probably due to the complex life cycle and polymorphism of *Plasmodium* parasites [1]. Additionally, although the RTS,S vaccine has shown modest efficacy in reducing clinical malaria in children, new data associated the use of the vaccine with a higher risk of fatal malaria in girls, and higher all-cause mortality in girls [22]. It is not clear why RTS,S increased the mortality in girls; however, potential risks and overall quality and efficacy of the vaccine should be assessed [21, 22].

Overall, the global elimination of malaria is still a major worldwide concern. Its success depends on the implementation of preventive programs, the search for effective new treatments and accurate early diagnosis [23, 24].

3.2. Hemozoin

The proliferation of *Plasmodium* in vertebrate hosts starts after an infected mosquito transmits the parasite sporozoites through the salivary gland, as depicted in **Figure 3.2.1**. The parasite circulates in the bloodstream and invades the host liver, where the sporozoites mature and multiply into merozoites [16]. Then, they are released into the bloodstream and enter the red blood cell (RBC) to start the asexual cycle [16] consisting of rings, trophozoites, and schizonts, which in turn will reinvade healthy RBCs [5].

The blood stage of malaria is characterized by symptoms consisting of fever, shaking chills, and overall flu-like manifestations [16]. In addition, during this stage, the parasite digests 60 to 80% of hemoglobin (Hb) in the RBC to sustain its growth and reproduction. This degradation takes

place within an acidic organelle called digestive vacuole (DV), and free heme is released during this process [5].

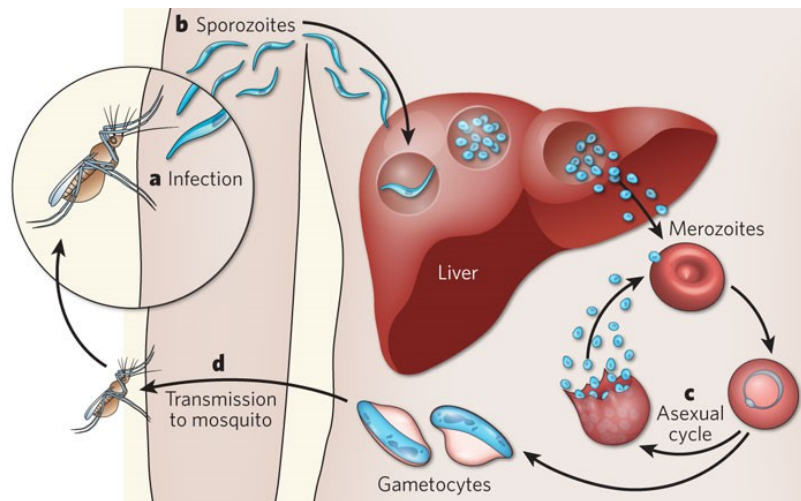


Figure 3.2.1. The life cycle of *Plasmodium* starts in the sexual stage inside a female *Anopheles* mosquito. During a blood meal, the mosquito transmits sporozoites into a human host, which infect liver cells where the parasite will mature for 10-14 days, followed by their release as merozoites into the bloodstream to invade red blood cells. In the blood stage, the schizont will feed on hemoglobin and proceed throughout various stages of asexual multiplication, consisting of rings, trophozoites, and schizonts. After schizont rupture, H₂O crystals and merozoites are released into the bloodstream and reinvade healthy red blood cells and start a new asexual cycle (Reproduced from ref. [25] with permission from Springer Nature).

Heme is a molecule of great importance in vital biological processes since it serves as a cofactor for many proteins known as hemoproteins, which are involved in oxygen transport and storage, ligand sensing and electron transfer [26]. Heme consists of a protoporphyrin ring bearing an iron ion at the center that can be present either as ferrous (Fe^{2+}) or ferric (Fe^{3+}), enabling catalytic activity to many enzymes [6]. Together with the highly hydrophobic nature of its protoporphyrin ring, heme can interact with lipophilic molecules, such as lipids and proteins, resulting in toxic effects inside the parasite [27], including the peroxidation of membranes, deficient leukocyte function, disruption of membrane potential and damage to cellular metabolism

due to inhibition of enzymes [1, 28]. Therefore, to avoid its harmful effects, the malaria parasite sequesters heme into hemozoin (Hz) in a non-enzymatic process known as biomineralization [8].

The formation of Hz, also known as the “malaria pigment”, seems to be the pathway to detoxify heme in other parasites besides *Plasmodium*, such as the avian Apicomplexan *Haemoproteus columbae*, the helminths *Schistosoma mansoni* and *S. hematobium*, the triatomine *Rhodnius prolixus* bug, the trematode *Echinostoma trivolvis* and probably the family of *Opisthorchiidae* [5, 29-31].

In 1991, Slater *et al.* used infrared spectroscopy, electron paramagnetic resonance, and X-ray absorption to study natural and synthetic Hz referred to as hematin anhydride or β -hematin. From this information, they proposed that the structure of Hz is a polymer chain constituted of heme moieties linked through the ferric iron ion center of one heme and a carboxylate bond of an adjacent heme [32]. For many years, the term “polymer” was used to refer to the malaria pigment, and a heme polymerase and a polymerization process for malaria pigment were the subjects of research for about a decade [33].

Then, in 2000, Bohle’s group carried out crystallographic studies using high-resolution synchrotron X-ray radiation of Hz and hematin anhydride. They showed that the structures of both Hz and hematin anhydride do not correspond to a polymer, but rather to cyclic dimers of hematin linked through reciprocal iron-carboxylate groups, and the dimers, in turn, are further linked by hydrogen bonds (**Figure 3.2.2**) [7]. The structure of Hz corresponds to a crystal with a triclinic unit cell, with space group P-1 and dimensions: $a = 12.196 \text{ \AA}$, $b = 14.684 \text{ \AA}$, $c = 8.040 \text{ \AA}$, and angles $\alpha = 90.22^\circ$, $\beta = 96.80^\circ$, and $\gamma = 97.92^\circ$ [7]. This work not only elucidated Hz structure, it also established that Hz and hematin anhydride were crystallographically, chemically and

spectroscopically identical [34]. Generally, the terms Hz and malaria pigment refer to the material originating from the parasite, whereas any of the isostructural synthetic phases will be termed hematin anhydride (HA). HA is often referred to as β -hematin; however, there are distinctive differences in synthesis and properties between these two materials [9]. The term β -hematin was conceived for the sodium bicarbonate insoluble phase of α -hematin ($\text{Fe}[\text{protoporphyrin IX}]\text{OH}$) (**Figure 3.2.2**) [11], whereas HA refers to the product resulting from the removal of water and replacement by the coordination to a propionate group of a neighboring $\text{Fe}(\text{protoporphyrin IX})$, and hence an anhydride product (**Figure 3.2.2**) [35].

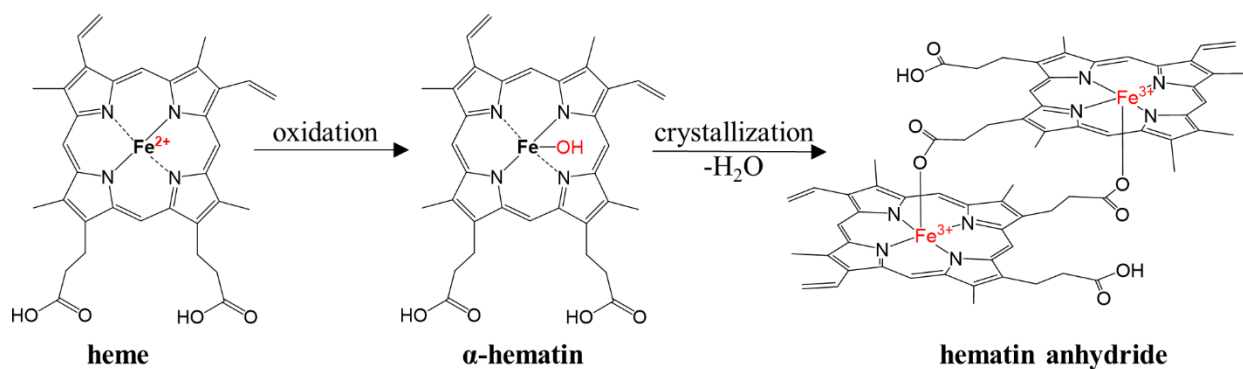


Figure 3.2.2. Schematic of the conversion of heme into HA. Free heme is oxidized into α -hematin at low pH, the hydroxyl group on the iron of α -hematin protonates and is replaced by the coordination with the propionate group of the neighboring hematin with loss of water, resulting in the crystallization of HA.

Scanning electron images of Hz isolated from diverse *Plasmodium* parasites reveal crystals with varied shape and size [29]; however, crystallographic studies present identical diffraction patterns, which implies that the structure of Hz is equivalent among *Plasmodium* species [5]. The overall morphology of Hz corresponds to brick-like shaped crystals with smooth sides, while the smallest face appears highly corrugated, suggesting that this is the fastest growing face [5, 29].

In general, the morphology and habit of a crystal are determined by the growth rate of its faces, which in turn can be affected by the solvent and components present in the medium [36]. These aspects of Hz are usually studied during HA formation in aqueous solutions or in the presence of components found in the DV of the parasite as an attempt to mimic the biological environment [35, 37]. Alternatively, more recent investigations on Hz are shifting to study the crystals within the DV to understand its biomineralization process *in vivo*. All these topics will be covered in **section 3.4**.

3.3. Synthetic analogues of Hemozoin

Increasing evidence points to a significant role of Hz not only in the life cycle of the parasite but also in the detection and pathology of the infection [11], which in turn impact the efficacy of the treatment selected after diagnosis [1]. Therefore, studying the properties of Hz isolated from the parasites have become a focus of attention. However, investigating Hz obtained from *in vivo* or *in vitro* models involves several challenges, such as contamination of the crystals with parasitic or host components after cell lysis and insufficient amounts of material obtained [14, 38]. Additionally, the cultivation of *Plasmodium* parasites requires laborious work and is limited to well-trained staff. Therefore, artificially grown crystals are used to overcome the challenges arising when employing Hz [38], and are useful for gaining insight into the properties of the natural material.

Synthetic crystals are typically produced using hemin (**Figure 3.3.1**) or hematin as precursor [8] and the crystallization of HA proceeds under different conditions that vary according to the protocol used [39]. These conditions involve the suspension of hemin or hematin in some media

(aqueous, anhydrous or a mixture of aqueous and organic media) under different conditions, such as slow acidification, heating or extended crystallization times [39]. Taking advantage of the differing solubility between monomeric hemin or hematin and HA, any insoluble or poorly aggregated hematin is separated from HA by rinsing the product with an alkaline buffer of sodium bicarbonate, although this step dissolves some of the HA as well [40]. The synthetic crystals are crystallographic and chemically similar or identical to Hz, as evidenced in previous reports by infrared spectroscopy and X-ray diffraction [5].

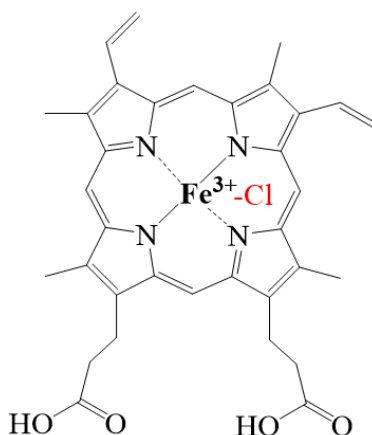
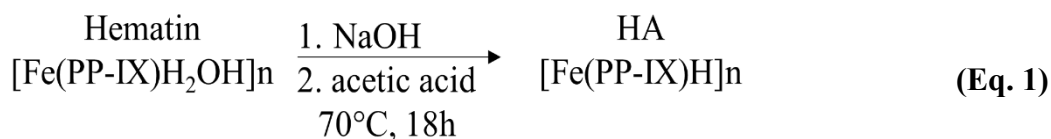


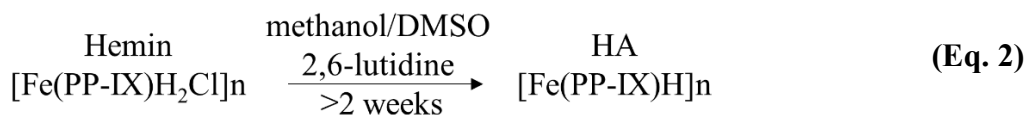
Figure 3.3.1. Molecular structure of hemin, the chloride equivalent of α -hematin. Hemin is formed when the central iron of a heme group coordinates with a chloride ligand.

One of the most widely used methods to prepare HA is the acid-catalyzed method [32]. In this preparation hemin is dissolved in aqueous media at elevated pH, followed by its conversion to hematin and subsequent crystallization into HA by the slow acidification with acetic acid at 70 to 80°C for 18 h [32] (**Eq. 1**). Modifications to this method involved the use of other acids to promote HA precipitation, such as propionic or benzoic acid, and decreasing the temperature to 60°C or 37°C [41]. Another variation of this method was introduced by Egan *et al.*, in which the formation of HA is carried out in a 4.5 M acetate solution, at pH 4.5 for 30 min [35], resulting in 40-50%

yield. The products of these methodologies are poorly crystalline precipitates that are rather heterogeneous or even nanocrystalline [14], with tapered ends and a large range in size from 200-1600 nm [29] (**Figure 3.3.2.A**). The acid-catalyzed method has been implemented to study the formation of HA in the presence of various promoters of HA formation, such as detergents or alcohols [42]; or to gain insights into the mechanism of HA inhibition by antimalarials [43]. Also, the crystals obtained from this method are used to study Hz's immunomodulatory role [8].



Bohle and Helms proposed another method to prepare HA in strictly anhydrous conditions, in organic media at room temperature [44]. In this reaction, chloride is removed from hemin in the form of HCl using the non-coordinating base 2,6-lutidine [39], while the organic solvents aid the solubilization and coordinate heme (**Eq. 2**). The reaction proceeds for two weeks to several months, which in turn produces high yields (>90%) of large HA crystals of around 4-10 μm , highly regular in size and morphology (**Figure 3.3.2.B**) [44]. These crystals are isomorphous to Hz and show remarkably large crystalline domains [14]; however, the length of the crystallites is larger than what the parasite produces *in vivo* (4-10 μm). This method has been used to investigate the role of neutral lipids in HA crystallization [45] and the crystals produced by this method have been largely used to study spectroscopic, structural and physical properties of HA [41], and more recently, the effect of HA in host immune response [14, 41].



In summary, *Plasmodium* produces Hz crystallites highly uniform in shape and size that varies between 50-500 nm (**Figure 3.3.2.C**) [38, 39]; however, in HA these features differ according to the preparation method [39]. Some of the synthetic products are also characterized by high surface areas with a random distribution of defects that lead to major differences in the diffraction patterns of the precipitates when compared to Hz [39].

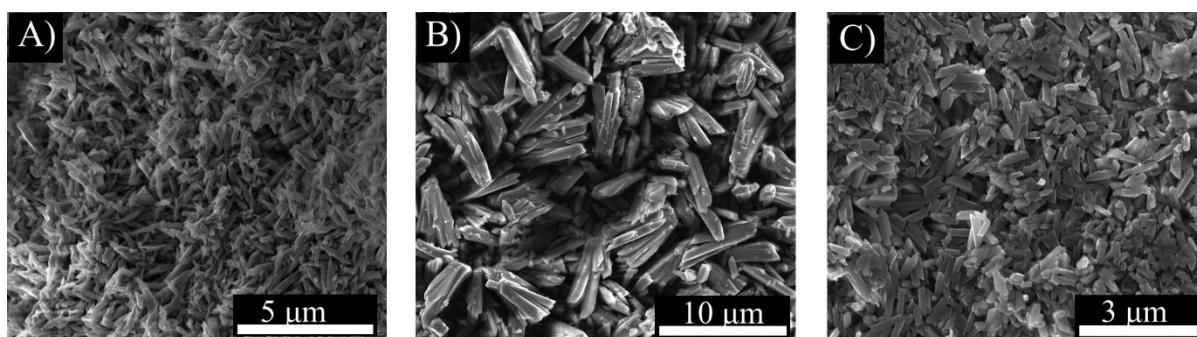


Figure 3.3.2. Scanning electron micrographs of A) HA produced by the acidic-annealing method at high temperature and B) HA crystallized in anhydrous conditions using DMSO, methanol and the base 2,6-lutidine and C) Hz obtained from *P. falciparum*.

At the present time, many pathways for Hz biomineralization have been proposed based on observations from the *in vitro* formation of HA [1]. Still these investigations are unable to clarify how Hz is so efficiently produced in the DV of the parasite under mild physiological conditions [40]; moreover, the exact molecular mechanism of Hz formation *in vivo* is still under debate [5].

3.4. Hemozoin biomineralization

The biomineralization of Hz has been extensively studied using HA formation assays. Egan and colleagues assessed HA crystallization in aqueous acetate solution varying the pH, temperature and acetate concentration [35]. The crystals were characterized using infrared spectroscopy (FT-

IR), scanning electron microscopy (SEM) and X-ray diffraction (XRD). The results showed that both the iron-carboxylate bond and crystallization of HA occur simultaneously through the loss of water and the fast precipitation of amorphous and highly soluble hematin, followed by the slow incorporation into more stable HA crystals [35]. More recent studies by Vekilov and co-workers showed that Hz follows a classical mechanism of growth where new crystal layers nucleate and extend the crystalline net by the attachment of new hematin molecules [46]. Additionally, theoretical models of HA's growth carried out by Buller *et al.* [47] reported that the habit of the needle-like crystallites of Hz and HA extends predominantly along the *c*-axis direction, exposing {100} and {010} side faces, and less-developed {011} and {001} face [36, 46, 47].

Egan's group proposed two possible models for Hz formation. In one model, free heme is released quickly in the DV, leading to saturation and precipitation of hematin; in such case, the biomineralization of Hz would be promoted by lipids acting as catalyst for the phase transition from heme to Hz, solubilizing hematin and facilitating Hz biomineralization [35]. In the second model, the release of heme in the DV is highly controlled to avoid surpassing the solubility limit of hematin, yet heme is found supersaturated, in comparison to Hz. In such a case, the nucleation of Hz could be promoted by a protein matrix. In fact, Sullivan *et al.* proposed that histidine-rich proteins (HRP) present in the DV of the parasite may bind heme to promote Hz biomineralization [48]. They hypothesized that carboxylate groups of Hz may bind weakly to amino acids in HRP, acting as templates for epitaxial growth or as stabilizers of Hz nuclei [35], as commonly observed in several biomineralization processes, such as hydroxyapatite in shells and bones [41, 49].

To date, several studies aim to identify the role of both lipids and proteins as potential promoters of Hz crystallization. The investigations on this subject will be discussed next, in **Chapter 3.4.1**.

3.4.1. The role of lipids in hemozoin biomineralization process

Many studies demonstrate a close relationship between lipids and hemozoin formation [50-52]. In 1995 Bendrat *et al.* reported that Hz crystals extracted with acetonitrile were contaminated with phospholipids [53]. Later on, Fitch and co-workers suggested that hemozoin formation was promoted inside unsaturated lipids [50] (**Figure 3.4.1.A**). Since then, the role of lipids in Hz formation has been widely investigated.

Huy *et al.* proposed that phospholipids, such as dilauroyl-phosphatidylcholine and dioleoyl-phosphatidylcholine, act as inducers of Hz formation in *Plasmodium* and other hematophagous parasites like *Schistosoma* and *Rhodnius* [54]. It was thought that the acyl chains present in lipid droplets and in phospholipid membranes (**Figure 3.4.1.A**) participate in the crystal nucleation inside the DV of the parasite [54]. However, only small amounts of phosphatidylcholine and phosphatidylethanolamine have been identified in Hz inside the DV [55].

To further understand the role of neutral lipids, Pisciotta *et al.* fixed DVs of malaria parasites in the trophozoite stage with malachite green to protect the lipid layer, and then proceeded to analyze their composition [55]. They found that Hz was surrounded by neutral lipids nanospheres, predominantly MSG (monostearic glycerol) and MPG (monopalmitic glycerol). A blend of fatty acids was also identified in minor proportions, constituted mostly of saturated palmitic and stearic fatty acids [55].

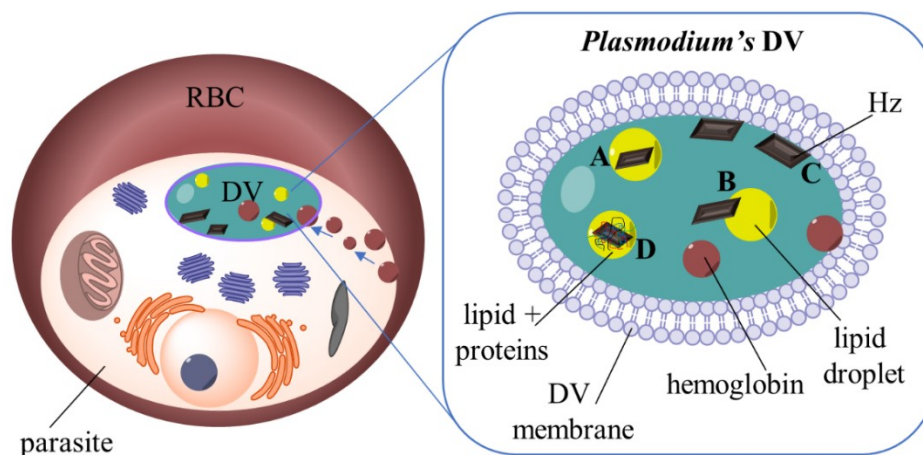


Figure 3.4.1. Schematic of a *Plasmodium*-infected RBC and Hb catabolism within the DV of the parasite (inset). It is proposed that after the proteolysis of hemoglobin, heme is released in the DV, and the parasite forms Hz crystals assisted by lipids in four possible ways: A) inside lipid droplets, B) at the water-lipid interface of lipid droplets, C) at the water-lipid interface of the DV membrane or D) in a complex of lipids and proteins.

Egan and co-workers also remarked the need for a lipid environment to grow HA or Hz as well, but in contrast to Pisciotto's work, they demonstrated that the mineralization was more efficient at the lipid-water interface (**Figure 3.4.1.B**), possibly due to lipids functioning as nucleation sites [41]. Kapishnikov *et al.* recently proved that Hz is produced at the aqueous-lipid interface near the inner membrane surface of the DV (**Figure 3.4.1.C**), instead of lipid droplets [56]. They proposed that Hz crystals are aligned and oriented within the DV, exposing their {100} faces along an acylglycerol lipid layer that coats the DV phospholipid membrane. The OH and C=O groups of the acylglycerols would serve as templates, lowering the surface free energy of the {100} face, and providing the specific crystal orientation [56], while the propionate groups of heme would remain in the aqueous phase [54, 56].

To further understand the process of Hz nucleation and growth in an aqueous-organic interface, Vekilov's group studied the surface of HA crystals grown in two different media, one at pH 4.8 in aqueous solution, and the other one in aqueous-saturated octanol, in which the organic

solvent mimicked the lipid regions within the DV [37]. HA crystals produced in aqueous solution at acidic pH showed spherical aggregations, rough surfaces, and crystal twinning. These characteristics are representative of crystals grown at high supersaturations of solute (heme) [57]; however, this crystal habit and morphology are not typical of Hz [37]. Conversely, the crystals grown in water-saturated octanol showed the presence of individual elongated crystals and a small fraction of amorphous aggregations. In general, the HA crystals produced in the presence of a mixed water-organic medium presented features that resembled more those observed in biological Hz. In this method, the supersaturated octanol maintained hematin solubilized, which *in vivo* accounts for the efficient conversion to Hz within the DV of the parasite [37]. The similarities between HA crystals formed in water-saturated octanol and Hz support the hypothesis that lipid nanospheres mediate the formation of Hz by keeping hematin below its saturation limit [37]. However, this work failed to replicate the efficient conversion of heme into Hz crystallites; additionally, these experiments did not explain the presence of a small fraction of amorphous precipitates despite their growth in conditions that resemble the DV.

This observation was also highlighted by Pesciotta's group when assessing HA formation in the presence of MSG and MPG. They demonstrated that neutral lipids enable heme crystallization [55]; however, the lipids were insufficient to produce HA with the morphology and size of Hz. They proposed that Hz formation may require not only of lipids but also proteins or other biomolecules (**Figure 3.4.1.D**) [55].

3.4.2. The role of proteins in hemozoin biomineralization

The production of histidine-rich proteins (HRP) by *Plasmodium* has been closely associated with Hz formation [48]. Sullivan and co-workers identified the HRP II and its homologues HRP III and

IV within *Plasmodium*. They proposed that these proteins promote Hz formation *in vivo* either as catalysts or nucleating initiators [48, 58]. Then, Ziegler's group used peptide dendrimers with the same repetitive sequence of HRP II to assess the formation of HA in acidic conditions [58]. Based on these experiments, they hypothesized that Hz formation is promoted by *P. falciparum* HRP II, acting as a template to seed the biomineralization [58]. However, later other researchers disputed the claim that HRP II is directly related to Hz formation since most of the HRP reside inside the membranes or the cytoplasm and just an estimated 3% is within the DV [59, 60]. Moreover, experiments made with parasites lacking HRP II and HRP III maintained the ability to produce Hz [61].

Recently, a protein named *Plasmodium* heme detoxification protein (HDP) was identified as a potent mediator involved in Hz formation. HDP is a 205 amino acids long polypeptide that converts heme into Hz very efficiently [62]. One hypothesis for the reaction mechanism is that the parasite traffics HDP and host Hb to the DV where two heme monomers bind to histidine residues present in HDP; then, a mutual iron-oxygen bond is formed and the heme dimer is released from the protein [62, 63], as depicted in **Figure 3.4.2**.

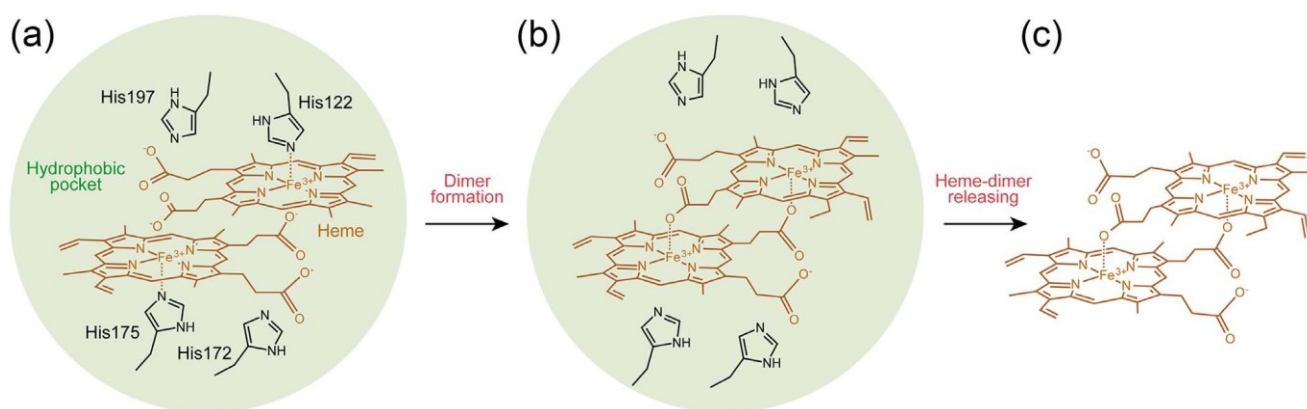


Figure 3.4.2. Hypothesized mechanism of Hz formation assisted by HDP, where histidine-residues in the protein interact with heme to allow the proper positioning of the heme monomers to initiate the nucleation of Hz (Reproduced from ref. [63] with permission from Springer Nature).

Chugh *et al.* showed HDP is present along with falcipain 2/2', plasmepsin II and IV and histi-aspartic protease in a protein complex found in the DV of the parasite [64]. They assessed the capacity of each of the proteins in the complex to convert Hb to Hz in an *in vitro* assay. The results from XRD and SEM showed that heme is efficiently converted to Hz by the action of HDP and falcipain 2. This evidence did not exclude the role of lipids as Hz promoters since they also demonstrated that Hz formation was enhanced by the addition of MOG or lipids extracted from parasite lysates [64]. Therefore, it is possible that HDP works synergistically with some lipids to produce Hz *in vivo* [59]. Jani *et al.* hypothesized that HDP promotes the formation of heme dimers to further incorporate them into lipid nanospheres to favor the hydrogen bonding of the propionic acid chains to extend the crystalline structure [62]. Moreover, HDP is also expressed at earlier stages of the *Plasmodium* lifecycle, indicating that this protein could have other possible functions [62].

Although the identification of HDP and its possible role bring advancement in our understanding of Hz formation, other important questions remain: how many proteases are present in the protein complex and how are they arranged within the DV? What is the main role of each of the constituents? Where is the complex exactly located in the food vacuole? [65] And when and how is heme oxidized into hematin? A reply to these questions will have important implications in the prevention of malaria and the development of new antimalarial drugs.

3.5. Hemozoin surface

The surface of a material is defined as the termination of a three-dimensional structure i.e. its outermost atomic layers; hence, the surface properties often differ from those of the bulk [66]. Understanding the surface properties of a material is critical for gaining insight into its physical

and chemical interactions, such as bonding and adhesion, electrostatic behavior, among other surface phenomena [66].

Currently, there is scarce information related to the structural and surface chemistry of Hz or HA crystals; studies carried out in this direction are focused on developing methods to understand drug-crystal interactions or Hz biomineralization. For example, Wood and co-workers studied Hz within a sectioned infected RBC using tip-enhanced Raman spectroscopy (TERS) to target the edges of the crystals [67]. TERS is based on surface-enhanced Raman spectroscopy (SERS), which uses a surface plasmon field to increase the Raman scattering; however, in TERS, the enhancement is produced by illuminating a metal nanotip smaller than the light wavelength, which allows its interaction with just a few molecules and thus it collects molecular information at the nanometer scale [67]. This methodology requires the use of atomic force microscopy (AFM) to image the surface morphology of Hz crystals and record the Raman spectra in the locations of interest [67]. The AFM images showed clusters of Hz covered with membrane and cellular components of the DV of the parasite, and crystal shape and size similar to those previously reported for Hz [67]. For the TERS experiments, the spectrum was recorded at the edge of the {001} face of Hz crystals because this is the fastest-growing face, and also because it is hypothesized that some antimalarials bind selectively to this face to inhibit Hz growth [36]. This analysis showed the characteristic bands of Hz in the region of 1600-1500 cm^{-1} related to the vibrations of the pyrrole ring. The spectrum also showed a band located at 1373 cm^{-1} , corresponding the symmetric vibration of the pyrrole ring of heme (ν_4). The latter peak is also known as the “electron density” or “oxidation state signal” because shifts in this band are associated to the oxidation state of the heme central Fe in the porphyrin, which in Hz corresponds to the ferric high spin state [67]. These experiments showed variations in the intensity of the

oxidation state band at 1373 cm^{-1} of TERS spectra acquired from Hz crystals in different DVs, probably as a result of using different tips. Although this technique does not bring new advancement in our knowledge about Hz morphology or its structural properties, due to the resolution of the AFM/TERS, this technique is expected to be used in the future as a label-free method to screen drugs that act by binding to Hz surfaces.

3.6. Understanding Hz biomineralization based on the characterization of HA surface

Vekilov's group developed a new method to synthesize large HA crystals and characterized the products with surface-sensitive techniques [68]. In an attempt to provide an environment that resembled the biological conditions of Hz formation, they carried out HA synthesis in a biphasic mixture consisting of water-saturated octanol to mimic the lipidic phase of the parasite's DV, and citric buffer at pH 4.8 to mimic the acidic aqueous phase. A solution of hematin was injected at the interface between the aqueous and the organic phase, and the preparation was left at 23°C for approximately 14 days. Samples were collected after 30 minutes and 2 weeks, and their morphology and size were evaluated using SEM and AFM. The materials collected after the first 30 min consisted of amorphous aggregates of varied size and elongated structures of around 600 nm in length (**Figure 3.6.1**). After 2 weeks of reaction, HA was present in the aqueous phase and the crystals were approximately $2\text{ }\mu\text{m}$ in length (**Figure 3.6.1**). These crystals were used as seeds to further enlarge them in a second step consisting of a supersaturated solution of hematin in octanol and the solution of citric buffer containing the previously produced HA. The pre-seeded crystals transferred to the octanol layer, and after 2 to 4 days the length of the crystals was about $35\text{-}50\text{ }\mu\text{m}$ (**Figure 3.6.1**) [68].

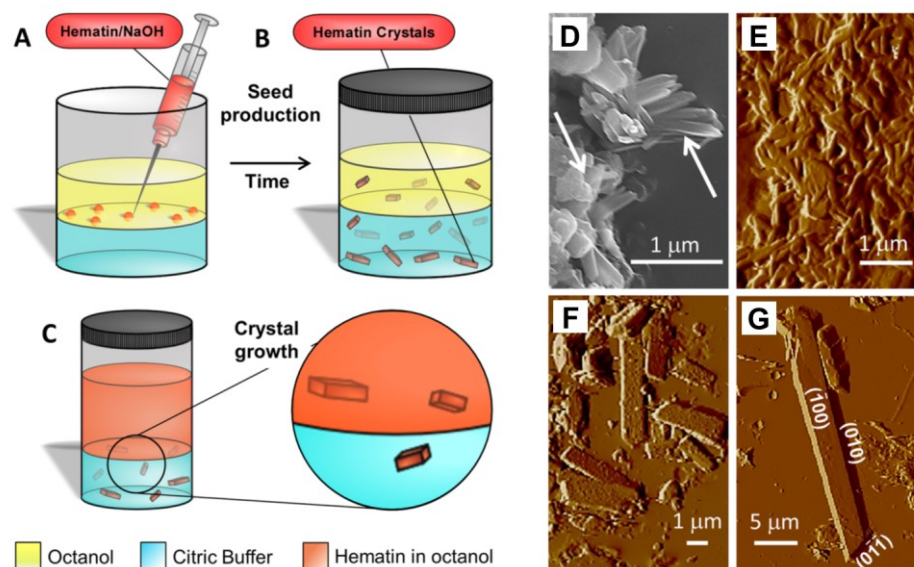


Figure 3.6.1. Illustration of the biomimetic synthesis of HA crystals. A) The crystals are produced at the interface between the wet octanol and the citric acid buffer. B) After 4-6 days HA is formed and is found in the aqueous phase; the crystals are removed and used as seeds in a second step. C) The seeds are suspended in a fresh citric buffer and this solution is incubated with an octanol phase saturated with hematin. After 2-4 days the crystals grew to an estimated size of 35-50 μm and migrate to the organic phase. D) SEM images of material collected from the preparation of HA seeds after 30 min of growth. The upward arrow indicates the presumably crystalline phase while the downward arrow is indicative of amorphous phases. E) AFM images of microcrystals isolated after 1.5 h of reaction, showing several faceted microcrystals of around 600 nm in length and not much amorphous material. F) AFM image of HA crystals of 3-5 μm in length obtained after 1.5 h of the second-step process involving saturated hematin. G) AFM image of a 28 μm HA crystal grown in the hematin-saturated octanol-citric acid buffer after 16 days. (Printed from ref. [68] with permission from American Chemical Society).

This study provided a methodology to produce large crystals of HA, which are advantageous to study its process of formation and relevant properties of Hz, such as antimalarial drug action, single-crystal X-ray diffraction, among others [37]. In addition, this investigation showed that the crystals grow at the lipidic phase, represented herein by the octanol layer. Also, based on surface imaging of the crystals throughout its formation, it was observed that the conversion of hematin into HA starts from mostly amorphous aggregates that mature into more crystalline and elongated materials over time [68]. However, no clear evidence of this mechanism was provided in this investigation since the crystals obtained in the first step were found in the aqueous phase.

Moreover, the methodology developed to produce HA in this investigation is not fully biomimetic since it involved extended periods of incubation at 23°C, (non-physiological temperature). This is not representative of the *in vivo* process within *Plasmodium*'s DV since the parasite produces Hz crystals very efficiently (15-30 h at the ring trophozoite stage [69]). Finally, the products obtained from these experiments were not evaluated to ensure the characteristic crystallinity of HA and Hz [7]. This characterization is critical to unambiguously identify Hz from heme aggregates, as reported in a previous study [70].

3.7. Antimalarial drugs that interfere with hemozoin formation

Many factors hamper the finding of a definitive cure for malaria, such as decrease of financial support, poverty, and highly dense population in malaria-endemic areas. However, the development of resistance to all current antimalarials and the lack of new drugs doomed initial efforts to eradicate the disease [1, 71]. This section describes the mechanism of action of some antimalarials that exert their antiplasmodial action by interfering with Hz formation.

3.7.1. Quinoline-based antimalarial drugs

Quinine is a natural compound present in the bark of the *cinchona* tree. Quinidine and its derived alkaloids were proven to have efficacy against malaria and were used for many years as a cure for malaria infections [72]. However, the administration of the drug was commonly accompanied by adverse side effects [72, 73]. Many drugs structurally related to quinine were developed as an alternative, defining the family of the quinolines [1]. The structure of quinoline-based antimalarials has a common heterocyclic aromatic quinoline group, with variations in the

side chain (**Figure 3.7.1**) [74]. Due to their low toxicity, low-cost production and clinical efficacy, this class of antimalarial drugs were the most important in the treatment and eradication of the disease for many decades [72]. The most important quinolines are quinine, piperazine, primaquine, mefloquine [74] and chloroquine (CQ) (**Figure 3.7.1.B**), the latter being the most widely used compound of this family.

After CQ penetrates the DV membrane, the molecule is protonated due to the acidic environment of the organelle, where it accumulates to millimolar concentrations causing the disruption of parasitic membrane function [75], inhibition of glutathione [76], peroxidation of lipids, proteins and DNA [77], inhibition of proteolytic enzymes and release of calcium necessary for the endolysosomal regulation system of *Plasmodium* [75, 78, 79].

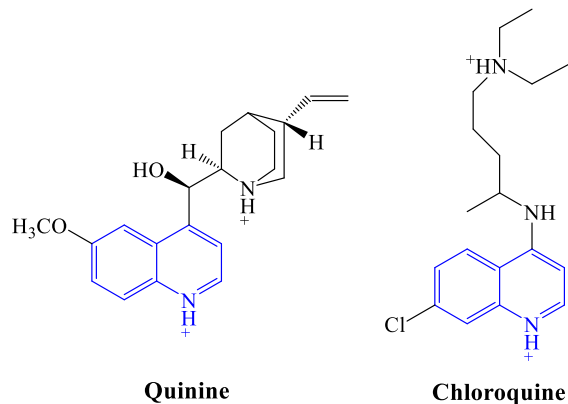


Figure 3.7.1. Chemical structure of quinine and its related antimalarial chloroquine, showing their protonation sites. The quinoline group is marked in blue in both molecules.

CQ exerts its antiplasmodial activity by inhibiting Hz formation in two hypothesized ways: either by forming complexes with hemozoin or by blocking hemozoin surface sites crucial for growth [75, 78].

In the first hypothesis, the drug binds to hemozoin through π - π interactions to form a hemozoin-chloroquine complex [80, 81]. It is proposed that the basic aminoalkyl side chains of CQ enhance

drug accumulation due to the acidic pH of the DV i.e. ion trapping [82], while the aromatic structure of the 4-aminoquinolines serves as a template to complex with hematin, and the 7-Cl group inhibits further growth of Hz [28, 78]. This process is influenced by electrostatic and hydrophobic interactions between CQ and the hematin molecule [75, 83] that stabilizes a derivative form of hematin known as μ -oxo-dimer [84]. The exact structure of the CQ-hematin complex is not known; however, one of the models proposes that the μ -oxo-dimer consists of two hematin molecules linked by an oxygen bridge between the two iron atoms of each molecule [28] (**Figure 3.7.2**). The hematin μ -oxo-dimer inhibits further aggregation of hematin into Hz, resulting in its accumulation in the DV and parasite's death [76, 81, 83]. More details on the structure and mechanism of complexation between CQ and hematin in solution are reviewed in the literature [85, 86].

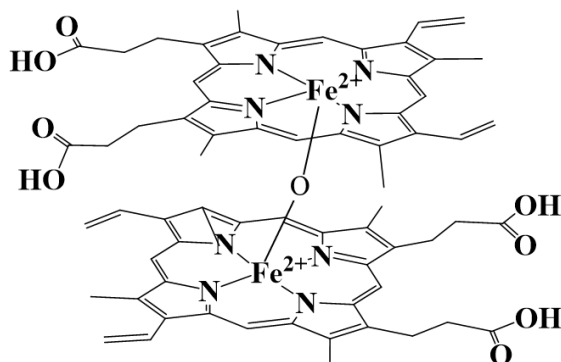


Figure 3.7.2. Structure proposed for the μ -oxo-dimer, a complex stabilized by the interaction between CQ and hematin.

The second hypothesis on the mechanism of action of CQ involves the adsorption of the drug on Hz surface [1]. Recently, Olafson and colleagues studied the surface of HA produced during HA formation in the presence of some common quinolines; the surface of these crystals was analyzed using time-resolved AFM [10]. They showed that quinine, chloroquine, and pyronaridine decreased the velocity of surface step formation on HA; this, in turn, decreased rapidly the

nucleation of new layers [10]. However, while amodiaquine and mefloquine gradually decreased the rate of step formation by about a half, only amodiaquine inhibited the nucleation of new layers. This mechanism is characteristic of inhibitor molecules that adsorb on kinks at the surface steps to further block the incorporation of new hematin molecules into the crystal structure [10]. Additionally, quinolines seem to chemisorb preferentially onto molecularly flat {100} faces to block crystal propagation, reinforcing the hypothesis that inhibition of Hz formation is the mode of action of this class antimalarials [1]. This mechanism has also been proposed by various groups [36, 81]; however, a definitive mechanism of CQ is still the subject of debate.

For almost 30 years, CQ was prescribed as first-line antimalarial therapy in endemic areas due to its effectiveness, low price, and low toxicity. CQ resistance was first reported in 1978 in East Africa and South America possibly due to the extensive overuse of the drug [87]. In resistant strains of *Plasmodium*, CQ is released from the DV at least 40 to 50 times faster than from sensitive strains, resulting in its accumulation at concentrations below those required to inhibit Hz formation [88-90]. Due to the important implications and impact on public health, alternative drugs were introduced to overcome these issues [1].

3.7.2. Artemisinin and its derivatives as antimalarials

Artemisinin (also known as qinghaosu) and its derivatives emerged by the 1980s after the first CQ-resistant strains of *P. falciparum* started to spread. The antiparasmodial activity of artemisinin was discovered in China in the 1970s by the research group led by Professor Tu Youyou [91], work for which she was awarded a Nobel prize in Physiology or Medicine in 2015. Youyou and colleagues analyzed 640 recipes to treat fever in traditional Chinese medicine; among them, the leaves of the wormwood *Artemisia annua* showed potent activity against CQ resistant and sensitive strains of

the malaria parasite [91]. After the success of the first clinical trials of *A. annua* extracts, in 1972 artemisinin was finally isolated and identified as the active compound in the plant.

Artemisinin is a sesquiterpene lactone that bears an endoperoxide bridge in its seven-membered ring structure and, unlike other antimalarials, lacks a nitrogen-containing heterocyclic ring, as shown in **Figure 3.7.3** [1, 92]. This compound is poorly soluble in water or oil; thus, new derivatives were developed to overcome these issues [1]. The most important semi-synthetic derivatives are artemether, dihydroartemisinin and artesunate (**Figure 3.7.3**) [93, 94], which show more oral bioavailability than artemisinin [93], resulting in a more efficient and faster antiparasmodial action, absorbance and elimination from the host bloodstream [1]. However, due to their poor pharmacokinetic properties and short half-lives, they are typically used in combination with longer-lasting antimalarials of other classes (for instance, in ACTs) [1, 93, 94]. Since 2006, ACT is the preferred first-line treatment for uncomplicated malaria [93] [95].

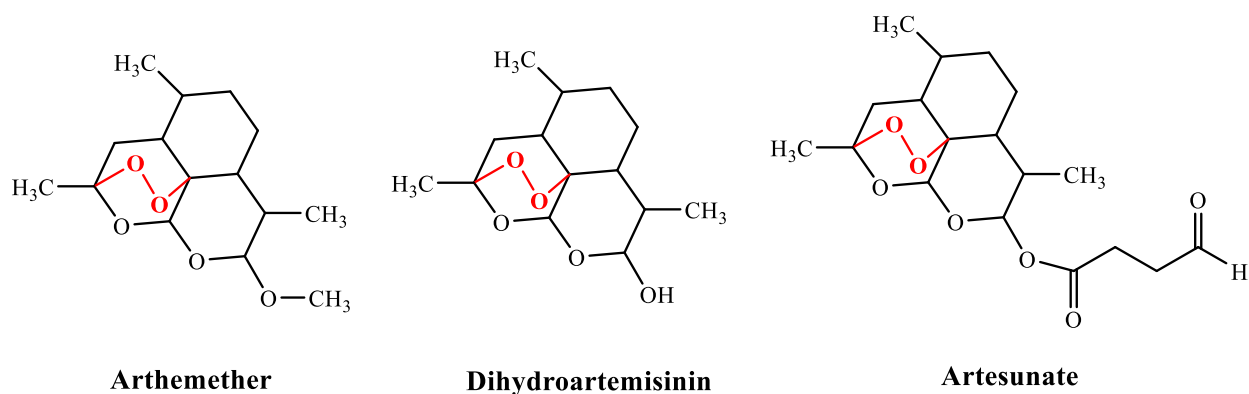


Figure 3.7.3. Structure of the most important artemisinins; the endoperoxide bridge is colored in red.

Although the mode of action of artemisinins remains unresolved, it is known that to be active against malaria, the peroxide bridge within the 1,2,4-trioxane system (marked in red in **Figure 3.7.3**) needs to be opened, either by intraparasitic heme or exogenous Fe^{2+} [96]. Initially, it was

hypothesized that the activation of the molecule resulted in the formation of reactive oxidative species (ROS) or secondary carbon-centered radicals within the parasite [96]. These radicals were thought to act as alkylating agents to form covalent adducts with parasite proteins, e.g. hemoproteins [97, 98]. However, this hypothesis is still debated as the alkylated proteins remain unidentified and undetected despite extensive studies [99].

Artemisinins are structurally similar to thapsigargin, another sesquiterpene lactone that inhibits with high affinity the sarcoendoplasmic reticulum Ca^{2+} ATPase enzyme (SERCA) [97]. Due to this similarity, it was hypothesized that artemisinins might target the *Plasmodium falciparum* ATPase-6 (PfATP6), the ortholog of SERCA in *Plasmodium falciparum* [100]. *In vitro* assays showed that once activated, artemisinins inhibit PfATP6 outside the food vacuole, with similar potency to thapsigargin [100]. This hypothesis is supported by many investigations; however, several studies showed no evidence of the antagonism between thapsigargin and artemisinins when their effect was evaluated on parasite growth, suggesting that the endoperoxides may exert their antimalarial activity by a different mechanism from that of thapsigargin [101]. Finally, and most importantly, it was found recently that the resistance of artemisinins is not related with mutations in the calcium ATPase [102], suggesting that the mechanism of these type of antimalarials should be further reevaluated [101].

In vitro assays that aim to monitor the inhibitory activity of artemisinins during HA crystallization are challenging since these assays typically use hemin or hematin as starting molecule, whereas artemisinins require freshly released heme to activate the endoperoxide bridge [10]. Several studies hypothesize that the selective toxicity of artemisinins may be due to the formation of adducts after the activation with heme, as depicted in **Figure 3.7.4**. This reaction is mediated by free radical intermediates, followed by the formation of covalent adducts with heme

or parasite proteins. In fact, Robert and Meunier [103] characterized an artemisinin-porphyrin adduct produced by the alkylation of a porphyrin after the activation of artemisinin, supporting the hypothesis that these drugs may exert their antiparasmodial activity by disrupting Hz formation [104]. Therefore, in this mechanism heme is both the activator and the target of artemisinins [104]. This hypothesis is also reinforced by the fact that artemisinins are highly effective in the intraerythrocytic stages of *Plasmodium* when Hz is produced. Conversely, these endoperoxides are ineffective against related intraerythrocytic Apicomplexa parasites that do not produce Hz, such as *Babesia microti* [104].

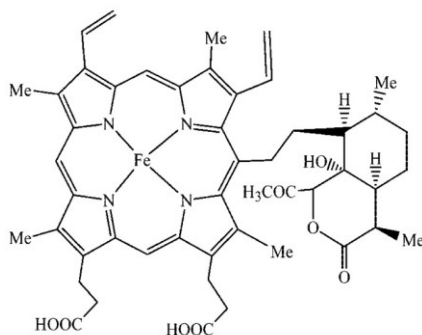


Figure 3.7.4. Heme-artemisinin adduct resulting from the alkylation of heme. (Printed from ref. [105] with permission of American Society for Microbiology).

ACTs have been introduced in most of all endemic areas as first-line antimalarial treatment, due to their excellent antimalarial properties and relative safety [95, 106]. However, there are several concerns on the efficacy of such treatments, most of all on the Thai-Cambodian border where there is evidence that partial artemisinin-resistant strains of *P. falciparum* started to appear in 2004 [107-109]. Consequently, there is an urgent need to develop new and potent antimalarial drugs as well as to search for new targets [110].

3.8. Relevance of Hz as tool in diagnosis and as immune modulator during malaria infection

Research activity involving Hz has increased considerably, not only to understand its physicochemical properties and biomineralization process but also as a potential target for malaria detection and as immune modulator during the infection [8]. In this section, we review both aspects of Hz investigations.

3.8.1. Hz as a tool for detection in malaria diagnosis

Successful diagnosis and treatment for malaria critically depend on timely and accurate detection of the infection [110]; the most commonly used methods to diagnose malaria are either optical microscopy or rapid diagnostic tests (RDTs). Light microscopy involves the staining of blood films with Giemsa stain; this type of diagnosis allows the identification of the *Plasmodium* species, the stage of their life cycle, and the quantification of parasitemia [111]. This test provides a reliable diagnosis (95% of accuracy with an average limit of detection of 88 parasites/ μ L of blood [112]); however, in malaria-endemic areas, the examination is challenging due to the need of trained technicians and the use of non-affordable microscopes and Giemsa tests [1]. To overcome these limitations, the use of malaria RDTs has increased significantly around the world.

A malaria RDT is a device that detects specific antigens produced by malaria parasites in blood cells [12]. The results are obtained quickly, the device is relatively inexpensive and is used by the individual without the assistance of a technician. However, RDTs differentiate only between a few human *Plasmodium* species, but not all of them [12], and the limit of detection is considerably higher than that of microscopy (over 100 parasites/ μ L of blood [113]). Also,

environmental conditions affect the device performance and it does not provide parasitemia quantification [114].

The limitations of current malaria diagnosis methods have prompted researchers to develop new cost-effective tools combining the advantages of microscopy and RDTs [114]. Recently, the paramagnetic and optical properties of Hz have been studied to develop new techniques for *in vivo* diagnosis of malaria based on the detection of Hz crystals in blood or tissues after their release from infected RBC [113]. A paramagnetic material has a magnetic moment only in the presence of an applied external magnetic field [115]. Although the magnetic susceptibility of Hz is weak compared to other ferromagnetic materials [11], this feature is used to separate infected RBCs from healthy ones [115], to purify the crystals after their isolation from cells [116] and to produce malaria diagnostic methods [117].

Additionally, in Hz and HA, the elongated shape of the crystals and the Fe^{3+} high spin ions of heme provide the crystals with magnetic anisotropy, causing the crystals to align in the presence of a magnetic field [115]. Hz also exhibits optical dichroism, a phenomenon occurring when a material is able to split a beam of light into two beams with different wavelengths [11, 115]. When suspended in a fluid, Hz crystals are randomly oriented without preferred direction of optical absorption. In the presence of a magnetic field, the paramagnetic crystals of Hz align in the direction of the magnetic field and the intensity and polarization of light lie along a preferred axis [118]. Hence, Hz turns into a dichroic polarizer i.e. an optical filter that converts a beam of mixed polarization into a beam of specific polarization [113]. Based on this magneto-optical phenomenon, which is directly proportional to the concentration of the crystal in a suspension, Mens' group was able to detect Hz from 13 patients with the accuracy of a RTD device, and calculated levels of parasitemia under 0.01 $\mu\text{g/mL}$ in Hz samples kept in PBS [113].

A popular method based on Hz detection in blood samples is laser desorption mass spectroscopy. In this technique, neutrals or ions are released from a condensed phase (usually solid) into the gas phase by the irradiation with an ultraviolet laser [119]. Then, the mass-to-charge ratio of the desorbed ions or neutrals is measured by a time of flight spectrometer to obtain their molecular masses [119]. Using this approach, Hz was detected in 0.3 μL of blood samples with levels of parasitemia below 0.1% in a mouse model, equivalent to around 10 parasites/ μL of blood [120]. Another method of detection was developed based on Raman spectroscopy [121-123], which enabled the detection of Hz in parasitemia levels as low as 0.05 – 0.2% [121]. Both techniques provide the diagnosis faster than using microscopy; however, they still rely upon acquiring blood samples and using sophisticated instrumentation [122, 124]. Other methods based on Hz as biomarker involve flow cytometry and polarization microscopy; however, they present similar disadvantages [117].

Recently, Lapotko and colleagues produced a non-invasive transdermal method to detect malaria based on acoustic signals generated by vapor nanobubbles produced by Hz in response to a short laser pulse [124] as illustrated in **Figure 3.8.1**. The lowest level of parasitemia measured was 0.00034% in mice models. The diagnosis can be obtained in seconds, the procedure does not require blood samples, is safe and does not require specialized personnel [124].

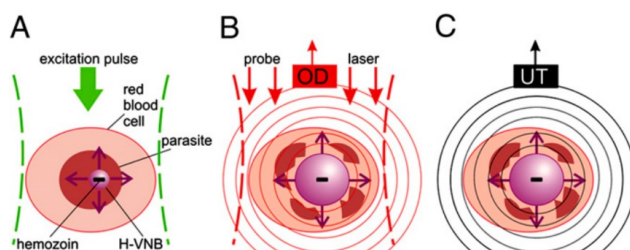


Figure 3.8.1. A) Vapor nanobubbles induced by short-laser pulses directed at Hz (H-VNB) inside infected RBCs. B) Optical detection (OD) scattering signals emitted by the vapor nanobubble and C) detection of pressure pulses of the vapor nanobubble via ultrasound transducer (UT) (Printed from ref. [124] with permission from Proceedings of the National Academy of Sciences of the United States of America).

Hz crystals also exhibit birefringence, which is the capacity of splitting a light wave into two beams that are refracted or transmitted unequally by an anisotropic medium [11]. This optical property together with Hz's absorbance can be used as biomarkers to detect malaria *in vivo*. Burnet *et al.* developed a “microvascular microscope” equipped with cross-polarized reflectance and transmission illumination. They detected Hz's birefringence and the absorbance of crystals circulating in the superficial vasculature of a biomimetic replicate of the oral mucosa of humans **Figure 3.8.2.A** [125]. In this study, the signal of Hz's birefringence was decreased by the random orientation within the tissue surrounding the crystals due to its phagocytosis by blood cells, e.g. macrophages and monocytes (**Figure 3.8.2.C**) [125]. However, Hz absorbance was still detectable under the same conditions **Figure 3.8.2.B**; therefore, only the absorbance was measured in the *in vivo* models with mice. The detection of Hz absorbance was achieved under 1 minute in mice with levels of parasitemia ranging from 0.03 to 50% [125].

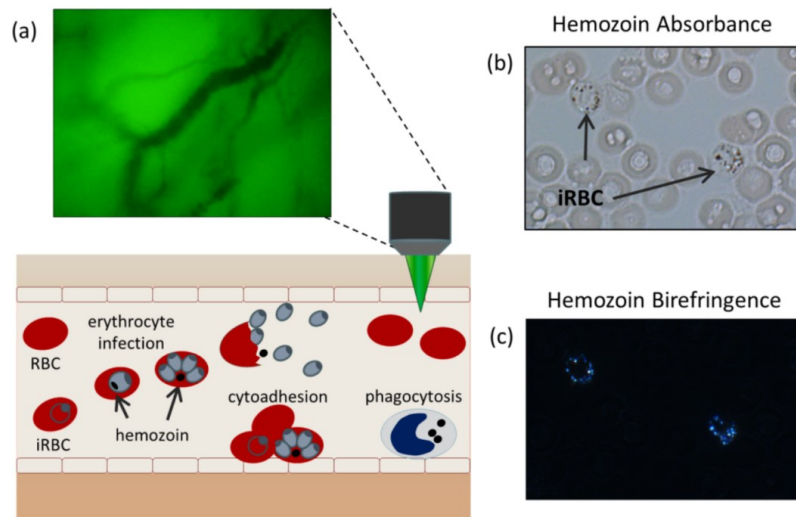


Figure 3.8.2. (a) Schematic illustration of the diagnostic concept of malaria-infected cells carried out through a microvasculature microscope. The crystals are typically circulating free in the bloodstream, or within the parasite's organelles, RBC membranes or phagocytized by blood cells. (b) Unstained blood smears showing Hz crystals within infected RBCs, the crystals are visualized under bright field and (c) cross-polarized illumination. (Printed from ref. [125] with permission from Journal of Biomedical Optics Express).

Overall, researchers have developed several rapid and highly sensitive platforms to diagnose malaria based on the detection of Hz. However, there are various limitations associated with the use of Hz as a biomarker for malaria diagnosis. After Hz is released from the RBC, the crystals remain circulating in the bloodstream for several months, even after clearance of the infection [126]. In addition, *Plasmodium* is not the only parasite capable of producing Hz; the crystals are also produced in humans by other parasites, such as *Schistosoma*, as mentioned before [77], which can result in false positives. Finally, while the concentration of the crystals can be correlated with levels of parasitemia [113], the quantification of malaria parasites based on Hz occurrence may lead to inaccurate results when malaria is a co-infection of another Hz producing parasite, such as in schistosomiasis [127].

Future experiments are necessary to translate the recent findings into commercial tools for malaria diagnosis, with special attention to identify early stages of the disease among diverse species of *Plasmodium* [124].

3.8.2. Hemozoin as immune modulator

Increasing evidence associates Hz in the pathogenesis of malaria [128]. Many biological effects have been studied by cultivating Hz or HA with murine or human-derived phagocytic cells, or by intraperitoneal injection of the crystals into mice [8, 129]. When the investigations are performed using HA, the crystals are commonly obtained from any of the preparations reviewed in **Chapter 3.3**. Meanwhile, the studies carried out using Hz involve lysing cells (RBC and parasites) to obtain natural crystals. In these processes, Hz comes in contact with many biological components, such as RBCs and parasitic membranes, proteins, lipids and even nucleic acids [8].

There is no standard procedure to purify Hz to remove the biological contaminants adsorbed on the surface prior to doing further experiments [14]; in fact, the immunological studies involving Hz are carried out using two types of crystals: either “purified Hz” or “native/crude Hz”. The first term refers to Hz extensively washed with detergents, enzymes, organic solvents or a mixture of them, in an attempt to reduce the biological contaminants as much as possible [8, 13]. The term “native Hz” or “crude Hz” refers to crystals used right after cell lysis, or just after a few rinses with a buffer or an organic solvent. The surface of these crystals presents unidentified biological contaminants remaining onto their surface, which in turn modulate the biological activity of Hz [8, 13]. For example, one study using native Hz cultivated with monocytes showed that the crystals inhibited the maturation of dendritic cells (DC), which in turn reduced their capacity to stimulate T cells [130], while another study showed that purified Hz enhanced DC maturation [129].

Basilico *et al.* showed that native Hz stimulates the inflammatory response of endothelial cells by stimulating the production of CXL8 and CCL5 inflammatory chemokines (chemokine C-X-C motif ligand 8 and chemokine C-C motif ligand 5, respectively) [131]. These chemokines contribute to the recruitment of neutrophils and leukocytes into inflammatory sites, which are associated with tissue inflammation and severe malaria [131]. In this work, it was also shown that crude Hz triggers the inflammatory response to a higher degree than HA, probably by the action of biological components adhered to Hz, such as parasitic DNA or host fibrinogen [131]. Hz is also known to produce an inflammatory response in lungs [132] and liver [133]. More information related to the inflammatory response of Hz is extensively reviewed in [15, 128, 134, 135].

Hz also accumulates in bone marrow, where osteoclasts and bone marrow-derived macrophages engulf Hz and other parasitic components such as nucleic acids and proteins that are thought to remain biologically active [136]. As result, these cells secrete proinflammatory and

osteoclastogenic cytokines, which in turn produces bone resorption (osteoclastogenesis) and growth retardation [137].

Furthermore, when Hz is released into the bloodstream after schizont rupture, the crystals interact with many cells, such as endothelial and blood cells (**Figure 3.8.3**), which in turn ingest the crystals, where they can stay for up to 72 h and disrupt cell function [131] [126]. It is thought that after the phagocyte expels Hz, the crystals are re-ingested by a new phagocytic cell, and this cycle is repeated several times due to the inability of the host to eliminate Hz [8]. In fact, in a study carried out with *P. berghei*-infected mice, it was shown that Hz or Hz-laden macrophages travel to different organs and tissues, such as spleen, liver and bone marrow, where they accumulate for prolonged times, even after successful treatment with antimalarials [126, 138]. As the crystals accumulate in organs and tissues, they form agglomerates that vary in size, depending on the site of accumulation [126]. For example, Hz from the liver and spleen formed larger aggregates over time; while Hz agglomerates in bone marrow were significantly smaller [126]. These variations in morphology and size could give rise to different immune responses associated with Hz, as demonstrated in *in vitro* experiments using different samples of HA with varied morphology and size [14].

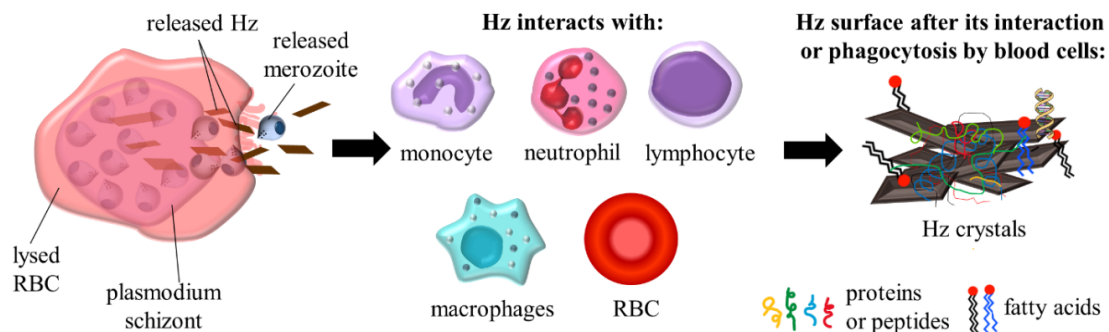


Figure 3.8.3. Schematic illustration of the interaction of Hz with blood cells after its release from a lysed schizont. The surface of Hz is prone to adsorb various components from the cells such as proteins or peptides, fatty acids, carbohydrates, and DNA.

Overall, these studies show that Hz and HA can act as an inhibitor or activator of the host immune response. However, these investigations are challenging and often contradictory due to several issues [13]. First, the most common methods to synthesize HA produce materials with different morphology, size and even surface defects [14, 38]. Thus, experiments using different preparations of HA show contradicting results. Additionally, the synthetic crystals may not mimic the inflammatory response observed in experiments carried out using natural crystallites of Hz [14]. Several biological molecules adhere to the crystals of natural Hz, and these can also have an immunogenic role (**Figure 3.8.3**); but since the nature of such adhered molecules is usually not analyzed before immunomodulatory tests, it is difficult to discriminate between the role of Hz crystals and that of the contaminating residuals [129].

Finally, studies on the impairment of the innate immune functions caused by Hz do not provide information about how the composition of what is adhered onto Hz surface vary over time, after several cycles of phagocytosis [8], and may differ according to the source used to generate the crystals, i.e. *in vivo* or *in vitro*. Analyzing the chemical, structural and temporal variations of the surface of Hz could significantly advance our understanding of the role of Hz in the host immune response [13].

Chapter 4. Surface characterization of hematin anhydride: a comparison between two different synthesis methods

As described in **Chapter 3.3**, HA is synthesized in the lab to study the crystallography and physicochemical aspects of Hz without having to address the issues related to the isolation and treatment of the natural material. Although the bulk properties of Hz and HA are mostly understood, their surface properties remain elusive. The absence of this knowledge hinders the full understanding of the role of HA or Hz as immune modulator, the mechanism of action of the current antimalarials, and the design of new ones, particularly those that exert their antiplasmodial activity by interfering with Hz formation.

In this study, we produced HA by two different methods of synthesis widely reported in the literature: the anhydrous and the acidic-annealing methods. We demonstrate that the surface properties of these materials differ significantly among methods and when compared to theoretical values. This study is essential to understand the impact of the protocol of synthesis on the surface chemistry of HA, which in turn affects its interaction with antimalarials and the biological environment.

In this chapter, we aim to address the following questions:

- i) How does the protocol of HA synthesis affect the surface properties of the crystals in terms of surface area, atomic environment, and elemental composition?
- ii) How do these results differ from the theoretical values and why?
- iii) Are carboxylate groups present on the surface of HA?

The findings of this study were published in the journal *Langmuir*, in 2016.

Guerra, E. D., Bohle, D. S., & Cerruti, M. (2016). Surface characterization of hematin anhydride: A comparison between two different synthesis methods. *Langmuir*, 32(18), 4479-4484.

4.1. Abstract

During the intraerythrocytic stage of malaria, the parasite digests hemoglobin and aggregates the released heme as an insoluble crystalline material called hemozoin. This detoxification step is an excellent drug target for developing new antimalarials, which can bind to hemozoin surface to inhibit further growth. Although the bulk crystalline properties of hemozoin are well known, the surface properties remain poorly defined. Here, we use a combination of spectroscopic and adsorption techniques to study the surface of synthetic hemozoin, hematin anhydride, produced by two different methods. We show that the two synthetic methods produce crystals with major differences, such as the amount of water adsorbed on the surface and surface carboxylate groups. These results imply that the methodology to produce hematin anhydride affects its surface reactivity; this information needs to be considered whenever hematin anhydride is used as a model to study host immune response or to design new antimalarials.

4.2. Introduction

In the last decade, fatalities attributed to malaria have dropped markedly due to the widespread deployment of bednets and improved therapies and diagnostics; however, the search for new antimalarial drugs continues as there are over 200 million new infections annually and resistance to all front line drugs has recently emerged.[139]

One of the most studied yet enigmatic antimalarial drug target is the heme detoxification pathway. During the infection, the parasite digests hemoglobin as a source of nutrients, followed by the detoxification of heme into an insoluble crystal called hemozoin.[140] Developing new inhibitors of this pathway remains an attractive target for the development of novel antimalarial drugs.[36, 141]

While the crystallography and bulk properties of hemozoin have been extensively studied,[7, 32] not much is known about its surface properties, such as functional groups exposed or the chemical environment of surface atoms. These details are important as they most likely modulate the immune response, crystal growth and reactivity to drugs.[8, 13] Nevertheless, contamination of organic residues in natural hemozoin and difficulty in isolating considerable amounts of the material severely hamper the possibility of performing surface studies on hemozoin.[8, 14]

As an alternative to hemozoin for in-vitro studies, synthetic crystals of hematin anhydride (HA, the chemical analogue to hemozoin) can be prepared. HA is often misleadingly termed β -hematin, and this nomenclature confuses the relationship between hematin and β -hematin, which corresponds to dehydration involving a carboxylic acid and thus an anhydride type of product. Although hematin anhydride and β -hematin often refer to the same synthetic material, the source and method of synthesis give these products distinctive properties.[9] Two methods have been suggested and are commonly used to prepare HA, namely the anhydrous[39] and the acidic-annealing method.[32] The two methods, though, produce materials with substantial differences in crystallinity and size.[39] Not only these differences represent a great challenge regarding data interpretation,[13, 41] they also impair our ability to model the biochemistry of this key drug target. A key question is thus which method produces the material that better mimics hemozoin?[8]

The answer to this question likely depends on the parameters that need to be mimicked. Since surface properties are so important when hemozoin is the target for antimalarial drug development, here we report the first analysis of the surface of HA synthesized by the aforementioned methods.

We characterized the surface of the samples with X-ray photoelectron spectroscopy (XPS) and N₂ adsorption at 77 K. Additionally, we used a derivatization technique in conjunction with XPS for the semi-quantitative detection of carboxylic groups on the surface.

We found differences in surface area, amount of water adsorbed, and the extent of surface carboxylation. This information may help to understand the role of surface species as intermediates of crystal growth and sites for interaction with proteins and biomolecules, facilitate pharmacokinetic data interpretation, and ultimately help to predict interactions between antimalarials and HA.

4.3. Experimental

4.3.1. Synthesis of hematin anhydride through the anhydrous non-coordinated-base (NB) method and aqueous acid-catalyzed (AC) method

The materials were prepared according to literature with minor modifications (SI 4.8.1 and 4.8.2) [32, 39]. As a final step, the materials were washed several times and dried overnight in a vacuum oven under P₂O₅ atmosphere.

4.3.2. Chemical derivatization of carboxyl groups with 2,2,2-Trifluoroethanol (TFE)

The chemical labeling was carried out following Giglio *et al.* methodology with some modifications[142] (SI 4.8.3). Briefly, after exposure to TFE vapors, the crystals were dried in vacuum for over three days before analysis with XPS. Both HA preparations and hemin chloride,

used as a control, were modified in the same conditions. See SI for details and schematic of the reaction (**Figure S.4.8.1**).

4.3.3. Characterization techniques

The specific surface area and porosity of the samples were obtained by measuring N₂ adsorption/desorption isotherms at 77 K and using the Brunauer-Emmett-Teller (BET) method to analyze surface area and the Barrett-Joyner-Halenda (BJH) method for pore size distribution.[143] All measurements were performed on a Micromeritics TriStar 3000 analyzer. The samples were degassed overnight at 150 °C prior to the analysis.

Surface composition of the samples was characterized by XPS on a Thermo Scientific K α spectrometer, using Al K α radiation (1486 eV) and an X-ray spot size of 200 μ m. To prevent surface charging, samples were hit with a flood gun shooting low energy electrons (around 14 eV) during the measurement.

Survey scans were taken with a pass energy of 200 eV and 1.0 eV resolution, while high-resolution scans were acquired with a pass energy of 50 eV and 0.1 eV resolution. The curve fitting analysis was performed using Avantage Software version 4.60 using Gaussian-Voigt curves functions and background removal through the Smart method.

The surface morphology of the materials was observed using an Inspect-50 field emission scanning electron microscope (SEM) (FEI, Japan), at 5 kV operating voltage. Images were acquired in low vacuum mode. ImageJ software was used to analyze the crystal size distribution.

X-Ray Diffraction (XRD) was used to confirm the characteristic crystalline structure of HA. (**SI Figure S.4.8.3**).

4.3.4. Statistical analysis

The data processing was performed on GraphPad Software, Inc. (2016). All data were expressed as mean \pm standard deviation (SD). Means that are significantly different are indicated with an asterisk (*). Unpaired t-test was performed to examine the statistic difference, where $P < 0.05$ was considered to be a significant difference.

4.4. Results and Discussion

As reported in previous works,[14, 39, 43] crystals prepared with the NB method (**Figure 4.4.10.A**) were larger than those prepared with the AC method (**Figure 4.4.10.B**) ($4.2 \pm 0.7 \mu\text{m}$ vs $0.6 \pm 0.3 \mu\text{m}$ average length, respectively, see **Table 4.1**). This is expected since the organic solvents in the NB method solubilize and coordinate hemin to slow down the crystallization kinetics producing larger crystals.[39] In contrast, the high temperature (70°C) at which the AC method reaction proceeds increases the crystallization kinetics generating smaller and less regular crystals.[41] This was further confirmed by XRD: while the NB material showed a fully crystalline nature, some amorphous or poorly crystalline phases were still present in the AC materials [41] (**SI Figure S.4.8.3**). This is also in accordance with previous results [14] and correlates well with the calculation of the domain sizes (**SI Table S.4.2**).

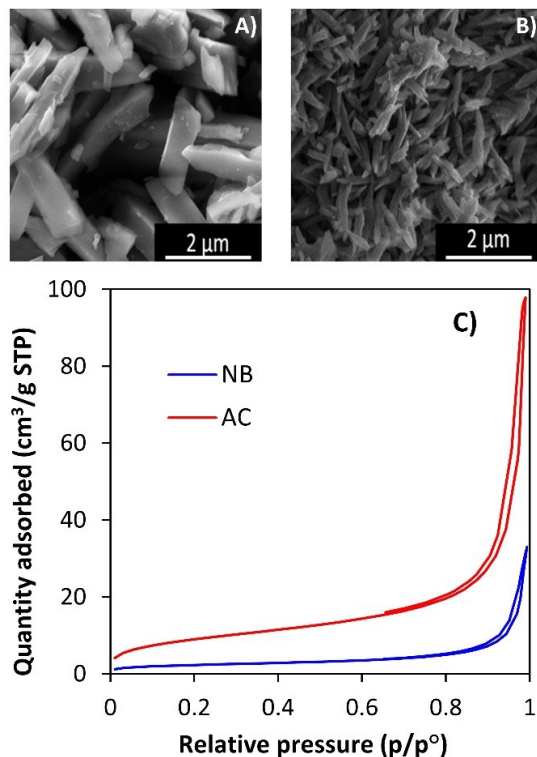


Figure 4.4.1. SEM images of HA obtained by the NB (A) and AC (B) methods showing different size and morphology of crystals. (C) N₂ adsorption-desorption isotherms measured at 77 K for NB (blue line) and AC (red line) crystals.

N₂ adsorption-desorption was used to determine the surface area and porosity of the HA materials (**Figure 4.4.1.C**). For both methods, the samples display a typical type II isotherm according to IUPAC classification,[143] which indicates that the materials are nonporous. The hysteresis loop starting at relative pressures of 0.9 indicates the presence of large macropores (diameter >50 nm). These are related to the empty spaces present between the small brick-shaped crystals of HA, as shown by the shape of the hysteresis loop (type H3), which suggests that the porosity is slit-shaped.[143]

We evaluated the specific surface areas (SSA) of both samples by analyzing the N₂ adsorption data with the BET model (**Table 4.1**). The SSA of HA synthesized by the NB method resulted in an experimental value of 25 ± 2 m²/g; whereas the SSA for the AC crystals was 34 ± 3 m²/g. The

significantly ($P=0.005$) higher SSA measured for the AC crystals was expected due to the smaller crystal size (**Figure 4.4.1**). Noteworthy, both methods produced HA with higher SSA than the expected theoretical surface area (TSA) calculations of $9.5 \text{ m}^2/\text{g}$ and $11.3 \text{ m}^2/\text{g}$ for NB and AC, respectively (**Table 4.1**). This discrepancy of SSA values may correspond to the heterogeneous crystal size distribution and possible fragmentation of the crystals upon heating during the degassing treatment.[144] (See **section 4.8.5** for calculation of TSA).

The BJH model was used to characterize the pore size distribution and pore volume of HA samples (**Table 4.1**). The pore volumes of both samples are very small ($0.02 \pm 0.01 \text{ cm}^3/\text{g}$ vs $0.08 \pm 0.05 \text{ cm}^3/\text{g}$, for NB and AC, respectively), and not significantly different ($P=0.2$). The pore diameters are large ($251 \pm 81 \text{ Å}$ vs $236 \pm 81 \text{ Å}$, NB and AC, respectively) and similar among samples ($P=0.8$), which is consistent with the macropores present between the particles.

Table 4.1. Experimental SSA, pore size distribution and pore volume estimated with BET and BJH models from N_2 adsorption-desorption measurements at 77 K for HA produced by the NB and AC methods. Each value represents the average of four measurements on different samples. Experimental SSA is compared with theoretical SSA evaluated based on crystal size. The crystal size is measured based on SEM image analysis (eight crystals analyzed per sample).

Method of synthesis	BET SSA (m^2/g)	Pore volume (cm^3/g)	Pore diameter (Å)	Theoretical SSA (m^2/g)	Crystal size (μm)
NB	25 ± 2	0.02 ± 0.01	251 ± 81	9.5	4.2 ± 0.7
AC	34 ± 3	0.08 ± 0.05	236 ± 81	11.3	0.6 ± 0.3

We used XPS to analyze the surface chemistry of HA. The survey scans for both samples of HA showed the presence of the expected elements C, N, O, and Fe. The absence of other elements confirms the purity of the synthesized materials. However, the atomic percentage differs among methods of synthesis. **Table 4.2** shows the experimental atomic percentage of the elements for both samples. The amount of C in the NB sample is very close to the theoretical value, while for

AC crystals is significantly less ($P=0.0009$). For both samples, the O content resulted lower ($P=0.004$) than expected. On the other hand, N and Fe content did not show a significant difference between the two methods.

We calculated the theoretical atomic percentages to compare them with the experimental values (**Table 4.2**). Both samples showed lower N content than the theoretical value, and somewhat lower amounts of C and Fe, especially in the samples prepared by the AC method. These smaller amounts are compensated by a larger O content than the theoretical value, especially for the AC method. Based on this data, and since the only element that is not detected by XPS is H, we propose that the difference between experimental and theoretical composition is to be related to the presence of water adsorbed on the crystals since HA is capable of reversible hydration.[144] The larger SSA of the AC-crystals would thus allow for larger amounts of water adsorbed and thus explain the higher percentage of O on this sample. The reversible hydration of HA crystals was previously studied by Bohle *et al.*:[144] however, this work used only bulk-sensitive techniques to analyze hydration, i.e. X-ray diffraction, infrared spectroscopy and thermal gravimetric analysis. Thus, this is the first demonstration of adsorption of water molecules on the surface of HA.

Table 4.2: Elemental composition evaluated by XPS, compared with theoretical values (See **SI 4.8.5** for details).

Element	NB	AC	Theoretical
C	$78.9 \pm 0.2^*$	$76.3 \pm 1.1^*$	79.1
O	$10.7 \pm 0.7^*$	$13.0 \pm 0.9^*$	9.3
N	8.4 ± 0.5	8.9 ± 0.9	9.3
Fe	2.0 ± 0.3	1.8 ± 0.3	2.3

* Significant at $P<0.005$; $n=6$.

We measured high-resolution C_{1s} , O_{1s} , N_{1s} , and Fe_{2p} spectra to analyze the atomic environment of surface atoms. (**Figure 4.4.2**). The spectra showed very similar components for both samples. The C_{1s} spectra (**Figure 4.4.2.A and B**) have a most intense component at 284.5 eV, assigned to single and double carbon bond (C-C, C=C), from the porphyrin ring.[145] The peaks at 286.5 and 288.4 eV are contributions from carboxylate groups (C-O and C=O, respectively),[146] which belong to the propionic chains that bind two different units of hematin.[47] These peaks may also include contributions from the pyrrolic carbon (C-N and C=N, respectively) of the porphyrin ring.[142, 147][148]

The O_{1s} spectra (**Figure 4.4.2.B and F**) showed two main peaks at 531.5 and 533.4 eV. The first peak has contributions from -OH groups [149] derived from water, either adsorbed on the surface or trapped within the crystalline structure.[144] This peak has also been assigned to the Fe-O-C(O) bond in the ester linkage[150] from the propionic chains that bind the hematin dimers. The second peak at 533.4 eV corresponds to C=O from carboxylates, which can be correlated with the peak at 288.4 eV in the C_{1s} spectra. The contribution from water in the peak at 531.5 eV explains why its area relative to the peak at 533.4 eV is higher than what would be expected from the theoretical amount of O atoms found in ester or carboxylate bonds. In fact, four oxygens of each type exist in the crystallographic structure of HA (**Figure S.4.8.1**); thus, one would expect the same area for the 531.5 and 533.4 eV components. Instead, the area of 533.4 eV peak is only 0.30 ± 0.01 the area of the 531.5 peak for the sample prepared by NB method, and even lower (0.22 ± 0.09) for the sample prepared by the AC method (**Table S.4.3**). These data show the important contribution of water on the 531.5 eV component of the O_{1s} spectrum. The somewhat higher relative intensity of the 531.5 eV peak compared to the 533.4 eV peak measured on the AC sample than on the NB sample is in agreement with our previous hypothesis, based on O%

measured by XPS survey (**Table 4.2**), that a larger amount of water is adsorbed on the AC sample. Still, the differences in relative peak areas are not statistically significant, probably due to the difficulty of separating the water and the Fe-O-C(O) contributions in the 531.5 eV peak.

The N_{1s} core level spectra of both samples (**Figure 4.4.2.C and G**) reveal two different N_{1s} signals. The peak at 398.2 eV corresponds to the four equivalent N atoms in the structure of the pyrrolic ring,[145] while the peak at around 401 eV can be attributed to the π - π^* transition related to the resonance of the delocalized electrons in the porphyrin structure.[151]

The Fe_{2p} spectra (**Figure 4.4.2.D and H**) show multiple peaks characteristic of the spin orbit splitting and satellite peaks of Fe.[152] For both samples, the doublets of the Fe_{2p_{3/2}} peak are found between 710.6 eV and 711.2 eV; while the Fe_{2p_{1/2}} peak is found at approximately 725 eV. The Fe_{2p_{3/2}} and Fe_{2p_{1/2}} satellite peaks for both methods are found around 717 eV and 730 eV, respectively. The positions of all the doublets and satellite peaks are in good correlation with the binding energy characteristic of Fe in oxidative state III.[152]

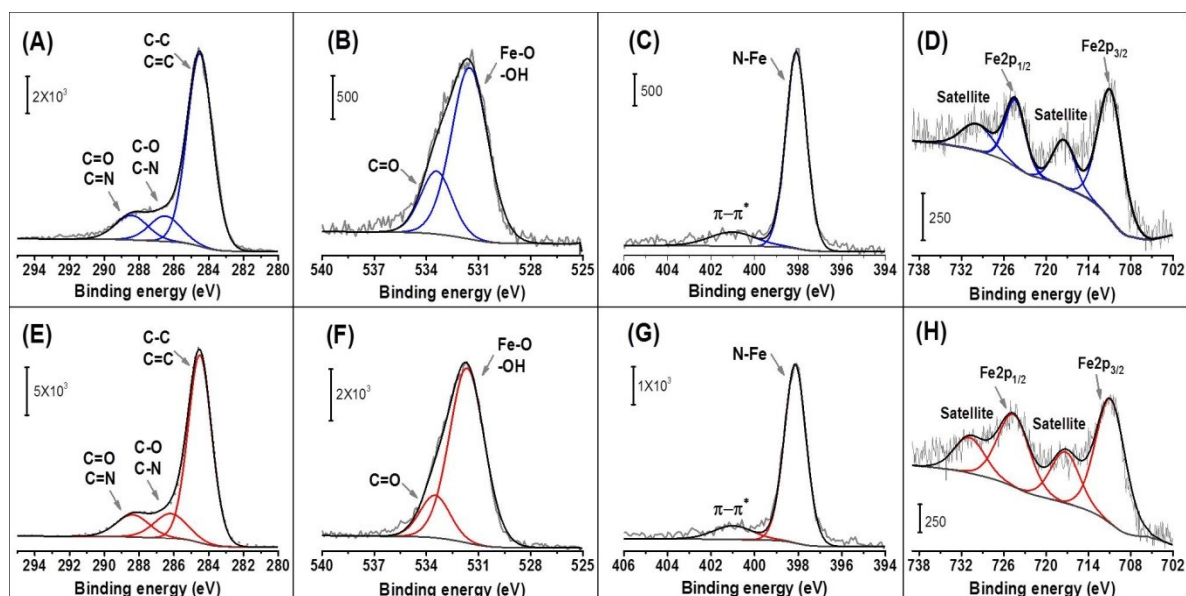


Figure 4.4.2: XPS high-resolution spectra of C_{1s} (A and E), O_{1s} (B and F), N_{1s} (C and G); and Fe_{2p} (D and H) core levels, collected for HA synthesized by NB (first row) and AC (second row) methods. Experimental data are shown in gray, peak fits in red or blue, and the overall fit in black.

In previous works, HA crystallites were indexed using transmission electron microscopy (TEM) electron diffraction. These studies indicate that the surface of HA may present propionic acid surface groups exposed at the {100} and {011} end faces;[47, 153] however, a supporting spectroscopic or chemical confirmation of this assignment is still missing. Showing the existence and quantifying such groups would be important since it was proposed that they may contribute to the high reactivity of the crystals and ultimately act as antimalarial binding sites to block hemozoin formation.[47]

To test this hypothesis, we functionalized HA with TFE. When carboxylates react with TFE in the presence of pyridine and di-*tert*-butyl-carbodiimide, the carbonyl of the acid group will be activated toward nucleophilic attack to incorporate the fluorine from CF₃CH₂OH onto the surface.[154],[155] (SI 4.8.3) We used hemin as a positive control due to its chemical resemblance to the HA heme unit.

After TFE functionalization, a fluorine signal (F_{1s}) appeared in the survey scans of NB and AC crystals, as well in hemin (**Figure S.4.8.1**), which confirmed the presence of carboxylate groups. **Table 4.3** shows the atomic percentages from XPS survey scans collected after TFE functionalization. More F was detected on the AC samples than on the NB crystals ($P=0.0001$), thus indicating a much larger amount of carboxylic groups on the AC sample. This result correlates well with the presence of more defects and larger surface area of the AC crystals.

Table 4.3: Atomic percentage measured with XPS survey scans of HA samples after TFE functionalization.

Element	NB	AC
	atomic %	atomic %
C	$76.4 \pm 1.6^*$	$74.6 \pm 1.0^*$
O	11.5 ± 0.8	11.8 ± 1.0
N	8.5 ± 0.6	8.3 ± 0.8
Fe	1.9 ± 0.3	1.9 ± 0.2
F	$1.7 \pm 0.8^*$	$3.4 \pm 0.4^*$

* Significant at $P < 0.0005$; $n=9$

Fluorination was further confirmed by high-resolution spectra: the C_{1s} spectra of TFE functionalized HAs exhibit an additional peak at 293 eV, corresponding to organic fluorine (CF_3) (**Figure 4.4.3.A and D**). Likewise, the O_{1s} spectra (**Figure 4.4.3.B and E**) exhibit a wider peak that once deconvoluted reveals a new component at 532.3 eV. This signal corresponds to the O in the $C-\underline{O}-CH_2-CF_3$ ester linkage.

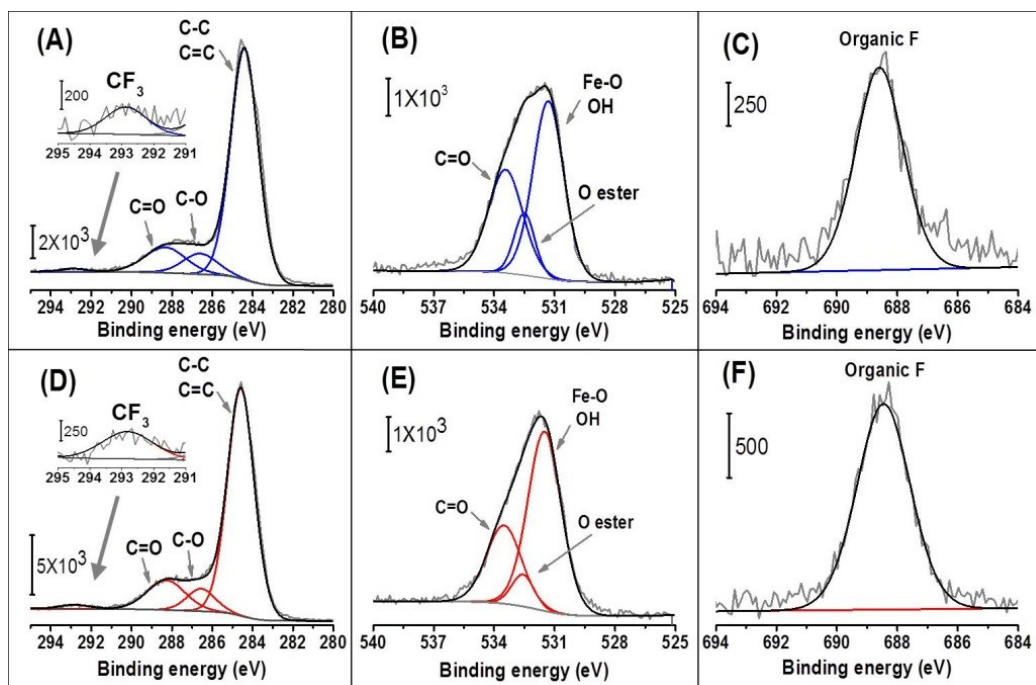


Figure 4.4.3: XPS high-resolution spectra of C_{1s} (A and D), O_{1s} (B and E) and F_{1s} (C and F) levels collected for HA synthesized with NB (first row) and AC (second row) method after TFE functionalization. Experimental data are shown in gray, peak fits in red or blue, and the overall fit in black.

Finally, a new peak appeared at 688.4 eV (**Figure 4.4.3.C and F**) which corresponds to the F_{1s} level of the organic fluorine ($-CF_3$).^[156] This shows the presence of CF_3 groups on the surface of the samples. Since any physisorbed TFE molecule is removed by the prolonged exposure to vacuum after functionalization and to ultrahigh vacuum for 30 minutes before XPS analysis, we can conclude that the CF_3 groups found on the sample surface are evidence of the covalent reaction between TFE and carboxylate groups from HA.^[142]

4.5. Outlook

This work shows that the method used to synthesize HA significantly affects the surface properties of the resulting materials, in terms of overall surface area, amounts of water adsorbed, and the presence of carboxylates. Such differences may very well impact the pro-inflammatory response

in macrophages and red blood cells and the production of reactive oxygen and nitrogen species.[13][8, 14] This is particularly important when HA is used as the synthetic analogues of hemozoin to test host response. In fact, such differences may explain challenges in data interpretation and the myriad contradictory results which have been reported.[13], [8, 14]

Additionally, the knowledge gained relative to the HA surface could contribute to the development of novel antimalarials, especially those whose mechanism of action is based on surface interactions with hemozoin, such as binding to the crystal surface or interrupting the nucleation process to prevent further growth.[36] The experimental confirmation of the presence of carboxylic groups on the surface of HA may also help understanding hemozoin nucleation and growth, since these groups may mediate the adhesion of lipids and proteins to hemozoin surfaces.[157]

It is surprising how little direct data concerning hemozoin's surface chemistry has been reported. To the best of our knowledge, this is the first to describe the surface characteristics of HA. An open challenge is to extend these studies to the natural *Plasmodium*-derived hemozoin;[67] some of the obstacles related to this are the poor amounts of hemozoin isolated from the parasites, variations in the characteristics of the crystals among *Plasmodium* genus, and organic contaminants present on the crystals after isolation.[8]

The characterization method applied for the first time to HA in this work could be used as a guideline to analyze surface properties of hemozoin; this is particularly true for XPS-based techniques, which require only small amounts of sample. This analysis will be crucial to understand hemozoin reactivity and to ultimately determine which synthetic method produces crystals that best resemble the properties of hemozoin.

4.6. Acknowledgments

E. D. Guerra thanks Consejo Nacional de Ciencia y Tecnología de México (CONACyT), Secretaría de Educación Pública de México (SEP) and the McGill Excellence Doctoral Award for their support. M. Cerruti and D. S. Bohle acknowledge the Canada Research Chair foundation and Natural Sciences and Engineering Research Council of Canada for funding.

4.7. Abbreviations

HA, hematin anhydride; NB, non-coordinated base method; AC, aqueous acid-catalyzed method; TFE, 2,2,2-trifluoroethanol; BET, Brunauer-Emmett-Teller; BJH, Barrett-Joyner-Halenda; XPS, X-ray photoelectron spectroscopy; SEM, scanning electron microscopy; XRD, X-Ray diffraction spectroscopy; SSA, specific surface area; TSA, theoretical surface area; TEM, transmission electron microscopy

4.8. Supporting information

4.8.1. Synthesis of hematin-anhydride through the anhydrous non-coordinated-base method (NB)

The material was prepared according to the literature without further modifications.[39] Briefly, in an inert atmosphere, hemin (0.8 mmol, 500 mg) was completely dissolved in 10 mL of 2,6-lutidine upon stirring. Then, 100 mL of a 50:50 mixture of anhydrous methanol: dimethyl sulfoxide were added. The flask was sealed and protected from light with aluminum foil for storage of a minimum of two weeks to several months. After opening the flask the precipitate was washed twice with methanol followed by centrifugation at 10,000 rpm for 1 hour, and the supernatant decanted. The crystals were washed twice with a solution of 0.1 M sodium bicarbonate for 3 hours

in an orbital shaker. The final washes consisted of distilled water 4 times and centrifugation. The samples were dried in vacuum in the presence of phosphorous pentoxide (P_2O_5) overnight.

4.8.2. Synthesis of hematin anhydride by the aqueous acid-catalyzed method (ACM)

The methodology was followed as reported [32] with none or minor modifications. Hematin (0.6 mmol, 380 mg) was dissolved in 80 mL of 0.1 M NaOH for 30 min under stirring. Precipitation was produced by the slow addition of propionic acid until a pH of about 4 was achieved. The suspension was allowed to anneal at 70°C for 18 hours, covered from light. After the allotted time, the flask was cooled down to room temperature. Then, the acidic suspension was decanted and washed twice with distilled water and centrifuged at 10,000 rpm for 30 min. Subsequently, the insoluble materials were removed twice by the addition of a 0.1 M sodium bicarbonate solution for 3 hours in an orbital shaker. Finally, the crystals were washed four times with distilled water and centrifugation. The samples were dried in a vacuum oven in the presence of P_2O_5 overnight.

4.8.3. Chemical derivatization of carboxylate groups with 2,2,2-Trifluoroethanol (TFE)

Chemical derivatization with TFE was coupled to XPS analysis to confirm the presence of COOH groups at the surface of HA. Prior to the experiment, all the glassware was washed with detergents in an ultrasonic bath, rinsed with deionized water and isopropanol followed by overnight drying. The samples of HA were placed separately in 10 mL beakers and they were placed in a glass container with hermetic seal. The reagents were introduced sequentially into the flask, outside the beakers at 15 minutes intervals in the following order and amounts: TFE (0.9 mL), pyridine (0.4 mL) and Di-*tert*-butyl-carbodiimide (0.3 mL). In this reaction, pyridine acts as a catalyst, whereas the carbodiimide is used as a drying agent.[156] The flask was sealed and the reaction proceeded at room temperature for 18 hours.[142, 155] After this time, the samples were dried under vacuum

for several hours at room temperature before XPS analysis. Hemin was used as positive control by exposing it to the same conditions.

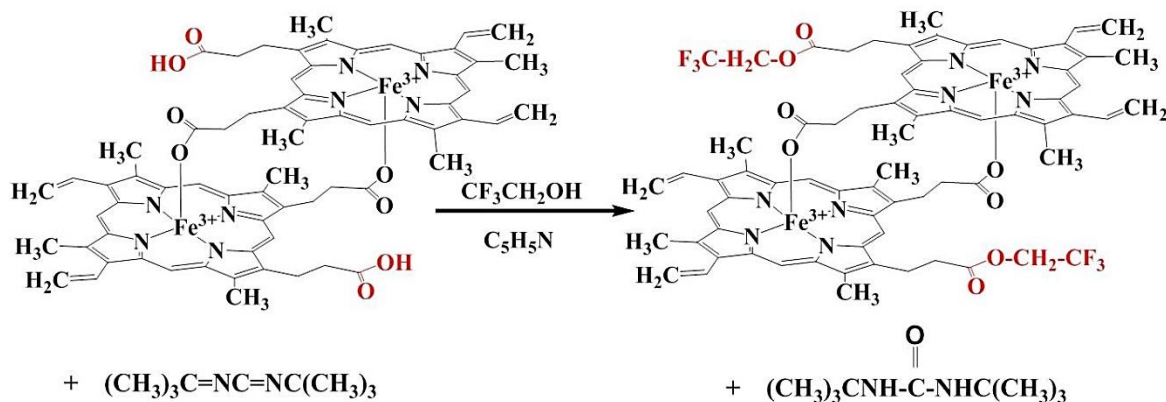


Figure S.4.8.1. Schematic of HA derivatization with TFE. The $-\text{COOH}$ groups susceptible to TFE labeling are marked with red.

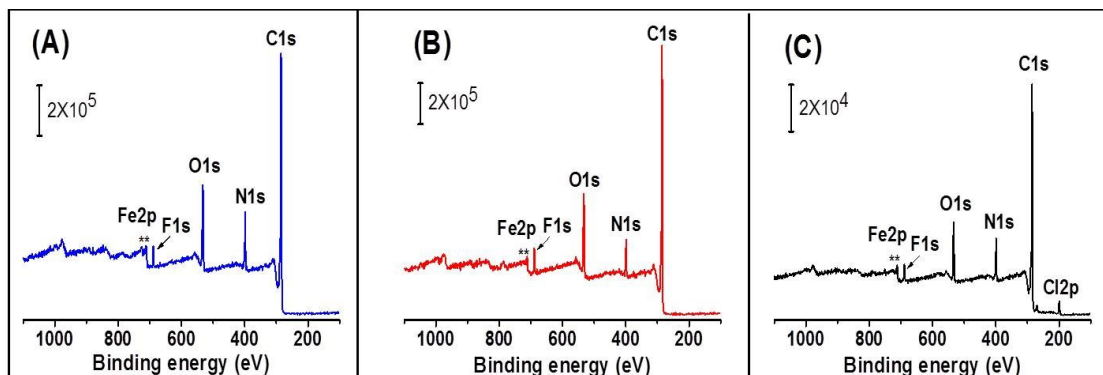


Figure S.4.8.2. XPS survey spectra of HA after TFE derivatization. (A) Samples of HA synthesized with NB method. (B) HA crystals obtained AC via and (C) Hemin chloride. All samples show an F1s signal at around 689 eV, confirming the incorporation of fluorine into the $-\text{COOH}$ termination groups of HA and Hemin.

Table S.4.1. Atomic percentage measured with XPS survey scans of HA samples after TFE functionalization.

Element	Hemin atomic %
C	74.5 ± 1.1
O	10.6 ± 0.7
N	8.1 ± 0.8
Fe	1.6 ± 0.2
F	3.3 ± 0.3
Cl	1.9 ± 0.3

4.8.4. Characterization with X-Ray Diffraction (XRD)

This technique was used to control the crystallinity of the synthesized HA samples. Powder diffraction data were obtained with a Siemens D5000 diffractometer using a Cu K α radiation source (K α_1 λ =1.54 Å), and a monochromator operated at 40 kV and 40 mA within the 5° to 27° range in 2 θ . All the samples were ground and transferred to a metallic holder.

Figure S.4.8.3 shows a very intense {100} reflection at 7.5° and also the characteristic peaks at 21° and 24° 2 θ for HA crystals obtained by the (i) AC and (ii) NB methods.[14],[34],[158] The spectrum of hemin is shown for comparison (iii). The quality of the crystals can be assessed by the shape and intensity of the diffraction peaks. The peaks corresponding to the AC-crystals are not as sharp as the ones obtained for the materials synthesized by the NB method.[34, 39] This is in good agreement with the SEM images.

We calculated the coherent domains sizes of two samples of HA for each method of synthesis. They were compared qualitatively using the Scherrer equation:

$$D = \frac{k\lambda}{\beta \cos \theta}$$

Where:

D=crystallite size

k=Scherrer constant

λ = X-ray wavelength

β =line broadening in radians

θ =Bragg angle

Overall, the domains sizes of HA synthesized by NB are larger, compared to the AC materials, as seen in **Table S.4.2**. This is in good correlation with the crystal sizes observed with SEM.

Table S.4.2. Experimental domain sizes of HA samples calculated from XRD data.

	2 θ (°)		FWHM (eV)		Domain size (nm)	
	NB	AC	NB	AC	NB	AC
Sample 1	7.4	7.5	0.4	0.6	26.52	17.68
	21.7	21.8	0.2	0.8	53.9	13.47
	24.2	24.5	0.4	0.6	27.07	18.05
Sample 2	7.4	7	0.5	0.6	21.22	17.68
	21.8	21.7	0.3	0.5	35.94	21.56
	24.3	24.2	0.3	0.7	36.1	15.46

4.8.5. Theoretical Specific Surface Area (SSA) calculation

The unit cell of hemozoin from trophozoites corresponds to a triclinic unit cell with approximate dimensions of 1 μm , 0.6 μm and 0.2 μm and a $\rho=1.45 \text{ g/cm}^3$. [7] For theoretical SSA calculations, we considered HA produced by either the NB or AC methods to be equivalent in width and

thickness but not in length, since SEM analysis average lengths of $4.2 \pm 0.7 \mu\text{m}$ and $0.6 \pm 0.3 \mu\text{m}$ for the two samples, respectively.

We approximated the geometry of the crystals to an orthorhombic system, instead of a triclinic unit cell. We started by calculating the total surface area of a crystallite with the mentioned dimensions in the following way:

$$\text{Eq. 1) } Total\ area = 2ab + 2ac + 2bc$$

Where:

a=Average crystal size obtained by SEM in μm

b= $0.6 \mu\text{m}$

c= $0.2 \mu\text{m}$

We then calculated the mass of the crystal using the value of density ($\rho=1.45 \text{ g cm}^{-3}$)

$$\text{Eq. 2) } V = a \times b \times c (\mu\text{m}^3)$$

$$\text{Eq. 3) } m = \rho \frac{\text{g}}{\mu\text{m}^3} \times V (\mu\text{m}^3)$$

Finally, the theoretical SSA was calculated according to:

$$\text{Eq. 4) } Theoretical\ SSA = \frac{\text{total area}}{\text{mass}}$$

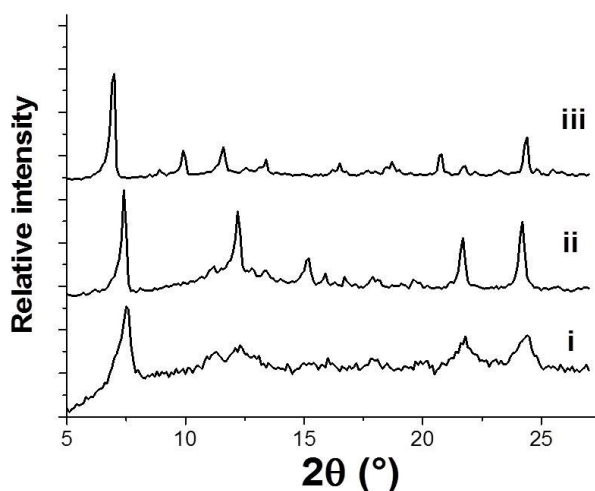


Figure S.4.8.3. XRD patterns showing the characteristic peaks of HA seen at 7°, 21° and 24° 2θ for HA ($C_{68}H_{60}Fe_2N_8O_8$) produced by the (i) AC and (ii) NB methods. The XRD spectrum of hemin ($C_{34}H_{32}ClFeN_4O_4$) is shown in (iii) for comparison.

4.8.6. Details relative to high-resolution XPS spectra collected after TFE functionalization of HA

Table S.4.3. XPS peak positions, and area ratios for the components fitted to the high-resolution C, O, N and Fe spectra measured for HA synthesized by NB and AC methods. Standard deviations are based on the measurements of at least three points on three different samples. The area ratios are standardized, for each element, to the most intense component. No statistically significant differences are found between any of the values reported for the NB and AC samples relative to either peak positions or area ratios.

Element	Binding energy (eV)		Assignment	Component area ratio	
	NB	AC		NB	AC
C _{1s}	284.5 ± 0.1	284.4 ± 0.1	C-C, C=C	1	1
	286.5 ± 0.1	286.4 ± 0.2	C-N or C-O	0.11 ± 0.04	0.15 ± 0.04
	288.4 ± 0.1	288.3 ± 0.2	C=N or C=O	0.15 ± 0.02	0.16 ± 0.01
O _{1s}	531.5 ± 0.0	531.6 ± 0.1	Fe-O and water	1	1
	533.3 ± 0.1	533.4 ± 0.1	C=O	0.30 ± 0.01	0.22 ± 0.09
N _{1s}	398.1 ± 0.1	398.2 ± 0.1	N-Fe	1	1.00 ± 0.00
	401.0 ± 0.0	401.0 ± 0.1	N _{π-π*}	0.15 ± 0.02	0.13 ± 0.02
Fe _{2p}	711.0 ± 0.1	710.8 ± 0.1	Fe2p _{3/2}	1	1
	724.4 ± 0.1	724.4 ± 0.3	Fe2p _{1/2}	0.60 ± 0.20	0.57 ± 0.05
	717.3 ± 0.3	717.2 ± 0.2	Satellite _{3/2}	0.34 ± 0.03	0.37 ± 0.04
	730.3 ± 1.1	730.9 ± 0.6	Satellite _{1/2}	0.26 ± 0.07	0.25 ± 0.04

Chapter 5. What is pure hemozoin? A close look at the surface of the malaria pigment

In the previous chapter, we showed the impact of the protocol of HA synthesis on its surface properties in terms of surface area and amount of water adsorbed and number of carboxylate groups as possible sites of interaction between HA or Hz and antimalarials or biomolecules. This knowledge helps us understand the mechanism of action of some antimalarials and the role of Hz as immune modulator. However, there is still no information related to the surface chemistry of Hz, which represents a challenge when the natural crystals are used to evaluate antimalarials activity or the immunomodulatory response in *in vitro* or *in vivo* models. Moreover, this information is crucial to clarify the conflicting results observed when comparing the activity of HA vs Hz.

In this chapter, we aim to study the surface properties of Hz extracted from parasites. Researchers use several protocols to treat crude extracts of Hz to remove the organic contaminants that adhere onto the crystals surface. However, it is not understood how these treatments affect Hz surface, both in terms of amount of contaminants and their composition.

In this chapter, our goal is to respond to the following questions:

- i) How does the cleaning protocol affect Hz surface? Which method is more effective to remove the organic contaminants?
- ii) Does the washing protocol introduce contamination to the crystal surface?
- iii) Is it possible to obtain pure Hz?
- iv) What are the main adsorption sites of biomolecules and antimalarials on Hz surface?

This manuscript has been published in the *Journal of Inorganic Biochemistry*.

Guerra, E. D., Baakdah, F., Georges, E., Bohle, D. S., & Cerruti, M. (2018). What is pure hemozoin? A close look at the surface of the malaria pigment. *Journal of Inorganic Biochemistry*, (194), 214-222

5.1. Abstract

The malaria parasite, *Plasmodium* spp., produces hemozoin (Hz) crystals as a by-product of hemoglobin digestion. Purification methods used to remove host or parasite products adsorbed on Hz surface lead to variable and undetermined residues. This compositional variation likely accounts for the assortment of contradictory results in studies of Hz's biomineralization, immunomodulating properties, and the mechanism of action of some antimalarials. In this work, we study the surface of Hz cleaned with two methods, both reported in the literature, one stricter than the other. We find that biomolecules are adsorbed on Hz treated with either method, they bind through carboxylate groups and may be present within Hz structure. Their composition and amount depend on the washing protocol, which also introduces contaminants. This finding led us to question the concept of "pure" Hz and to propose X-ray photoelectron spectroscopy (XPS) and matrix-assisted laser desorption/ionization time of flight (MALDI-TOF) as characterization tools to assess surface contamination prior to further work on Hz crystals.

Keywords: hemozoin, malaria pigment, surface composition, purification, contamination, characterization

Highlights:

- Organic contaminants remain adsorbed onto hemozoin even after purification.
- The purification protocol introduces contamination to hemozoin surface.
- The residual biomolecules could also be part of the crystalline structure of hemozoin.
- Surface carboxylate groups in hemozoin are the main adsorption sites for biomolecules.

5.2. Introduction

Malaria is a blood infection caused by parasites of the *Plasmodium* genus, causing an estimated 216 million infections annually and almost half a million deaths worldwide.[159] During the intraerythrocytic asexual stage of *Plasmodium*, the parasite feeds from hemoglobin to sustain its development,[8] with the released heme rapidly converted into an insoluble crystal called hemozoin (Hz) as a detoxification mechanism.[8] Hz, also known as “malaria pigment” due to its dark brown color, is a crystalline biomineral, consisting of dimers of heme linked reciprocally by iron-carboxylate bonds; the dimers are further arranged in chains linked by hydrogen bonds.[7] Lipids, proteins, the digestive vacuole membrane, and acidic pH are thought to play significant roles in Hz biomineralization; however, the overall process is still not entirely resolved.[8]

Hz formation is the target of several quinoline-derived antimalarials, and possibly artemisinins, which are thought to inhibit Hz growth either by forming drug-heme complexes or by adsorbing on Hz surface.[10] Given the widespread parasitic resistance to these antimalarials, a deeper understanding of their mechanism of action and of the mechanism of Hz biomineralization[41] are topics of utmost urgency.

Hz seems to be also involved in the immunopathology of malaria. Many studies have investigated this by adding Hz or its synthetic counterpart, hematin anhydride (HA), to phagocytic

cell cultures,[8] but the results are often contradictory and poorly reproducible.[13] For example, several groups reported that Hz and HA induce the production of pro-inflammatory cytokines and chemokines,[15, 134, 160] while others have reported that HA decreases the anti-inflammatory response.[161] Hz also contributes to malarial anemia by suppressing red blood cells (RBC) proliferation;[136, 162, 163] but HA has lower activity compared to Hz.[136]

Both using HA and Hz to perform these experiments has challenges: different preparations of HA result in crystals with varied morphology and size, which impact their surface reactivity;[164] and when Hz is isolated from schizonts, various biomolecules bind to Hz surface.[8] Such components may be lipids, parasitic DNA, fibrinogen, digestive vacuole membrane residues, RBC membranes[8] and fibrin during placental infection.[165] These compounds could be involved in the biological effects observed in Hz; thus, it is still not clear whether the immune activity of Hz is caused by the crystals themselves or by its surface contaminants.[8]

The lack of a standardized protocol to purify native Hz after its extraction contributes to the difficulties in studying Hz formation and properties.[8, 14] The methodologies reported aim to remove a variety of biomolecules that are thought to adhere to Hz during parasite incubation and lysis.[13] The procedures to purify Hz include washing the crude extract with a hypotonic solution of phosphate buffer saline (PBS);[166] separation of Hz from cell debris by ultrafiltration and/or magnetic-activated cell sorting (MACS) separators.[116] Other procedures involve extracting the proteins with organic solvents and water,[167] or digesting Hz organic coating by proteinase K, followed by washes with a detergent and urea.[129] More thorough treatments include a combination of organic solvents, extensive digestion by proteinase K, DNase I and RNase A, and final washes with detergents and water.[31] Clearly, the different methods used to purify Hz may produce crystals with different compositions, which would ultimately impact the host response

and produce the observed contradictory results.[15] Hence, to clarify these issues, the surface of Hz should be carefully studied after its extraction and purification.[13]

Surprisingly, not many studies focus on Hz surface. The few studies on this topic analyze crystal morphology and size,[7, 29, 67] or are carried out on HA.[10, 164] The elemental composition, atomic environment and main adsorption sites of Hz surface are still unknown. Moreover, none study how the purification method influences Hz surface.

In this report, we address this knowledge gap by analyzing the surface of Hz with XPS to study the composition and chemical environment of atoms on Hz surface, and MALDI-ToF to understand the nature of the adsorbed molecules. We washed Hz with an extensive purification procedure in an attempt to obtain highly pure crystals; this methodology includes using organic solvents and water to precipitate proteins,[167] three types of enzymes, detergents, and water.[31] We also performed a shortened version of the same protocol to study the impact of the cleaning procedure on surface composition. Then, we compared these samples to HA, since these crystals are devoid of adsorbed organic matter,[8] and suspended HA in solutions that mimic the natural environment of Hz to assess the sources of the organic components adsorbed on Hz and its surface adsorption sites.

5.3. Experimental

5.3.1. Materials

Reagent grade sinapinic acid (SA), trifluoroacetic acid (TFA), acetonitrile and calcium chloride were obtained from Sigma-Aldrich Canada. Methanol, chloroform, sodium chloride, magnesium chloride hexahydrate, and sodium hydroxide pellets ACS grade were purchased from Fisher Scientific. Proteinase K (20 mg/mL) PCR grade, DNase I (100 U/mL), RNase A (DNase and

protease-free, 10 mg/mL) and Halt protease inhibitor (single use cocktail, 100x) were obtained from Thermofisher Scientific. *N*-2-hydroxyethylpiperazine-*N'*-2-ethanesulfonic acid (HEPES), L-glutamine and RPMI1640 were purchased from Gibco (by Life Technologies), saponin from Quillaja Saponaria Molina, from Acros Organics MS and sorbitol from Sigma life sciences. A+ blood was obtained from The Interstate Blood Bank, INC.

Stock solutions of 25 mM HEPES, 0.05 % saponin in PBS (1x) were prepared in advance. Also, 2% sodium dodecyl sulfate (SDS), phosphate-buffer saline solution (PBS 1x, pH 7.4), 10 mM Tris hydrochloride (Tris-HCl, pH 8) and 10 mM 3-[(3-Cholamidopropyl)dimethylammonio]-1-propanesulfonate hydrate (CHAPS) were prepared from reagents purchased from BioShop, Canada Inc. The 10 mM CHAPS buffer was prepared by mixing 150 mM NaCl, 1 mM CaCl₂ and the protease inhibitor in 50 mM Tris HCl, the pH was adjusted to 7.4.

Proteinase K (2 mg/mL) was prepared in a buffer solution of 2% SDS/Tris-HCl, pH 8. DNase I (100 U/mL) and RNase A (1 mg/mL) were mixed in the same buffer solution consisting of 10 mM Tris-HCl, 2.5 mM MgCl₂ and 0.5 mM CaCl₂, pH 8.0. The pH of the stock solutions was adjusted with 0.1 M HCl or 0.1 M NaOH (reagents were ACS plus grade, purchased from Fisher Scientific). Milli-Q water from a Barnstead purification system (resistivity of 18.2 MΩ-cm) was used to prepare all the solutions and experiments unless specified. Protein LoBind tubes were purchased from Eppendorf.

5.3.2. Methods

5.3.2.1. Cultivation of *P. falciparum* asexual blood stages and Hz extraction

Plasmodium falciparum chloroquine sensitive strain 3D7-H was maintained in a synchronous culture by implementing a modified version of Trager and Jensen's cultivation method.[168] In

brief, parasites were cultivated in RPMI 1640 media supplemented with L-Glutamine and 25 mM HEPES in 10% human plasma and A+ human erythrocytes in a 2% hematocrit. 5% sorbitol was used for synchronization of the parasite blood stages. The parasites were collected at the late trophozoite stage and processed as follows: washed in PBS, treated with 0.05% saponin in PBS to lyse the RBC, washed in PBS and extracted in CHAPS buffer, and finally centrifuged at 15k rpm for 10 min at 4°C. The supernatant was removed to give cytosolic free samples of Hz, followed by re-suspension in PBS to store at 4°C for further cleansing steps.

5.3.2.2. Extensive washing of hemozoin (ewHz)

This method of purification followed what Lvova *et al.* reported, with minor modifications.[31] Each sample consisted of 300 µL of Hz suspended in the lysis buffer. The sample was centrifuged for 1 min at 9,000 rpm and the supernatant removed. Protein traces were removed by extraction with chloroform, methanol, and water, according to the Wessel and Flügge method.[167] Briefly, 400 µL of methanol were added and the sample was vortexed until obtaining a uniform suspension, followed by centrifugation (30 s at 9,000 rpm). Then, 200 µL of chloroform were added and the sample was vortexed and centrifuged again (30 s at 9,000 rpm). 300 µL of water were added and the suspension was vortexed and centrifuged (2 min, 9,000 rpm). The top phase was removed, 300 µL of methanol were added and the pellet was mixed and centrifuged (2 min, 9000 rpm). The supernatant was removed, and the resulting Hz was treated with 2 mL proteinase K (2 mg/mL); the suspension was gently mixed by flipping the tube upside down, and was left at 37°C for 18 h. After this time, the suspension was centrifuged at 14,000 rpm for 20 min, the supernatant discarded and the pellet washed three times (2% SDS, 10 mM Tris-HCl, pH 8) with centrifugation in between and the supernatant discarded. Later, the resulting material was treated with 2 mL of a solution of

DNase I (100 U/mL) and RNase A (1 mg/mL) for 2 h at 37°C. The suspension was centrifuged at 14,000 rpm for 20 min and the top phase removed. Then, the crystals were washed three times with a solution of 2% SDS and three times with milli-Q water. The resulting sample was dried at room temperature and stored under vacuum prior to the characterization. This sample is referred to as extensively washed hemozoin (ewHz) in the text.

5.3.2.3. Partial washing of Hz (pwHz)

As described in **section 5.3.2.2**, Hz was first purified using the Wessel-Flügge method [167] to precipitate most of the proteins and lipids, followed by a treatment with 2 mL of a solution of proteinase K (2 mg/mL) for 18 h at 37°C. The resulting material was washed three times with a solution of 2% SDS/Tris-HCl (pH 8), and three times with milli-Q water with centrifugation in between steps and supernatant removal. The sample was dried at room temperature and kept under vacuum until characterization. This sample is referred to as partially-washed hemozoin (pwHz) in the text, since it involves only one enzyme (proteinase K) to digest the surface contaminants of Hz, and lacks DNase I and RNase A.

5.3.2.4. Characterization techniques

The surface composition of all materials was studied by X-ray photoelectron spectroscopy (XPS) using a spectrometer from Thermo Scientific K α , equipped with an Al cathode with an incident K α radiation of 1486 eV, and a spot diameter of 200 μ m. A flood gun of low energy electrons was used to prevent surface charging during the measurement. The analyses were carried out with a pass energy of 1 eV for all survey scans, and 0.1 eV for high-resolution scans of individual core levels. Data processing was performed using Advantage Software version 5.956, using Gaussian-

Voigt curve functions, while the background was removed using the Smart method. Peaks in the elemental high-resolution spectra were fitted according to the parameters reported in **Supporting Information Table S.5.1** and **Table S.5.2**. Three points were randomly selected along each sample and at least three samples were analyzed. High-resolution spectral energies were normalized by fixing the position of the C-C/C=C component of C_{1s} at 284.5 eV.

Matrix-assisted laser desorption/ionization time of flight (MALDI-ToF) was used to compare the adsorbed biomolecules of Hz to the surface of HA. To prepare the matrix, 20 mg/mL of sinapinic acid (SA) were dissolved in a mixture of 70:30 v/v acetonitrile : trifluoroacetic acid (0.1%, prepared in water). The mixture was vortexed, followed by centrifugation at 5,000 rpm for 1 min to remove the excess of SA. The supernatant was transferred to another tube to be used as matrix, while undissolved SA was discarded. The sample (Hz or HA) was mixed thoroughly with 10 µL of the matrix; then, 3 µL of this suspension were dropped on the stainless steel MALDI target plate and dried under a stream of air. The analysis was performed on an Autoflex II Smartbeam MALDI-ToF mass spectrometer (Bruker Daltonik GmbH), equipped with a frequency-tripled Nd:YAG laser of 355 nm and frequency of 200 Hz. Measurements were performed in the positive ion reflectron mode with an accelerating voltage of 20 kV, with detector bias gating set to 1.3 kV. The power was set at 20% with a global attenuator offset at 80%, reflectron at 10x and the digitizer was fixed at 1.0. Three spots were selected along each sample and at least three samples were analyzed. The spectra were produced by averaging 30 consecutive shots. The data was normalized with respect to the intensity of the peak at 616 Da, which corresponds to the molecular mass of heme.

5.3.2.5. Statistical analysis

Three independent experiments were performed for each sample. All the data are expressed as mean \pm standard deviation (SD). Means that are statistically different are indicated with a subscript asterisk (*). Microsoft Excel 2016 was used to perform the One-way ANOVA tests followed by Bonferroni's test correction to evaluate the statistical difference of multiple samples, where $P < 0.01$ was considered a significant difference.

5.4. Results

5.4.1. The cleaning method impacts the composition and amount of residual biomolecules on Hz surface

A flow chart for the purification of Hz is shown in **Figure 5.4.1.A** with the main distinction between extensively washed Hz (ewHz) and partially washed Hz (pwHz) being the steps after proteinase K treatment. Survey XPS analysis for ewHz shows the expected elements of C, O, N and Fe (**Figure 5.4.1.B, red**), and the atomic percentages of this sample do not show significant differences compared to HA (**Figure 5.4.1.B, grey**). No other elements were found on this sample. The lack of magnesium, phosphorus, and zinc on both, ewHz (**Figure 5.4.1.B, red**) and on pwHz (**Figure 5.4.1.B, blue**) clearly indicates that nucleic acids, with their phosphate backbone and zinc and magnesium counterions,[169] are not present. The absence of sulfur and sodium in all the samples also indicates that sodium dodecyl sulfate was removed after the rinses with water, or at least its concentration was below XPS detection limit of 1 to 0.1 atomic %. [170]

In contrast, the sample treated with fewer enzymes, pwHz, shows the unexpected presence of Si and Ca (**Figure 5.4.1.B, blue**). To determine if these elements are contaminants resulting from the purification, we studied the surface composition of dead *Plasmodium* parasites of the same

strain and clone cultivated to obtain Hz (*Plasmodium falciparum* 3D7). We rinsed the dead parasites with hexane and dichloromethane to extract the water and facilitate drying (see **Supporting Information Section 5.11.2.2** for details) for XPS analysis. We found Si in this sample (**Figure S.5.11.1**), which suggests that this element is *Plasmodium*-derived. The origin of Si in *Plasmodium* is unclear, as to date there is no information about this element in Apicomplexa parasites. Nevertheless, there is evidence indicating an important role of silicon in bone and connective tissue health,[171] and in plant defense.[172]

We did not detect a significant concentration of calcium in the elemental composition of the parasites; however, Ca is critical for vital functions in apicomplexan parasites, such as host cell invasion and egress, motility and differentiation.[173, 174] In *Plasmodium*, this element could originate from its intracellular constituents, such as the endoplasmic reticulum, acidocalcisomes, mitochondria, Golgi apparatus, nuclei, or the food vacuole where Hz is produced.[173, 175] Since XPS is a highly surface-sensitive technique, we may not have sampled these inner storage organelles, which explains why we did not find Ca in the dead parasites.

The atomic percentages of N and Fe in pwHz are close to the theoretical values, while C is significantly lower and O significantly larger (**Figure 5.4.1.B, blue**). To understand these differences as well as learn more about the nature of the adsorbed biomolecules on Hz, we ran high-resolution XPS measurements for O, N, C, and Fe on both pwHz and ewHz, and compared them to those measured on pure HA. C_{1s} and Fe_{2p} spectra do not show significant differences between the two samples (**Figure S.5.11.2**).

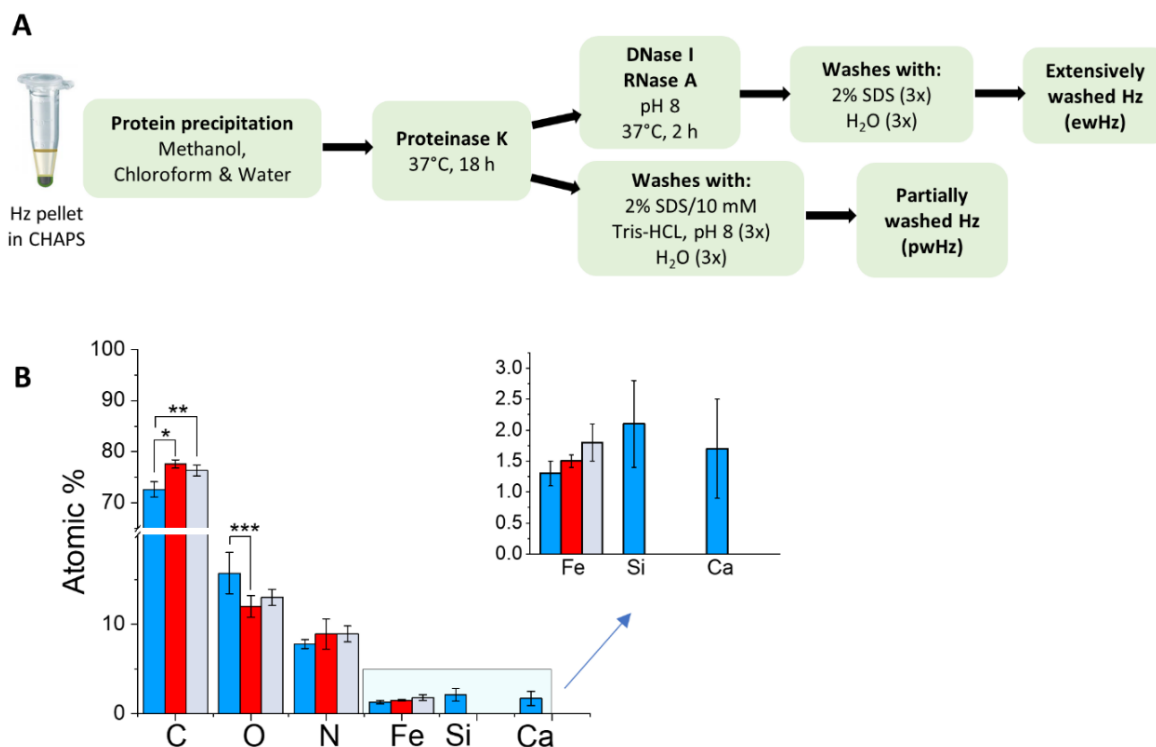


Figure 5.4.1. (A) Flow chart of the methodologies used to treat Hz to produce pwHz and ewHz. (B) Elemental composition of pwHz (blue bars) and ewHz (red bars) evaluated by XPS and compared with HA (gray bars). Values represent mean \pm SD calculated for three independent experiments and three different spots analyzed along the same sample. *Significant differences between area ratios, with * $P < 0.0004$, ** $P < 0.003$ and *** $P < 0.002$.

High-resolution O_{1s} spectra of pwHz, ewHz and HA (**Figure 5.4.2.A-C**) show a peak located at 531.5 eV that corresponds to both the Fe-O-C(O) bond and the -OH group of water adsorbed on the crystals surface; while the peak at 533.5 eV is assigned to C=O from carboxylates of the propionic side chains.[164] In the absence of water, the 531.5 and the 533.4 eV peaks should have the same areas since there are four oxygen atoms of each type in the crystalline structure of both Hz and HA.[164] However, HA and Hz are hygroscopic, with the crystals being able to absorb up to 14% of their mass in water on their surface and possibly within the heme layers.[144]

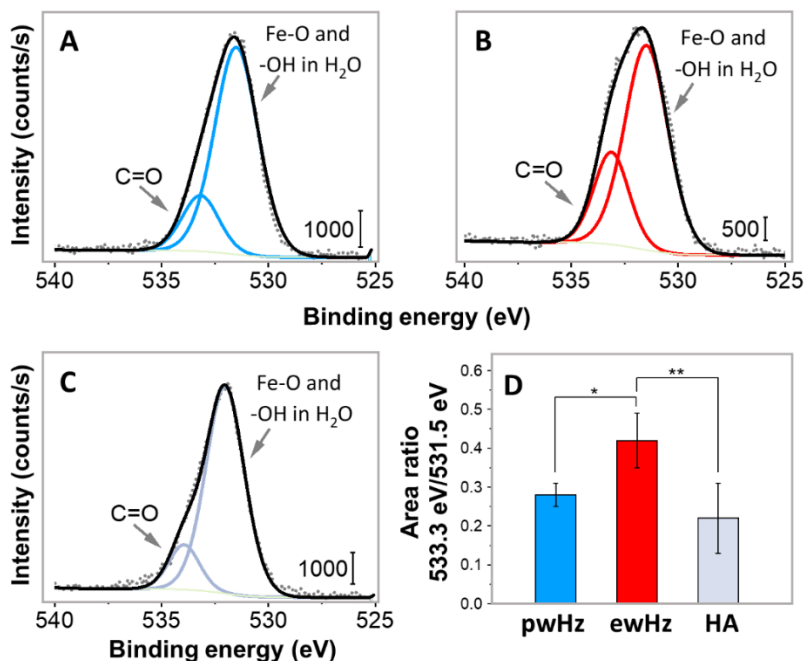


Figure 5.4.2. XPS high-resolution spectra of the O_{1s} level collected for (A) pwHz (B) ewHz, and (C) HA. Experimental data are shown in dark gray dotted line, peak fits in continuous blue, red or light gray (A, B, or C, respectively), and the overall fit in black. (D) Area ratios of the 533.3 eV/531.5 eV peaks for the O_{1s} core level measured for pwHz (blue bar), ewHz (red bar), and HA (gray bar). Values represent mean ± SD calculated for three independent samples and three different spots analyzed along the same sample. *Significant differences between area ratios, with *P<0.0003 and **P<0.006.

In pwHz, the 533.3 eV/531.5 eV peak area ratio is close to HA (**Figure 5.4.2.D**); this suggests that water may be associated with the adsorbed species on pwHz. These compounds may be constituted by small peptides, which were not digested by proteinase K alone, and are prone to interact with water.[176] This is in good agreement with the high oxygen content in this sample, as discussed earlier (**Figure 5.4.1.B, blue bars**). Conversely, in ewHz the 533.3 eV/531.5 eV peak area ratio is significantly larger than in pwHz and HA (**Figure 5.4.2.D**). This indicates less water on the surface of ewHz, probably due to fewer adsorbed species on it, resulting in a surface with more -COOH groups exposed. Although ewHz is very close to HA in composition, the difference in water content most likely arises due to the methodology used to synthesize the HA used in this work (**Supporting Information Section 5.11.2.1**). While the XPS high-resolution spectra of C_{1s},

N_{1s} and Fe_{2p} from HA among methods are equivalent, the O_{1s} spectra show varied water content among synthesis methods, as demonstrated in a previous work.[164] Therefore, it can be expected that ewHz and HA differ in amount of water adsorbed.

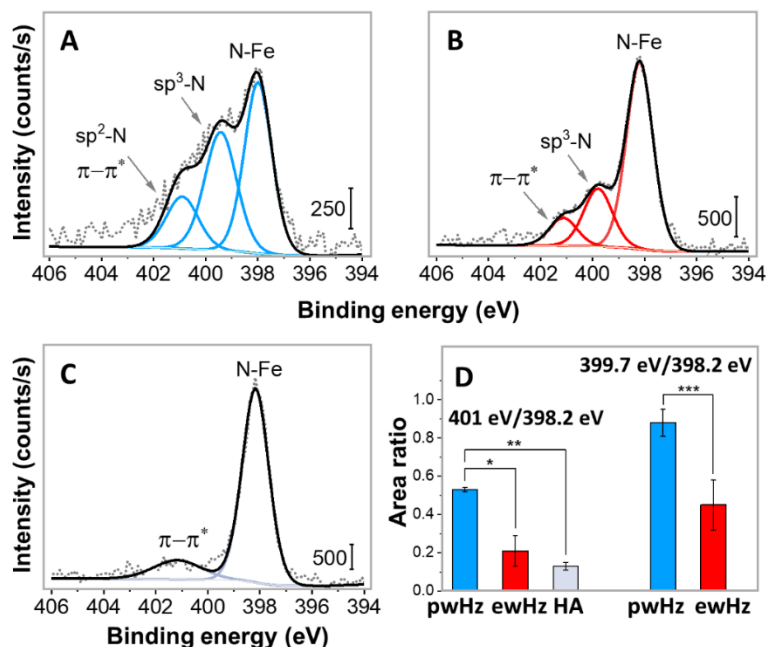


Figure 5.4.3. XPS high-resolution spectra of the N_{1s} core level collected for (A) pwHz (B) ewHz and (C) HA. The dashed blue line in pwHz distinguishes the contribution from the $\pi-\pi^*$ delocalization. Experimental data are shown in dark gray dotted line, peak fits in blue, red or light gray, and the overall fit in black. (D) Area ratios of the XPS N_{1s} 401.0 eV/398.2 eV and 399.7 eV/398.2 eV peaks acquired for pwHz (blue bars), ewHz (red bars), and HA (gray bars). Values represent mean \pm SD calculated for three independent experiments and three different spots analyzed along the same sample. *Significant differences between area ratios, with $*P < 9 \times 10^{-7}$, $**P < 5 \times 10^{-8}$ and $***P < 1 \times 10^{-6}$.

The analysis of the N_{1s} spectra of pwHz and ewHz (Figure 5.4.3.A and B, respectively) show an intense peak at 398.2 eV, which corresponds to the four equivalent N-Fe bonds in the pyrrole of each porphyrin ring, as confirmed by their presence also in the spectrum of HA (Figure 5.4.3.C).[164] Both samples also show a peak at around 401 eV that is related to the $\pi-\pi^*$ transition of the delocalized electrons, as shown for HA.[164] However, the 401 eV/398.2 eV peak area ratio in pwHz (Figure 5.4.3.D, blue) is significantly higher than that in ewHz (Figure 5.4.3.D, red)

and HA (**Figure 5.4.3.D, gray**). This could be related to a contribution from sp^2 hybridized nitrogen components (sp^2 -N) derived from the adsorbed biomolecules.[177] Both pwHz and ewHz show a new signal at 399.2 and 399.7 eV, respectively, which may arise from sp^3 hybridized nitrogen components (sp^3 -N) bound or adsorbed onto the surface of the crystals. Overall, the significantly higher area ratios (both 401 eV/398 eV and 399.2 eV/398.2 eV) in pwHz (**Figure 5.4.3.D, blue**) confirm that larger quantities of biomolecules are adsorbed on the surface of these crystals.

5.4.2. Residual biomolecules adsorbed on Hz surface are related to protein fragments or amino acids

To assess the origin of the adsorbed biomolecules found on pwHz and ewHz, we put our synthetic model crystal, HA, in contact with compounds that are part of the natural cycle of Hz production or extraction, i.e. parasite schizont lysates and RBC membranes, respectively. HA crystals were incubated with these components at 37°C for 24 h, and then treated with the same extensive purification procedure used to obtain ewHz (**Supporting Information, Sections 5.11.2.6 and 5.11.2.7**). Additionally, we prepared a control sample of HA only treated with the extensive purification used to produce ewHz (see **experimental section 5.3.2.2**), to investigate whether the methods and enzymes used can introduce additional adsorbed molecules on Hz. We studied these materials with XPS and analyzed the high-resolution N_{1s} spectra to compare with what was found on ewHz and pwHz.

First, we put HA crystals in contact with dead parasite lysates. The XPS N_{1s} spectra (**Figure 5.4.4.A**) show three peaks centered at 398.1, 399.7 and 401.2 eV. The location of these peaks is very close to the signals found on pwHz and ewHz (**Figure 5.4.3.A and B**, respectively), indicating

a possible contribution of parasite cell debris, constituted mostly by aggregated and denatured plasmodial proteins[178] on the surface of these samples. However, the 399.7 eV/398.2 eV peak area ratio in this sample (**Figure 5.4.4.D, turquoise**) is lower compared to that found on pwHz and ewHz (**Figure 5.4.3.D**). This indicates that part of the residual sp^3 -N components in pwHz and ewHz arise from other biological sources, besides schizont debris.

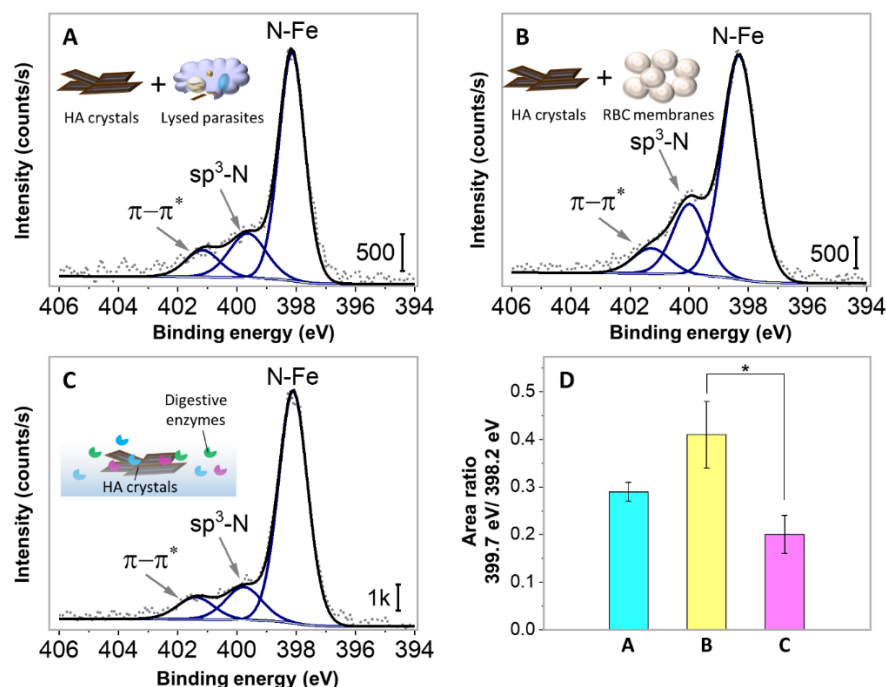


Figure 5.4.4. XPS high resolution of the N_{1s} core level acquired for purified HA after suspension in (A) dead parasites of *P. falciparum* of the clone 3D7, (B) RBC membranes, (C) enzymes and detergents used to prepare ewHz. Experimental data are shown in dark gray dotted line, peak fits in blue and the overall fit in black. (D) N_{1s} 399.7 eV/398.2 eV peak area ratio calculated for the spectra shown in A, B, and C. *Significant differences between area ratios, with *P<0.006. Values represent mean \pm SD calculated for three independent experiments and three different spots analyzed along the same sample.

Then, we tested the interaction of HA with RBC membranes. The XPS analysis revealed three peaks in the N_{1s} spectra of this sample (**Figure 5.4.4.B**) at 398.1, 399.8 and 401.1 eV, again very close to the peak locations measured on pwHz and ewHz (**Figure 5.4.3.A and B**, respectively), indicating that residues of RBC membranes interact strongly with Hz and may be predominant on

the surface of the crystals.[178] Indeed, the high 399.7 eV/398.2 eV area ratio in this control (**Figure 5.4.4.D, yellow**) suggests that many of the sp^3 -N species adsorbed on pwHz and ewHz derive from the interaction between RBC membranes and HA, despite the extensive washes. These results suggest a strong affinity between Hz and RBC components that may attach during the process of Hz formation, as proposed by Goldie *et al.*,[178] or during Hz release.[40, 179]

Finally, we looked at the N_{1s} spectrum of HA treated with the thorough purification used to produce ewHz, to understand if the purification itself may introduce adsorbed biomolecules on Hz. The XPS N_{1s} spectrum (**Figure 5.4.4.C**) presents three peaks located at 398.1, 399.7 and 401.3 eV. The similarity between this spectrum and those recorded for ewHz and pwHz (**Figure 5.4.3.A and B**) shows that the adsorbed biomolecules found on the surface of pwHz and ewHz could also arise from the purification process itself. These compounds could be either fragments of proteins degraded by the enzymes used during the purification, or fragments of the enzymes themselves. However, the 399.7 eV/398.2 eV peak area ratio (**Figure 5.4.4.D, pink**) is significantly smaller compared to pwHz and ewHz (**Figure 5.4.3.D, blue and red, respectively**), indicating that even though the purification step may be introducing contamination on Hz, it is not the only source of organic material containing sp^3 -N compounds on Hz surface.

Overall, while these results cannot definitely show which molecules are adsorbed on Hz surface, they highlight the importance of studying the surface of Hz prior to its use in antimalarials evaluation or immune response tests since the chemical composition may be similar to the theoretical values despite the presence of adsorbed biomolecules. This was the case in this work for ewHz, where the survey XPS analysis was indistinguishable from that of HA.

Also, these results confirm the highly adhesive character of Hz, probably as a result of its amphiphilic nature[8], and prove that there are multiple biological compounds that can adhere to

Hz, such as components of the digestive vacuole membrane, proteins, carbohydrates, lipids, and RBC membranes.[8] These compounds could be related to Hz formation and may also be implicated in the physiological effects observed during malaria infection.[8] Additionally, the residues derived from the purification procedure are likely to be part of the molecules adsorbed on Hz, and our elemental analysis clearly shows that the protocol used to purify Hz affects the composition and amount of species adsorbed on its surface.

To better understand the binding mechanism between biomolecules and Hz surface, we assessed the interaction between HA and some amino acids (see **Supporting Information section 5.11.2.8**). These molecules are not only the monomers of peptides and proteins,[176] but they also represent traces of any of the enzymes used in the purification procedure,[180] as well as the fragments left by the enzymes after proteolysis. We selected two basic amino acids, histidine (His) and arginine (Arg); two nonpolar, alanine (Ala) and leucine (Leu); and a polar one, serine (Ser), since all of them may interact with the amphiphilic Hz surface. All the selected amino acids present sp^3 -N in their structure, and His and Arg also present sp^2 -N; thus, their XPS N_{1s} spectra signals are similar to those of Hz samples and control experiments.[177]

Figure 5.4.5.A shows the N_{1s} spectrum obtained from the surface of HA crystals after contact with amino acids. The spectrum shows three peaks located at 398.1, 399.4 and 401.4 eV, similarly to what we found on pwHz, ewHz (**Figure 5.4.3.A and B**, respectively), and on all our previous control experiments (**Figure 5.4.4.A-C**). This may indicate that amino acids and small peptides are the possible adsorbed biomolecules in the samples of washed Hz. Like in the previous control experiments, the 399.4 eV/398.1 eV peak area ratio (0.25 ± 0.14) is lower than that measured on pwHz and ewHz (**Figure 5.4.3.D**, **blue** and **red**, respectively). While this may be due to the concentration of amino acids used in this experiment (see **Supporting Information section**

5.11.2.8), this result shows that amino acids interact strongly with the surface of Hz and remain attached despite the washes with detergents and water.

Amino acids may be adsorbed onto HA and Hz via hydrophobic interactions (e.g. between the vinyl or methyl side chains of heme and the alkyl side chains of Ala and Leu[181]), or hydrogen bonding and electrostatic interactions (e.g. between the hydroxyl group of Ser or the amino group of Arg or His and the propionic acid chains of HA [182]).

5.4.3. Surface carboxylate groups act as main adsorption sites on Hz

To understand if hydrophobic interactions or hydrogen bonds and electrostatic interactions are predominant, we masked the carboxylate groups on HA by esterification with 2,2,2-trifluoroethanol (TFE) (see **Supporting Information section 5.11.2.9** and **Figure S.5.11.4**),[164] and we incubated the resulting fluorinated HA with the previously selected amino acids (see **Supporting Information section 5.11.2.8**). The difference in N_{1s} spectrum between this sample (**Figure 5.4.5.B**) and all other controls (**Figure 5.4.4** and **Figure 5.4.5.A**) is striking: the spectrum does not show a peak at 399.7 eV and overall, it is very similar to the N_{1s} spectrum measured on HA (**Figure 5.4.3.C**). This implies that amino acids did not adsorb significantly on fluorinated HA, and that the carboxylate groups on the surface of Hz are the crucial sites for biomolecule adsorption. The molecules on Hz may be either H-bonded or electrostatically interacting with carboxylates, as in our control experiments, or covalently bonded to them. In fact, amide bonds between amino groups and Hz carboxylate groups may be catalyzed *in vivo* by proteases [183] and ribosomes and non-ribosomal peptide synthetases, e.g. ATP-dependent enzymes and ATP-grasp enzymes.[184] Amide bonds are quite resistant to hydrolysis; thus, they could persist on Hz surface after thorough washes.

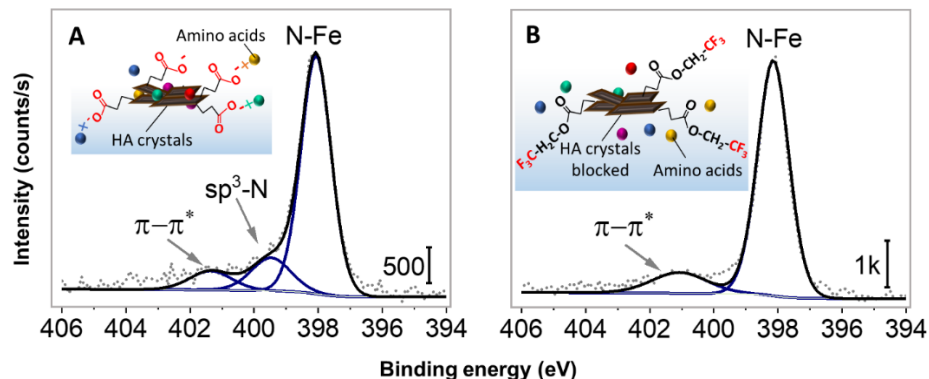


Figure 5.4.5. XPS high resolution of the N_{1s} core level acquired for (A) HA after interacting with amino acids, (B) fluorinated HA crystals after interacting with amino acids. Experimental data are shown in dark gray dotted line, peak fits in blue and the overall fit in black. All data are representative of three independent experiments and three different spots analyzed along the same sample.

5.4.4. The cleaning procedure introduces partial contamination on Hz surface

Finally, we used MALDI-ToF to further analyze the molecules adsorbed on ewHz and pwHz. We compared the spectra relative to the fragments ablated from Hz crystals and from HA, and ascribed any signal present in the spectra of pwHz or ewHz but not in HA to molecules adsorbed on Hz. The HA spectrum (**Figure 5.4.6.A, green**) shows the characteristic MALDI fragment ion at m/z 616, which corresponds to an intact heme monomer.[185] In addition, other molecular masses related to the heme signature are observed at m/z 471, 484, 498, 511, 526, 557 and 571, as previously reported,[185] The three peaks located in the low m/z region at 206, 224 and 246 (**Figure 5.4.6.B, green**) are assigned to ion fragments of sinapinic acid used as matrix (**Figure S.5.11.5**).

The mass spectrum of pwHz (**Figure 5.4.6.A, blue**) also shows the signal of intact heme; however, the peak intensity and peak resolution are lower compared to the HA spectrum. For example, some isotopic masses relative to the average masses of 498, 511 and 526 are lost; whereas the signals at m/z 471 and 484 associated with heme monomers are missing. This decrease in the signal may be related to abundant species with high molecular weight adsorbed onto the surface

of the crystals, which compete for the charges during the ionization process and suppress the signal from less abundant components.[186] These macromolecules would require further preparation for mass spectra analysis; e.g. gel electrophoresis (SDS-PAGE or agarose) for proteins.[186]

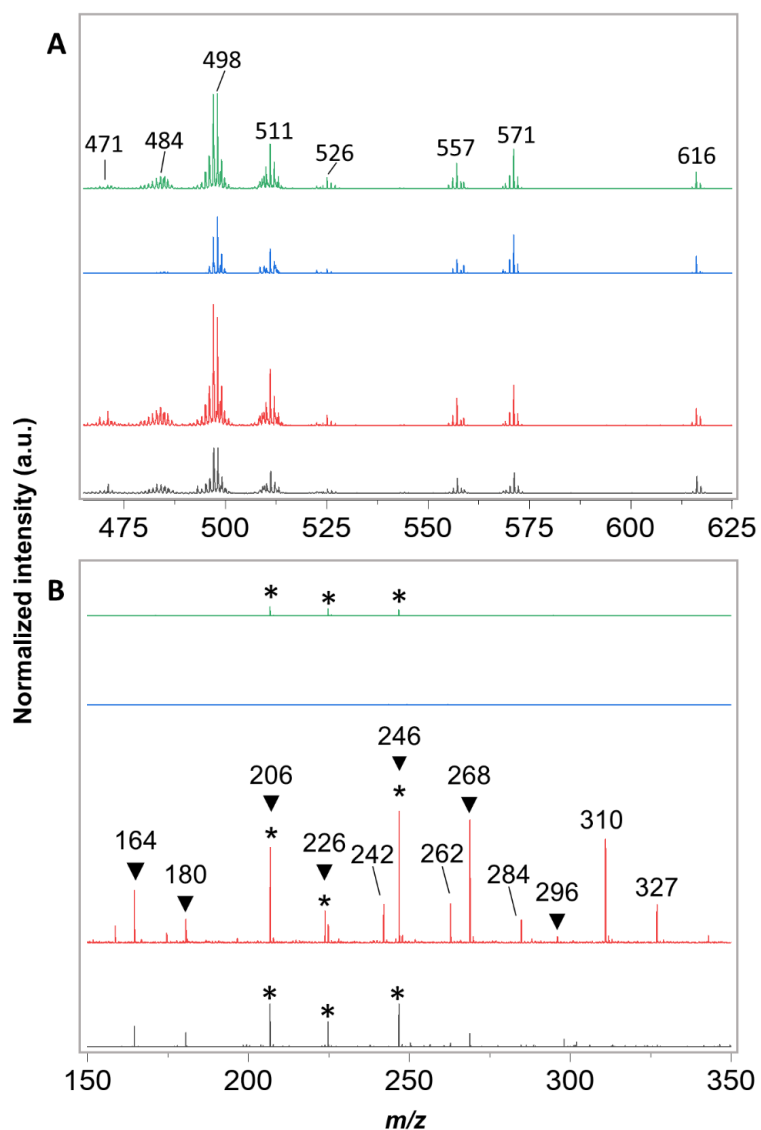


Figure 5.4.6. Representative MALDI-ToF mass spectra of positive ions in reflectron mode collected in the m/z region of (A) 150-350 and (B) 465-625 for HA (green), pwHz (blue), ewHz (red) and HA treated with the extensive washes (black). All experiments were repeated three independent times with similar results. The intensity was normalized with respect to the intensity of the peak at 616 Da. The peaks related to the matrix are marked with an asterisk (*). The peaks arising after the washing procedure are marked with an inverted triangle (▼).

The mass spectrum of ewHz shows the heme signals in the m/z region of 471 to 616 (**Figure 5.4.6.A, red**). The spectral resolution and intensity are comparable to those found for HA (**Figure 5.4.6.A, green**), which confirms that the presence of large molecules on the surface of pwHz suppressed the MALDI signal of heme and related ions on that sample (**Figure 5.4.6.A, blue**), and this issue is solved by extending the purification procedure of Hz. However, several peaks appear in the low m/z region of the spectrum of ewHz (**Figure 5.4.6.B, red**), which are not present in the spectra of either HA (**Figure 5.4.6.B, green**) or pwHz (**Figure 5.4.6.B, blue**). We hypothesize that these signals are related to ion fragments of species produced by the enzymes used during the extensive purification, such as peptides and amino acids, as discussed before.

To prove this hypothesis, we collected the MALDI-ToF spectrum of HA treated with the extensive methodology used to obtain ewHz. The spectrum of this sample shows both the characteristic peaks of intact heme monomer in the m/z range of 471-616 (**Figure 5.4.6.A, black**) and peaks in the low m/z region (**Figure 5.4.6.B, black**). Some of these new peaks are in the same positions as the ion fragments present in the low m/z region of the ewHz spectrum (**Figure 5.4.6.B, black**, marked with an inverted triangle). Also, the peaks assigned to sinapinic acid at 206, 224 and 246 were significantly larger on both this sample and on ewHz than on HA, which suggests that some of the adsorbed biomolecules on ewHz and this sample produce ions with the similar molecular masses as the matrix.

5.5. Discussion

Understanding the surface properties of Hz has remained a major challenge due to the difficulty of isolating sufficient material from the parasites,[38] and the lack of a standardized protocol to

purify and characterize the crystals after extraction.[14, 164] In this work, we used XPS and MALDI-ToF to compare the composition of Hz surface after purification with an extensive methodology involving organic solvents, detergents and three types of enzymes, and a shorter one, which involves only one enzyme in the final treatment. In addition, we used synthetic HA crystals put in contact with biomolecules that mimic the natural environment of native Hz to understand the nature of the adsorbed molecules on Hz samples.

Our results showed that even after the extensive washing procedure several low molecular weight residues such as lipids, carbohydrates, amino acids, and peptides persist on Hz surface, while after the shorter procedure larger amounts of contaminants of higher molecular weight are present. The molecules remaining after the shorter washing procedure also contained unexpected elements, such as calcium and silicon.

We did not detect any nucleic acids on either sample. This implies that the thorough purification activity in the extensive treatment cannot be attributed to the use of the DNase I and RNase A. Instead, the high pH of the buffers used to suspend the enzymes during the extensive wash may be responsible for the greater purification observed with this treatment since high pH degrades the outermost layer of Hz.[8] Thus, the addition of enzymes to degrade nucleic acids may not be necessary to treat Hz. Although the use of an alkaline buffer is essential to obtain cleaner crystals, there is a sacrifice in yield from this step.

The macromolecules found on both pwHz and ewHz may have adhered on Hz surface during its extraction from the parasite digestive vacuole and RBC, but they may also be fragments or whole proteins involved in the biocrystallization of Hz. Most biominerals are formed under the direction of proteins,[49, 187, 188] which can then remain adsorbed at the biomineral surface or included within the crystals. Thus, even inorganic biominerals that show excellent crystallinity

contain a large amount of organic material.[49] In fact, Chugh *et al.* proposed that heme detoxification protein (HDP) is required to rapidly convert heme into Hz,[62] and Nakatani *et al.* hypothesized that some histidine residues in HDP direct the proper alignment of heme monomers to enable the formation of the axial ligand of the heme iron in Hz.[63] Thus, the biomolecules we found adsorbed onto Hz surface may be traces of its biomineralization process.

5.6. Conclusions and Outlook

Our results show that the methodology chosen to purify Hz affects the surface of the crystals in terms of both the amount and nature of contaminants. This explains the discrepancies related to the immunomodulatory properties of Hz. The use of different protocols to purify Hz produce crystals with different species on its surface that in turn modulate different host responses.[8] A standardized procedure that researchers could use prior to analyzing biological effects of Hz would clarify the state of Hz each work is dealing with, and prevent generating controversial results. We propose that XPS and MALDI-ToF become standard characterization tools to evaluate Hz surface since they require small amounts of sample and are highly sensitive.

The finding that carboxylate groups are critical for adsorption of molecules on Hz surface is of outstanding relevance for antimalarial drug design, particularly for those that act by inhibiting Hz growth.[10] Drug screening should probably focus on carboxylate binding candidates.

Overall, this work suggests that the surface of Hz may never be free from contaminants, and ultimately questions the concepts of “pure” Hz crystals. We showed that many compounds adhere onto the amphiphilic surface of Hz during its formation and extraction; but if these compounds adhere during the process of Hz crystallization, they are likely to be present not only at its surface but also as integral components of the bulk of Hz crystals. Carboxylate groups, here shown to bind

the adsorbed molecules, may serve as substrates for nucleation and growth inside the digestive vacuole of the parasite.[153, 157] The organic coating bound to native Hz could be part of an organic matrix present within Hz structure to coordinate its crystal nucleation and formation.[15, 38] The proposed mechanism raises an intriguing question: how much of the adsorbed molecules associated with Hz originates from contamination and how much represents material involved in the biomineralization? Further work is needed to explore this fascinating concept.

ABBREVIATIONS

HA	hematin anhydride
Hz	hemozoin
ewHz	extensively washed hemozoin
pwHz	partially washed hemozoin
sp ² -N	sp ² hybridized nitrogen components
sp ³ -N	sp ³ hybridized nitrogen components
RBC	red blood cell
MALDI-ToF	matrix-assisted laser desorption/ionization time of flight
XPS	x-ray photoelectron spectroscopy

5.7. Associated content

Supporting information

Electronic Supplementary Information (ESI) available: Details relative to materials and methods, XRD and FT-IR analysis of hematin anhydride, characterization of HA fluorinated with TFE, and details relative to the parameters used for XPS analysis of all samples.

5.8. Author information

Corresponding author

*Marta Cerruti

3610 University Street

Wong Building, 2250

Montreal, QC H3A 2B2

Email: marta.cerruti@mcgill.ca

Telephone: +1 (514) 398-5496

5.9. Author Contributions

The manuscript was written through the contributions of all authors. All authors have given approval to the final version of the manuscript.

Notes

The authors declare no competing financial interest.

5.10. Acknowledgments

E. D. G. thanks Consejo Nacional de Ciencia y Tecnología (CONACyT) de México (CVU 354150), Secretaría de Educación Pública (SEP) de México (grant BC-3262), and the McGill Excellence Doctoral Award (MEDA) for their financial support. M. C. and D. S. B. acknowledge the Canada Research Chair (CRC) foundation and Natural Sciences and Engineering Research Council of Canada (NSERC) for funding.

5.11. Supporting information

5.11.1. Materials

The following materials were obtained from Sigma-Aldrich Canada, ACS grade: hexane, dichloromethane (DCM), hematin, sodium bicarbonate, L-alanine, L-leucine, L-arginine, D-histidine, L-serine, 2-(N-Morpholino)ethanesulfonic acid (MES) hydrate, 2,2,2-trifluoroethanol (TFE), pyridine and Di-*tert*-butyl-carbodiimide. Sodium hydroxide, propionic acid and monosodium phosphate (NaH_2PO_4) ACS grade were purchased from Fisher Scientific. Phosphate buffer saline (PBS) (1x) tablets and sodium dodecyl sulfate (SDS) were purchased from BioShop, Canada Inc. Stock solutions of PBS (1x) pH 7.4, 2%SDS, MES (1x) pH 6, 0.01 M sodium bicarbonate, 0.1 M NaOH and 5 mM NaH_2PO_4 pH 8, were prepared and used freshly. The pH of the stock solutions was adjusted with a solution of 0.1 M HCl or 0.1 M NaOH. Milli-Q water from a Barnstead purification system (resistivity of 18.2 $\text{M}\Omega\text{-cm}$) was used to prepare all the solutions and experiments, unless specified. Protein LoBind tubes were purchased from Eppendorf.

5.11.2. Methods

5.11.2.1. Synthesis and characterization of hematin anhydride (HA)

Crystals of HA were produced by the acid-annealing method, as reported in the literature, [32] with minor modifications. 0.6 mmol of hematin were dissolved in 80 mL of 0.1 M NaOH for 30 min under stirring. Then, 49 mmol of propionic acid were added drop-wise to precipitate the crystals until reaching a pH of around 4. The suspension was left to react overnight at 70°C, covered from light. After this time, the flask was cooled down to room temperature, the suspension was decanted and washed twice with distilled water and centrifuged at 9,000 rpm for 30 min in between. Unreacted and poorly aggregated heme was removed by the addition of a 0.01 M sodium

bicarbonate and left in an orbital shaker for 3 h followed by centrifugation at 9,000 rpm for 30 min and supernatant was decanted; this step was repeated twice. The resulting crystals were washed four times with distilled water with centrifugation in between at 9,000 rpm for 30 min. The sample was dried at room temperature and kept in vacuum.

The crystallinity of synthesized HA was assessed with X-ray diffraction (XRD). The sample was ground and transferred to a metallic holder and the diffraction patterns (**Figure S.5.11.7.A**) were acquired with a Siemens D5000 diffractometer, using a Cu K α radiation source (K α_1 λ =1.54 Å). The monochromator was operated at 40 kV and 40 mA within the 5° to 27° range in 2 θ .

Fourier Transform – Infrared (FT-IR) spectroscopy was used to ensure the chemical composition of synthesized HA. FT-IR spectrum was collected for HA mixed with KBr (**Figure S.5.11.7.B**) on a Bruker Tensor 27 spectrometer equipped with a diffuse reflectance (DRIFT) accessory and a DTGS detector. The spectrum was acquired in transmittance mode from 400 to 2000 cm⁻¹ with 56 scans at 4 cm⁻¹ resolution. The data analysis was performed using OPUS software version 7.0.0, (Bruker, Karlsruhe, Germany).

5.11.2.2. Preparation of *Plasmodium falciparum* parasites for XPS analysis

100 μ L of a suspension of dead parasites of *Plasmodium falciparum* of the clone 3D7 (see **Experimental Section 5.3.2.1**) were washed with hexane, dichloromethane and a final wash with hexane with centrifugation in between (1 min, 9,000 rpm) and supernatant removal. The resulting material was dried at room temperature to evaporate the residual solvents and was kept in vacuum until analysis.

5.11.2.3. Preparation of red blood cell (RBC) membranes

RBC membranes were prepared following the methodology reported by Steck, T.L *et al.*, [189] with minor modifications. First, packed red blood cells were obtained from whole blood by centrifugation at 5,000 $\times g$ for 7 min to remove cells, followed by centrifugation at 12,500 $\times g$ for 5 min to remove acellular components. 1 mL of these packed RBCs were suspended in 6 mL of PBS (1x) pH 7.4 and mixed by gentle trituration. The mixture was centrifuged at 1000 $\times g$ for 10 min and the supernatant removed, this step was repeated twice. The packed RBCs were suspended in 35 mL of 5 mM NaH_2PO_4 pH 8.0, and left incubating on an ice bath for 30 min. Then, the suspension was centrifuged at 12,000 $\times g$ for 10 min. The supernatant was discarded and the resulting pellet was resuspended again in 5 mM NaH_2PO_4 pH 8, until the pellet color changed to white/translucent, showing that most hemoglobin was removed. Finally, the volume of the RBC ghosts was adjusted to 1 mL using 5 mM NaH_2PO_4 and the solution was kept at 4°C and used right away.

5.11.2.4. Chemical derivatization of HA with 2,2,2-trifluoroethanol (TFE)

Prior to the experiment, all the glassware was thoroughly washed with soap, rinsed with deionized water and isopropanol followed by overnight drying. HA was placed in a 10 mL beaker inside a glass flask with an airtight seal. The reagents were introduced sequentially into the flask, outside the beaker, at 15 minutes intervals in the following order and amounts: TFE (0.9 mL), pyridine (0.4 mL) and Di-*tert*-butyl-carbodiimide (0.3 mL). [156] The flask was sealed and the reaction proceeded at room temperature for 18 h to expose the crystals to the reagents vapors. [142, 155] After this time, the sample was dried at room temperature and kept under vacuum for several days

before its analysis. XPS characterization was used to ensure the complete derivatization of HA by corroborating a new signal at around 292 eV in the C_{1s} spectrum of this sample (**Figure S.5.11.4**).

5.11.2.5. Suspension of HA in solutions used as control

HA was suspended in different solutions used as control, and treated with the extensive cleaning procedure used to produce ewHz, (see **Experimental section 5.3.2.2** of the main manuscript), unless specified. The resulting crystals were dried at room temperature and left under vacuum until characterization.

5.11.2.6. HA suspended in *Plasmodium falciparum* parasites

P. falciparum parasites of the clone 3D7 were cultivated as described in the Methods section of the main manuscript. The parasites were kept in PBS at 4°C until their use. 3 mg of HA were dispersed in 1 mL of parasites using short lapses of sonication at 4°C to lyse the parasite's cell and obtain a uniform dispersion of HA, while avoiding heating the cells. The suspension was left at 37°C for 24 h, and the crystals cleaned with the extensive purification method. The resulting material was dried at room temperature and kept in vacuum until its analysis.

5.11.2.7. HA suspended in RBC membranes

3 mg of HA were added to 1 mL of RBC ghosts with an absorbance of 0.7 measured at 280 nm[13]. The mixture was vortexed to open the RBC membranes and the suspension was incubated at 37°C for 24 h. After this time, the mixture was centrifuged at 9,000 rpm for 10 min and the supernatant removed. The resulting material was cleaned using the extensive cleaning to produce ewHz as

described in **Experimental Section 5.3.2.2** of the main manuscript. Finally, the crystals were dried at room temperature and kept in vacuum until analysis.

5.11.2.8. HA suspended in a mixture of amino acids

A solution containing 1 mg/mL of each of the following amino acids was prepared in MES (1x) buffer by adding the following amino acids: L-alanine, L-leucine, L-arginine, D-histidine, and L-serine. The pH of the solution was adjusted to 6.0 using 0.1M HCl. Later, 3 mg of HA were added in 1 mL of the amino acids solution and sonicated, followed by incubation at 37°C for 1 h. This material was not cleaned under the extensive purification procedure used to obtain ewHz, to avoid introducing species derived from the enzymes. Instead, the suspension was centrifuged at 14,000 rpm for 20 min and the supernatant discarded, followed by three washes with milli-Q water, one with 2% SDS and three more with milli-Q water with centrifugation in between at the same rate and time. The sample was dried at room temperature and kept in vacuum until its analysis.

5.11.2.9. Suspension of HA functionalized with TFE in a mixture of amino acids

For this control, we repeated the procedure followed in **section 5.11.2.8** for the suspension of intact HA in amino acids); however, instead of using pristine HA, we used HA functionalized with TFE, obtained following the procedure described in **section 5.11.2.4**.

5.11.2.10. UV-Vis measurement of RBC membranes

The absorbance of the RBC ghosts was measured using a microplate reader (SpectraMax i3, Molecular Devices, California, USA) at a wavelength of 280 nm, where the 5 mM NaH₂PO₄ buffer at pH 8 was used as a blank.

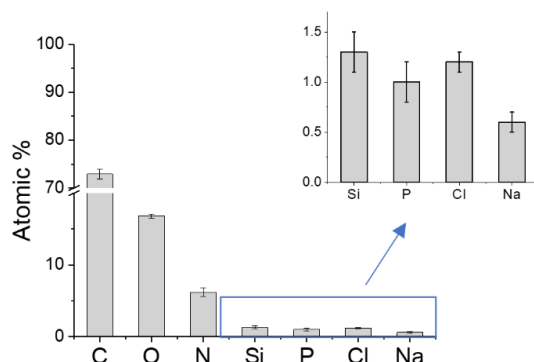


Figure S.5.11.1. Experimental atomic percent measured from XPS surveys for dead parasites of *P. falciparum* 3D7 washed with hexane and dichloromethane.

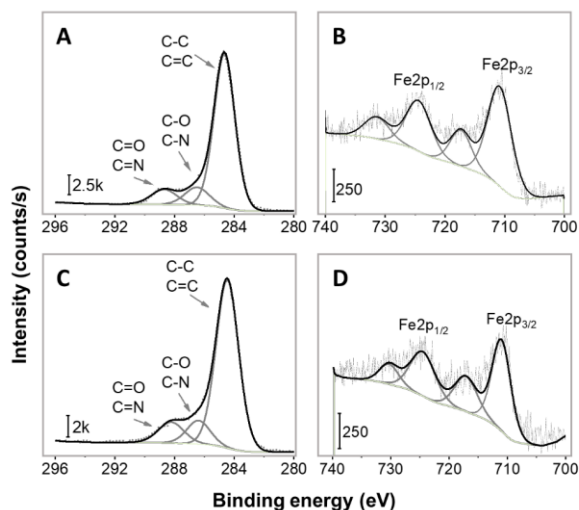


Figure S.5.11.2. XPS high resolution of C_{1s} collected for (A) pwHz and (C) ewHz. XPS Fe_{2p} obtained for (B) pwHz and (D) ewHz. Experimental data is presented in gray dotted line, peaks fit in gray continuous line, and the overall fit in black. The C_{1s} spectra of both samples show a signal at 284.5 eV corresponding to C-C/C=C from the porphyrin ring and side chains; while the peaks at 286.5 and 288.4 eV are assigned to C-O and C=O, respectively from the carboxylates. These peaks also have contributions from C-N and C=N from the porphyrin ring [164]. The Fe_{2p} spectra show the characteristic peaks of the spin-orbit splitting of Fe. The Fe_{2p_{3/2}} and Fe_{2p_{1/2}} doubles at 711.2 and 725 eV, respectively, are representative of Fe in oxidative state III.[164]

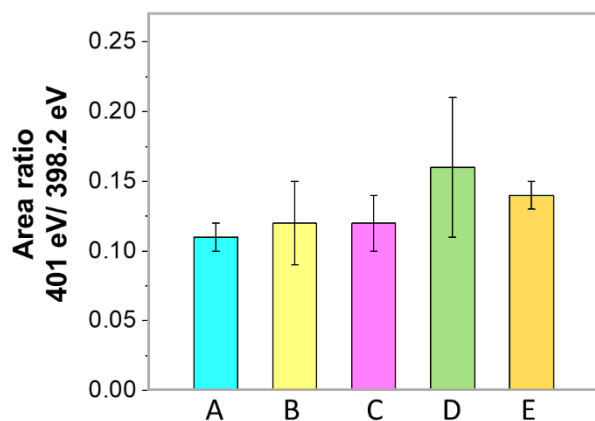


Figure S.5.11.3. Area ratios of the XPS N_{1s} 401 eV/398.2 eV peak acquired for HA suspended in: (A) dead parasites of *P. falciparum* of the clone 3D7 (turquoise bar), (B) RBC membranes (yellow bar), (C) enzymes and detergents used to prepare ewHz (pink bar), (D) mixture of amino acids (green bar) and (E) mixture of amino acids after derivatization of HA surface carboxylate groups (orange bar).

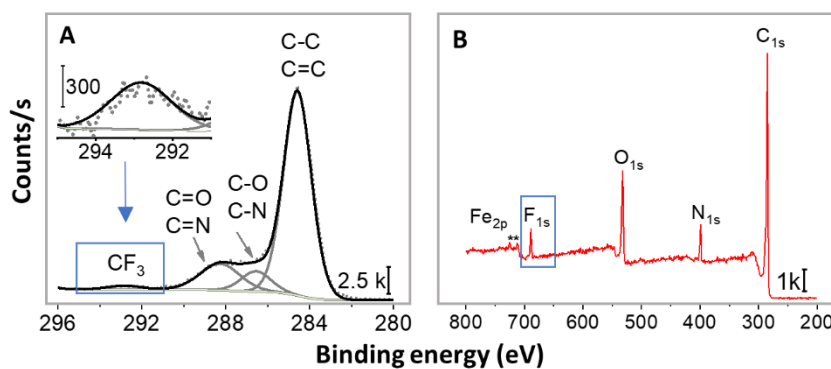


Figure S.5.11.4. XPS data of (A) high resolution of C_{1s} and (B) survey of HA after a surface esterification of the -COOH groups by TFE. The new peak around 292 eV in the C_{1s} spectra (inset in panel A) and the new signal at 688.4 eV in the survey evidence the successful functionalization of HA surface.

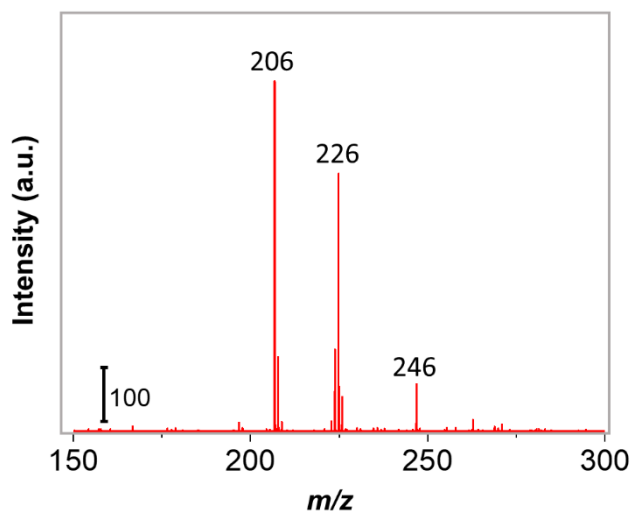


Figure S.5.11.5. Mass spectrum of sinapinic acid used as matrix for the analysis with MALDI-ToF showing the molecular masses at m/z 206, 224 and 246, also found in HA, ewHz, and HA washed with a thorough procedure. The matrix was mixed with trifluoroacetic acid and the spectrum acquired as described in **Experimental Section 5.3.2.4** of the main manuscript.

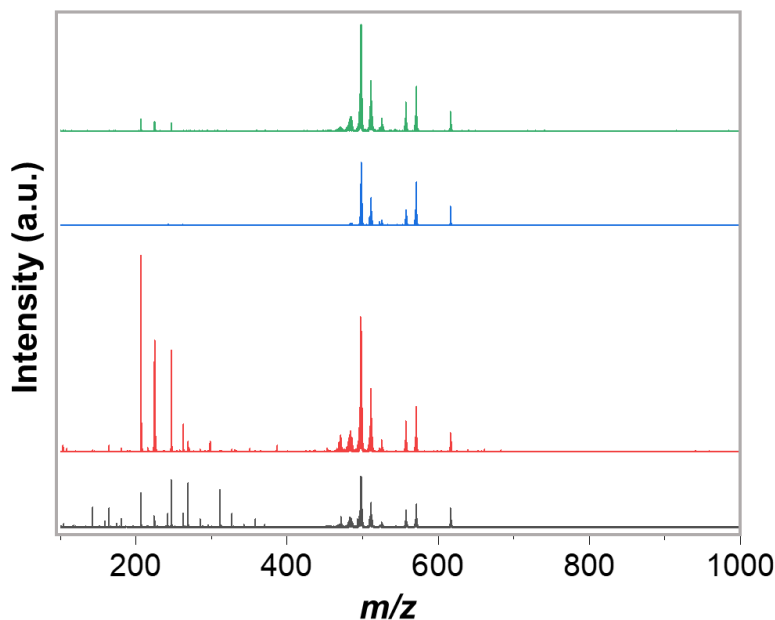


Figure S.5.11.6. Representative MALDI-ToF mass spectra of positive ions in reflectron mode collected in the m/z region of 100-1000 for HA (green), pwHz (blue), ewHz (red) and HA treated with the extensive washes (black). The intensity was normalized with respect to the intensity of the peak at 616 Da.

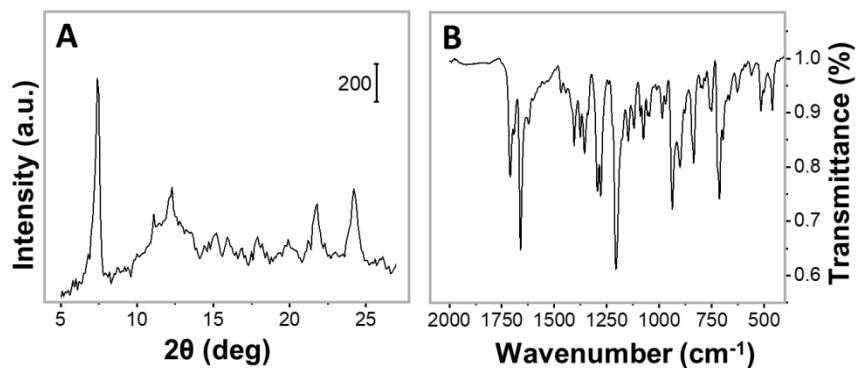


Figure S.5.11.7. (A) XRD spectrum obtained for HA synthesized by the acid-annealing method and used for all the controls presented in this work. The spectrum shows the characteristic peaks of HA at 7.5°, 21°, and 24°.[14] (B) FT-IR spectrum of HA showing the peaks of at 1664 and 1209 cm⁻¹, representative of the coordination between the iron in heme and a propionate group. The peak located at 1712 cm⁻¹ is characteristic of the hydrogen-bonded carboxylate group that links the heme dimers to extend the crystalline array.[32, 190]

Table S.5.1 XPS binding energies and area ratios of O_{1s} obtained for HA, pwHz, and ewHz. The peaks at 531.5 and 533.3 eV for all the samples were fitted according to the experimental FWHM obtained for HA.

Sample		<u>O</u> -Fe and OH from water	C= <u>O</u>
HA	BE (eV)	531.6 ± 0.1	533.3 ± 0.1
	Area ratio	1	0.22 ± 0.09
	FWHM (eV)	2.5 ± 0.1	2.1 ± 0.1
ewHz	BE (eV)	531.5 ± 0.1	533.3 ± 0.1
	Area ratio	1	0.42 ± 0.07
	FWHM (eV)	2.5 ± 0.1	2.1 ± 0.0
pwHz	BE (eV)	531.7 ± 0.2	533.3 ± 0.1
	Area ratio	1	0.28 ± 0.03
	FWHM (eV)	2.5 ± 0.0	2.1 ± 0.0

Table S.5.2. XPS binding energies and area ratios of N_{1s} obtained for HA, pwHz, ewHz and all the controls used, in which HA was suspended in different solutions. The peaks at 398.2 and 401.1 eV for all the samples were fitted according to the experimental FWHM obtained for HA; whereas the peak at 399.7 eV was fitted according to the FWHM obtained for ewHz.

Sample		N-Fe	sp ³ -N	sp ² -N / π - π^*
HA	BE (eV)	398.2 \pm 0.2	-	401.0 \pm 0.1
	Area ratio	1	-	0.13 \pm 0.02
	FWHM (eV)	1.2 \pm 0.1	-	1.8 \pm 0.3
pwHz	BE (eV)	398.1 \pm 0.2	399.2 \pm 0.5	401.0 \pm 0.8
	Area ratio	1	0.88 \pm 0.07	0.49 \pm 0.07
	FWHM (eV)	1.3 \pm 0.1	1.5 \pm 0.1	1.5 \pm 0.1
ewHz	BE(eV)	398.2 \pm 0.1	399.7 \pm 0.2	401.2 \pm 0.2
	Area ratio	1	0.45 \pm 0.13	0.21 \pm 0.08
	FWHM (eV)	1.3 \pm 0.1	1.5 \pm 0.2	1.5 \pm 0.1
HA in parasites	BE (eV)	398.1 \pm 0.1	399.7 \pm 0.1	401.2 \pm 0.1
	Area ratio	1	0.29 \pm 0.02	0.11 \pm 0.01
	FWHM (eV)	1.1 \pm 0.0	1.5 \pm 0.0	1.4 \pm 0.1
HA in RBC membranes	BE (eV)	398.1 \pm 0.1	399.8 \pm 0.1	401.1 \pm 0.3
	Area ratio	1	0.41 \pm 0.07	0.12 \pm 0.03
	FWHM (eV)	1.2 \pm 0.1	1.4 \pm 0.2	1.5 \pm 0.1
HA treated with enzymes	BE (eV)	398.1 \pm 0.0	399.7 \pm 0.1	401.3 \pm 0.1
	Area ratio	1	0.25 \pm 0.04	0.12 \pm 0.2
	FWHM (eV)	1.2 \pm 0.0	1.5 \pm 0.0	1.5 \pm 0.1
HA in amino acids	BE (eV)	398.1 \pm 0.0	399.4 \pm 0.1	401.4 \pm 0.1
	Area ratio	1	0.25 \pm 0.14	0.14 \pm 0.21
	FWHM (eV)	1.2 \pm 0.1	1.5 \pm 0.1	1.8 \pm 0.2
HA-TFE in amino acids	BE (eV)	398.2 \pm 0.0	-	401.0 \pm 0.1
	Area ratio	1	-	0.12 \pm 0.1
	FWHM (eV)	1.2 \pm 0.0	-	1.7 \pm 0.1

Chapter 6. Inorganic ions on hemozoin surface provide a glimpse into

Plasmodium biology

In the previous chapter, we showed that the protocol to clean Hz affects the surface composition of the organic residuals adhered onto its surface after isolation of the crystals. We also showed that the cleaning protocol introduces partial contamination on Hz surface. In fact, the crystals may never be free of surface contamination, possibly because the “contaminant” molecules may be part of the crystalline structure of Hz. This knowledge clarifies the conflicting results reported in the literature when Hz is used as a model to assess its role in the pathogenesis of malaria. In addition, we proposed XPS and MALDI-ToF as powerful characterization techniques to assess the surface of Hz before its use for immune response tests. This would allow researchers to discriminate between the role of Hz and that of surface contaminants during their tests.

We also found that shortening the washing steps resulted not only in a larger amount of residuals unable to be removed but also in the presence of extra inorganic compounds such as sodium, chlorine, silicon, calcium, and phosphorus. These inorganic compounds have not been previously reported or identified; moreover, there is not much information related to the biochemical composition of what is bound to native Hz.

In this study, we attempt to address the following questions:

- i) What inorganic species are present in native Hz?
- ii) What is the chemical environment and possible source of the unidentified inorganic species? And do these components vary according to the model used to obtain Hz, i.e. *in vivo* or *in vitro*?

The findings of this work are submitted to a peer-reviewed journal.

Guerra E.D., Baakdah F., Gourgas O., Tam M., Stevenson M. M., Georges E., Bohle D. S., Cerruti M.

6.1. Abstract

In malaria, *Plasmodium* parasites produce hemozoin (Hz) as a route to detoxify free heme released from the catabolism of hemoglobin. Hz isolated from the parasites is encapsulated in an organic layer formed after the interaction between the crystals and parasite and host constituents. The components of this organic coating may play a role in Hz formation and in the immunomodulatory properties attributed to Hz, and they also may influence the mode of action of antimalarials that block Hz formation. Proteins, carbohydrates, and traces of nucleic acids and lipids have been identified among the constituents of the organic layer adsorbed on Hz, but the actual composition is likely to depend on the models used to produce Hz. In this work, we analyze the organic layer adhered to Hz collected from *in vitro* and *in vivo* models of *Plasmodium*, and find Na, Cl, Si, Ca and P present, in addition to organic material. Our results suggest that Na, Cl, and P adsorb during Hz release from the red blood cells, while Si and Ca derive from components present during Hz biomineralization within the digestive vacuole of the parasite. In fact, we find Si in *Plasmodium* is present both as SiO₂ and hydrated solubilized silica or Si covalently bound to organic cell components; we propose that these Si compounds may be involved in the parasite's survival, as observed in plants, diatoms, and mammals, and may be among the causes of the immunogenic response to Hz in humans. Overall, we show that inorganic elements adsorbed on the surface of Hz organic coating provide insights into the biological functions of *Plasmodium* parasites.

6.2. Introduction

Malaria is a life-threatening disease caused by parasites of the *Plasmodium* genus that are transmitted by the bite of an infected female *Anopheles* mosquito [5]. During the asexual stage of *Plasmodium*, the parasite feeds on hemoglobin, releasing heme inside its digestive vacuole (DV). Free heme can inhibit multiple enzymes, disrupt cell membranes and produce cell lysis [141]. Therefore, to avoid its deleterious effects, the parasite sequesters heme to form an insoluble crystal called hemozoin (Hz), also known as the malaria pigment [5].

Hz crystallization starts with two heme molecules binding through an iron-carboxylate bond forming dimers; the dimers are further linked through hydrogen bonds in a crystalline structure [7]. Although the structure and biochemistry of Hz are mostly understood, its biomineralization process is not completely elucidated at the molecular level, especially the role of different biomolecules in promoting crystal nucleation and growth [191].

Hz is the antimalarial target of the quinoline family of drugs and probably of artemisinins, which exert their effect by interfering with the crystal formation [10]. However, the exact mechanism of action of these drugs is still under debate [8], and the widespread resistance to this class of antimalarials threatens their efficacy [2]. Hz birefringence and optical dichroism [11] are exploited in malaria diagnosis *in vivo* [113]; while its paramagnetic properties serve as biomarker for malaria diagnosis in blood smears [11]. This property is also extensively used for the separation of infected RBC from healthy ones *in vitro* [115] and further crystal purification in magnetic separators [116]. In addition, Hz modulates the immune response during malarial infection [8].

The biological activity of Hz and its role in the host immune response is a controversial topic. It is usually tested using Hz synthetic counterpart, hematin anhydride (HA) (also known as β -hematin), or different Hz preparations obtained from *in vitro* or *in vivo* models [15]. However,

these reports often produce inconsistent or irreproducible results [13]. For example, one study showed that by cultivating fresh extracts of Hz with monocytes, the cells were unable to mature into dendritic cells [130]. Contrary to these observations, another study showed that purified Hz enhanced dendritic cell maturation [129]. Hz also contributes to malarial anemia by suppressing red blood cells (RBC) proliferation *in vivo* [136, 162, 163], but HA has lower activity compared to Hz [136]. Also, it was observed that Hz remains unaltered inside macrophages for extended periods, whereas HA is vulnerable to degradation by phagocytosis of macrophages [13].

The differences in biological activity between HA and Hz may be associated with differences in crystal size and morphology [136]. Additionally, several studies indicate that during the isolation of Hz, the crystals interact with lysed parasitic cells and erythrocytes [178], whose constituents may ultimately adsorb onto Hz [8], forming a coating that is often considered “contamination” [5]. Some groups have also proposed that this coating is implicated in the immune response associated with Hz [13]; thus, it is not clear whether the immunomodulatory properties of Hz are caused by the crystals or the material adsorbed onto their surface [8]. Furthermore, there are many reported procedures to purify Hz prior to its analysis, which lead to a variety of unidentified biomolecules adsorbed onto Hz that in turn may impact the immunogenic response [8, 13, 192].

Previous attempts to elucidate the composition of the organic coating adhered onto Hz revealed that it is mainly constituted by proteins, carbohydrates, amino acids, traces of lipids and nucleic acids [178, 193]. The amounts of these constituents differ depending on the technique used to purify the crystals since some material is lost or degraded during Hz isolation and treatment [178]. Some researchers identified histidine-rich proteins in crystals obtained from different species and strains of *Plasmodium* [29], while others found neutral and polar lipid mixtures associated to Hz

isolated from *P. falciparum* and treated by a sucrose cushion method [55]. These compounds may be related to components inside the DV of the parasite or the host RBC [8].

Also, the composition of the organic material on Hz extracted from *in vitro* cultures may differ from the crystals obtained from *in vivo* models due to several cycles of Hz phagocytosis by circulating monocytes and tissue macrophages [8]. Ingestion of Hz by many generations of phagocytes causes the adsorption of a variety of biomolecules onto its surface, producing Hz with altered morphology and biochemical composition. All of these differences could be responsible for the variable results obtained when evaluating the biological activity of Hz [8].

Last but not least, while most works debate over the type of biomolecules present in the coatings (lipids, proteins, carbohydrates, etc.), our previous study identified Si and Ca in the coating of Hz derived from *in vitro* cultures of *P. falciparum* [192], and another work mentioned the presence of Ca derived from Ca²⁺-dependent protein kinase 1 (CDPK1) in DV membranes and the organic material adsorbed on Hz [174]. Nothing is known about the role of these inorganic ions in Hz biomineralization, and their presence could also influence the mode of action of some antimalarials. Also, additional inorganic species could be adsorbed on Hz, which may have been missed by previous reports due to the extensive washing.

Some key questions are thus: what is present on the coating adsorbed on Hz? How does its composition vary among the different models used to grow the parasite? And, more deeply: can we learn something about Hz formation and *Plasmodium* functions by analyzing this layer?

In this work, we answer these questions by studying the composition of the material adhered on Hz obtained from an *in vitro* and an *in vivo* model of *Plasmodium* using a surface-sensitive technique, X-ray photoelectron spectroscopy (XPS), combined with near-edge X-ray absorption fine structure (NEXAFS) and scanning electron microscope (SEM)/energy-dispersive X-ray

spectroscopy (EDS). We find that several inorganic ions are consistently present on all Hz models we analyzed. To understand the origin of these elements, we compared the elemental species found on Hz and on HA immersed in solutions that simulate the components that may adhere onto Hz during its synthesis and ejection from the RBC. Based on these results, we suggest some hypotheses on the biological function of these elements in *Plasmodium*.

6.3. Results and Discussion

We extracted Hz from Chloroquine (CQ)-sensitive *P. chabaudi* AS infected macrophages (Mφ), and *P. falciparum* *in vitro* cultures of the strains 3D7-H (also CQ-sensitive) and 7G8 (CQ-resistant). The materials were washed mildly with organic solvents (**Methods 6.5.2.3**) to remove the parasitic cell debris and host components weakly adhered to the crystals surface, while preserving the components strongly adsorbed. For this reason, these samples are referred to as native hemozoin (nHz) in this work.

XPS analysis of these samples (**Figure 6.3.1.A**) showed the presence of C, O, and N, but no Fe. This implies that the mild washes with hexane and dichloromethane were not sufficient to eliminate all the organic coating and expose a “pure” Hz surface. This was confirmed by SEM (**Figure 6.3.1.B**), which showed Hz crystals coated by a thin shroud of organic matter, in contrast with Hz treated with enzymes and detergents after isolation (**Figure 6.3.1.C**). This result implies that the signals of C, O, and N are mostly due to the proteins, cell debris and traces of lipids and carbohydrates that may constitute the organic coating, rather than the porphyrin ring of Hz [178]. This is also confirmed by the finding of the unexpected inorganic elements Na, Cl, P and Si in all the samples, and additionally Ca in Hz collected from *P. chabaudi*-infected murine Mφ and *Pf* 3D7-H strain.

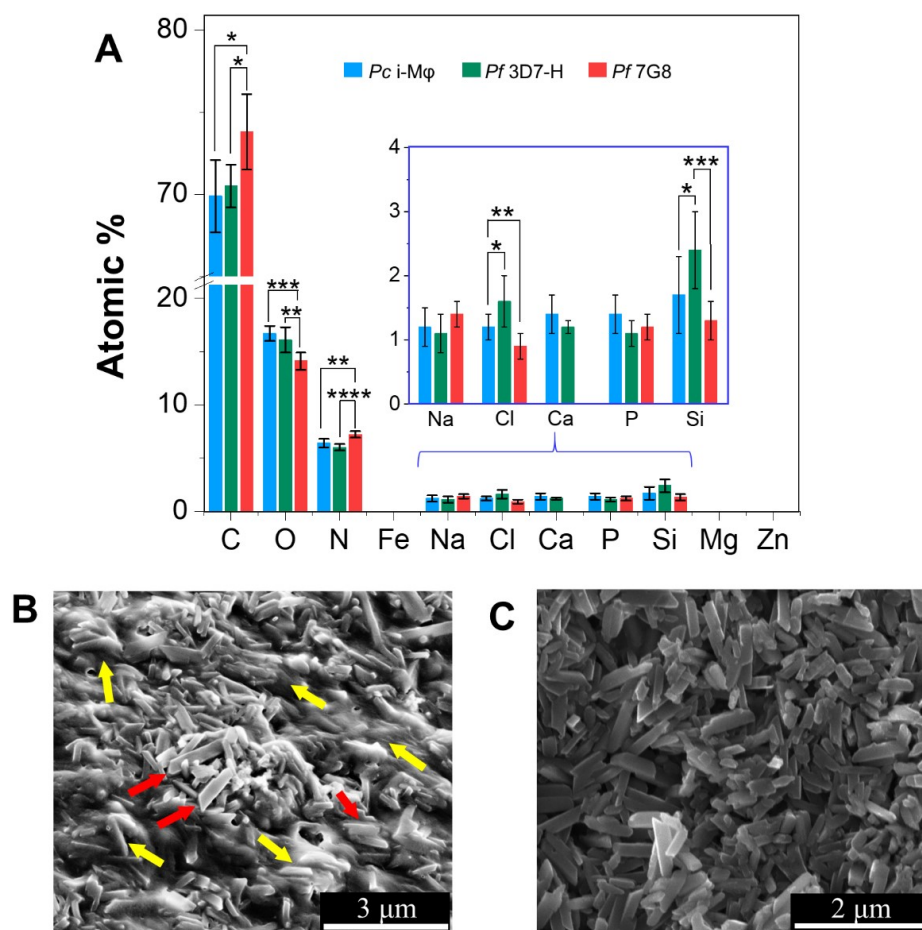


Figure 6.3.1. A) XPS survey collected for nHz samples obtained from CQS *P. chabaudi* AS infected-macrophages (blue) and *P. falciparum* of the strains 3D7-H (CQS, green) and 7G8 (CQR, red), (no significant differences were found among samples). Data represent mean \pm s.d. of 3 independent samples and three different spots analyzed along the same sample. One-way ANOVA test was used for statistical analysis, followed by Bonferroni's test correction to evaluate the statistical difference of multiple samples, where $P < 0.01$ was considered a significant difference. All data are expressed as mean \pm standard deviation (SD). *Significant differences between atomic percentage, with $*P < 0.01$, $**P < 0.001$, $***P < 1 \times 10^{-5}$ and $****P < 1 \times 10^{-6}$. SEM images of B) nHz crystals rinsed with hexane and dichloromethane. The red arrows indicate the crystals devoid of most of the cell components, while the yellow arrows note the crystals still coated with biological residues. C) Clean sample of Hz showing individual crystals lacking most of the organic residues as a result of treatment for proteins precipitation, enzymatic hydrolysis, and rinses with detergents and water, as reported in [192]. Data represent mean \pm SD of 3 independent experiments.

The fact that the inorganic species are present in all nHz samples regardless of the source suggests that these elements are introduced during Hz biomineralization, its egress during schizogony or from the RBC. Calcium was not found in one of the nHz collected from *in vitro* cultures probably due to the strain of *P. falciparum* used to collect the Hz. The absence of Mg and

Zn in all the samples of nHz indicates that nucleic acids are not present in significant amounts [194], as these ions are typically arranged within the structure of DNA and RNA [169, 195].

We previously reported the presence of Si and Ca on the surface of Hz samples extensively washed with solvents, proteinase K in an alkaline buffer, and detergents [194]; however, we did not detect any Na, Ca and P on these samples. This shows that while Si and Ca adsorb strongly and possibly are part of the bulk structure of Hz crystals, P, Na and Cl are just weakly adsorbed on the outer layer of the crystal, along with organic material. This suggests that Si and Ca may be introduced during Hz formation in the DV of the parasite, while Na, Cl, and P may be adsorbed during the release of Hz from the DV and RBC.

To study the spatial distribution of the inorganic elements associated with nHz, we collected energy dispersive spectroscopy (EDS) maps of samples of nHz produced from *in vitro* cultures of *P. falciparum* 3D7-H. These samples were rinsed with water to remove any excess ions present in the extraction buffers (**Methods 6.6.2.14**). **Figure 6.3.2.A** shows the crystals “encapsulated” in the organic layer. The EDS map of nHz showed the presence of C, O, N, Fe, characteristic of Hz, as well as Na, Cl, Si, Ca and P, confirming the XPS data. EDS detected Fe (**Figure 6.3.2.B**) because it is a less sensitive surface technique than XPS, sampling approximately 0.2-1 μm [196] rather than the 3-10 nm analyzed by XPS [197].

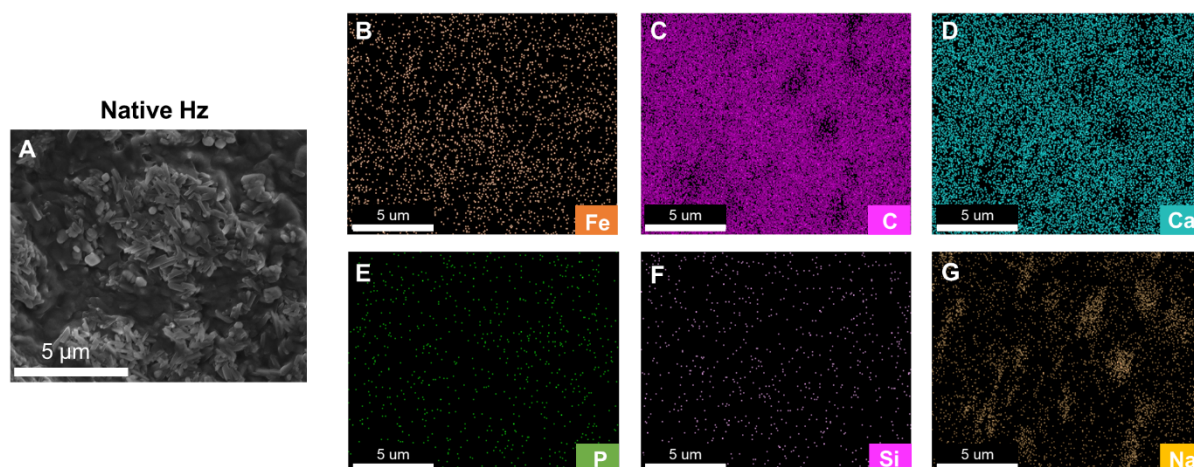


Figure 6.3.2. A) Scanning electron microscopy (SEM) images of nHz obtained from *P. falciparum* strain 3D7-H and energy-dispersive x-ray spectroscopy elemental (EDS) mapping for B) Fe, C) C, D) Ca, E) P, F) Si and G) Na.

The EDS maps showed a close correlation between the location of C and Ca (**Figure 6.3.2.C** and **D**, respectively), but no correlation between Ca and P. This indicates that Ca may be present in an organic environment. Si appears distributed evenly along the whole area mapped in small quantities, while Na and Cl are present in the spots lacking C and Ca. This suggests the presence of adsorbed Na and Cl salts on the organic layer of Hz.

To determine if the inorganic elements found in nHz derive from parasitic debris, we studied the surface composition of *P. falciparum* parasites of the 3D7-H strain, rinsed with the same organic solvents used to prepare nHz (**Methods 6.6.2.1**). XPS analysis showed Na, Cl, Si, and P (**Figure S.6.6.1**), indicating that these elements indeed may originate from the parasites themselves. Na^+ and Cl^- are ions commonly found within the parasite, erythrocytes and the buffers used to extract Hz [168, 198, 199]; therefore, it is not surprising to find these elements associated with nHz and the parasites, probably as Na and Cl salts, as mentioned above. However, XPS did not detect any significant amount of Ca on *Plasmodium*, possibly because this element is found

mostly within parasitic organelles, which are beyond the sampling limit of surface-sensitive XPS [194].

In the following sections we focus on understanding the speciation of Ca, Si and P found on nHz as a means to understand their possible origins.

Atomic environment of silicon

The XPS Si_{2p} spectra of nHz obtained from *P. falciparum* 3D7-H cultured *in vitro* showed two peaks located at 101.9 ± 0.1 and 103.2 ± 0.0 eV (**Figure 6.3.3.A**). The peak located at 103.2 eV has been related to Si in SiO₂ [200] or Si in carbon-silica composites [201], while the peak at 101.9 eV has been assigned to Si in a more reduced state. These same results were obtained for nHz collected from different strains of *Plasmodium* in an *in vitro* and *in vivo* model (**Figure S.6.6.2**).

To determine if the observed Si derives from the parasite cultivation media or the process of Hz extraction, we suspended HA in blood serum, RBC membranes and in the buffers used to lyse the parasites (**Methods 6.6.2.3**). The XPS survey spectra did not show any Si on these samples (**Figure S.6.6.3**), suggesting that the Si in nHz is most likely parasitic-derived. To confirm this hypothesis, we analyzed *Plasmodium* parasites (**Methods 6.6.2.1**). The Si_{2p} spectra of this sample (**Figure 6.3.3.B**) showed two signals located at 101.9 ± 0.1 and 103.1 ± 0.2 eV, identical to the peaks found in nHz ($P=0.79$ and $P=0.27$, respectively).

To understand the origin of the two observed Si species in nHz and *Plasmodium*, we suspended HA crystals in different solutions containing Si compounds and studied the chemical environment of the Si_{2p} signal coming from the crystal surface afterward. First, we suspended HA in a solution of silicic acid (**Methods 6.6.2.7**), also known as hydrated silica (Si(OH)₄). This compound is slightly soluble in water and is naturally absorbed by vascular plants [202, 203]. The Si_{2p} spectrum on this sample (**Figure 6.3.3.C**) showed a peak centered at higher energy (104.2 ± 0.0 eV,

$P=5.2 \times 10^{-11}$) than the peaks found on nHz (**Figure 6.3.3.A**), suggesting that the Si species found on the organic coating of Hz do not contain silicic acid.

Next, we evaluated cucumber skin (*Cucumis sativus*) since this plant is Si-rich. The XPS Si_{2p} analysis of this sample (**Figure 6.3.3.D**) revealed two peaks located at 101.9 ± 0.1 and 103.2 ± 0.3 eV at positions very close to those found on Hz ($P=0.25$ and $P=0.34$). We analyzed also the branch of another Si-rich plant commonly known as horsetail (*Equisetum hyemale*) and obtained similar results ($P=0.06$ and $P=0.79$, with respect to Hz) (**Figure 6.3.3.E**). The XPS Si_{2p} signals of both plants are very close to those found in nHz, which suggests that the Si-species in these two plants are similar or equivalent to those found on nHz. In addition, the location of the 102.0 eV peak has been reported for compounds containing SiO_4^{4-} anions in the form of oligomerized hydrated silica in studies of silicon-substituted apatites [204, 205].

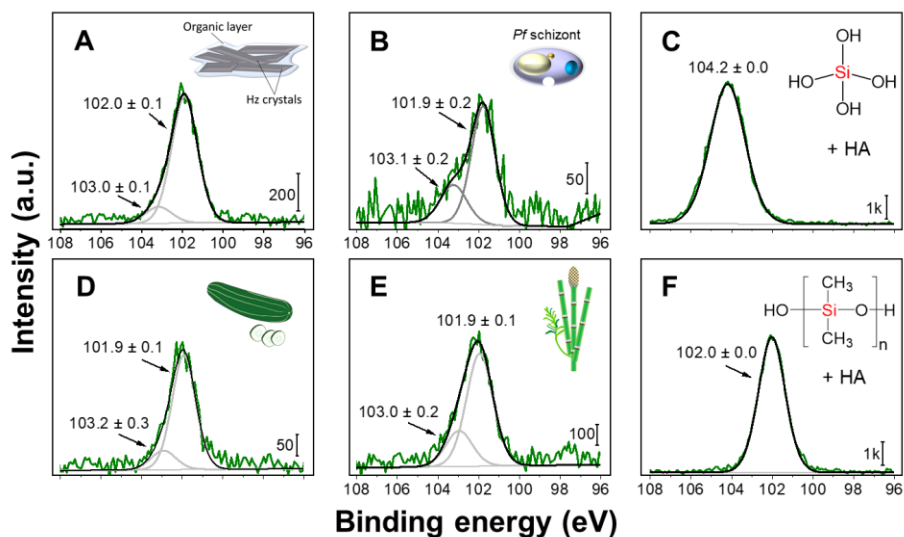


Figure 6.3.3. XPS high-resolution spectra of Si_{2p} collected for A) Hz extracted from *P. falciparum* of the strain 3D7-H, B) *P. falciparum* parasites of the strain 3D7-H, C) HA suspended in silicic acid, D) cucumber skin (*Cucumis sativus*), E) horsetail (*Equisetum hyemale*) and F) HA suspended in PDMS (Mn~550). Experimental data is shown in green, peaks fit in gray, and the overall fit in black.

The peak at approximately 102 eV could also correspond to silicon oxycarbide compounds in the form of SiO_3C and SiO_2C_2 [206]. To explore this option, we suspended HA in a solution of poly(dimethylsilane) (PDMS) (**Methods 6.6.2.8**), a polymer containing a silicon oxycarbide (SiO_2C_2) bond in its structure. The XPS Si_{2p} spectrum of this sample revealed a single peak centered at 102.0 ± 0.0 eV (**Figure 6.3.3.F**). This analysis highlights the unusual biochemistry of the Si species associated with nHz. Since no other groups ever reported Si in *Plasmodium* parasites, we can only hypothesize its physiological role. In plants, Si enhances the activity of the enzymes responsible for the defense against biotic stress due to pathogen attacks, and abiotic stresses such as drought, temperature, salinity and metal toxicity [207-209]. Hence, Si is required for the growth and development of many plants species [207].

In diatoms, the metabolism of silicic acid provides a vital source of nutrients for structural growth; they incorporate Si into the cell walls to form a structure called frustule [210]. Diatoms possess intracellular pools of soluble silicon at supersaturated concentrations, ranging from 19 to 340 mM, depending on the diatom species and the water content within the cell [210]. This silicon is maintained in a soluble form by interaction with organic components to produce mono-silicic acid or low molecular weight poly-silicic acid bound to biological components [210, 211].

In mammals and some fruits, Si is found covalently bound to the backbone of some polysaccharides through Si-O-C links formed between silicic acid and hydroxyl groups, resulting in a bridge of Si-O-C, i.e. as an ether (or ester) [212]. The Si-O-C link formed between silicic acid and hydroxyl groups is highly resistant to diluted alkali and acid. However, strong alkali and acid hydrolyze the Si-polysaccharide bond, releasing the silicon in the form of SiO_2 [212]. This observation suggests that the two Si_{2p} signals arising from nHz and *Plasmodium* may derive from Si bound to intracellular components of the parasite, as reported for diatoms and mammals. Thus,

the Si_{2p} contribution at 102.0 eV could be related to Si in Si-O-C bonds due to Si covalently bonded to carbohydrates, which were previously found on nHz [178], or to oligomerized hydrated silica. Meanwhile, the Si_{2p} signal at 103.2 eV could result from SiO₂ released from the partial hydrolysis of covalently bonded Si due to the acidic conditions of the DV.

It is possible that the parasite acquires silicon compounds from the host blood [213] as it is estimated that humans and other mammals average 0.5 mg of silicon per liter of blood plasma [202]. Based on these reports and our Si_{2p} spectra analysis, we hypothesize that inside the parasite there may be some reserves of soluble oligomerized hydrated silica chains, complexed by cell components, in addition to some SiO₂.

Since silica particles are known to cause acute inflammatory response [214, 215], the presence of Si on Hz surface could contribute to the immune modulation attributed to the crystals during malaria infection.

Atomic environment of calcium

We used both XPS and NEXAFS to study the atomic environment of calcium. The XPS high-resolution spectra of Ca_{2p} of nHz from *P. falciparum* 3D7-H (**Figure 6.3.4.A**) showed the two characteristic peaks associated with the spin-orbit splitting of Ca_{2p}. The samples showed the Ca_{2p_{3/2}} peak centered at 347.3 ± 0.1 and the Ca_{2p_{1/2}} peak at 350.7 ± 0.1 eV. As before, we suspended HA in blood serum, RBC membranes and in the buffers used to lyse the parasites (**Methods 6.6.2.6**) to determine if Ca came from the parasite culture media or the reagents used for Hz isolation. The XPS survey analyses did not show Ca on the surface of these samples (**Figure 6.6.2.6**), indicating that this element is *Plasmodium*-derived. In fact, there are various reserves of Ca²⁺ in the parasite, such as the endoplasmic reticulum, acidocalcisomes, mitochondria, Golgi apparatus, nuclei, and

even the DV where Hz is formed [173]. In the intraerythrocytic stage, Ca is found in the DV at an elevated concentration (250-300 nM), which is approximately 5 or 6 times higher than Ca in the cytosol [216]. During schizogony, free Ca^{2+} leaves the DV and redistributes in the intermembranes of each merozoite segment, followed by a rapid decrease in Ca content [216]. Since Hz is also released during schizont rupture, it may come into contact with this element during its egress.

To further understand the origin of the Ca species, we first suspended HA in a solution of calcium acetate (**Methods 6.6.2.9**), as a representative compound for calcium in an organic environment, e.g. calcium coordinated to carboxylates. The spectrum measured on this sample (**Figure 6.3.4.B**) was very close to that of nHz ($\text{Ca}_{2p_{3/2}}$ at 347.3 ± 0.1 , $P=0.86$), strongly suggesting that calcium atoms are derived from organic salts. This chemical environment also corresponds to Ca in calcium carbonate, which gives rise to a $\text{Ca}_{2p_{2/3}}$ signal at 347.2 eV [217], equivalent to what found in nHz. However, there are not sources of calcium carbonate in the parasite, thus, this compound is unlikely to be associated with nHz.

We also measured the Ca_{2p} spectrum on cucumber skin and found the $\text{Ca}_{2p_{3/2}}$ peak at 347.1 ± 0.0 eV, similar to Hz ($P=0.06$) (**Figure 6.3.4.C**). Plants and some Apicomplexa parasites share common Ca^{2+} - binding proteins [218], and the finding of similar Ca species suggests that the organic coating adhered onto nHz may contain Ca in a similar environment. These results suggest that Ca associated with nHz may be found in an organic matrix or coordinated to cellular components.

Calcium is also present in *Plasmodium* within acidocalcisomes; these acidic organelles serve as storage for cations, amino acids and concentrated phosphorous [219]. Calcium is pumped in the acidocalcisomes by Ca^{2+} -ATPase, where it is thought to bind to other molecules such as short and long chains of polyphosphate, within an acidic environment [173]. Acidocalcisomes are involved

in calcium homeostasis, intracellular pH and osmoregulation in bacteria, mammals, algae and other Apicomplexa besides *Plasmodium*, such as *Schistosoma*, *Toxoplasma* and *Trypanosoma* [220].

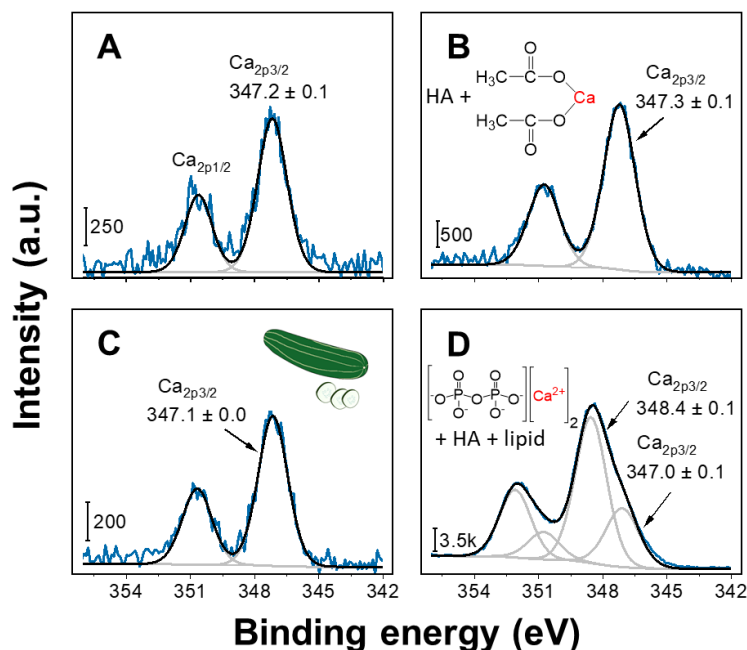


Figure 6.3.4. XPS high-resolution spectra of Ca_{2p} collected for A) Hz extracted from *P. falciparum* of the strain 3D7-H, B) HA suspended in calcium acetate, C) dried cucumber skin (*Cucumis sativus*) and D) HA and calcium pyrophosphate suspended in cholesterol. Experimental data is shown in blue, peaks fit in gray, and the overall fit in black.

To determine if the Ca in nHz coating could be related to Ca complexed with phosphorous from acidocalcisomes, we suspended HA in a solution of calcium pyrophosphate (Ca pyroP) (**Methods 6.6.2.10**). The XPS analysis of this control sample showed no adsorption of Ca pyroP on HA surface (**Figure S.6.6.5**). We hypothesized that this is because the synthetic crystals are devoid of the organic coating that is naturally present on nHz and could act as a binding intermediate.

To test this hypothesis, we evaluated the adsorption of Ca pyroP on HA crystals suspended in cholesterol (**Methods 6.6.2.11**). We selected this lipid to simulate the adherent capacity of the organic material adsorbed on nHz; also, this compound does not contain inorganic elements that

could give rise to overlapping signals. In the presence of cholesterol, the calcium pyrophosphate adsorbed onto HA crystals (**Figure 6.3.4.D**). This result shows the importance of an intermediate layer (lipidic in our example, but possibly proteinic too), as a means to adhere insoluble salts or solid particles on Hz.

The XPS analysis of Ca pyroP adhered to HA through cholesterol reveals two different $\text{Ca}_{2p_{3/2}}$ signals located at 347.0 ± 0.1 and 348.4 ± 0.1 eV (**Figure 6.3.4.D**). The signal at 347.0 eV is very close to that found on nHz ($P=0.13$) and is also found in calcium hydrogen phosphate (CaHPO_4 , **Figure S.6.6.4.A**); however, the presence of an additional $\text{Ca}_{2p_{3/2}}$ peak indicates that this compound produces Ca in two different chemical states, unlike what we found on nHz. This suggests that Ca pyroP are not likely to be the origin of the Ca found on nHz, confirming the EDS map results that did not show a strong association between Ca and P.

To determine more precisely the composition of the calcium compounds in nHz, we used Ca K-edge near-edge x-ray absorption fine structure spectroscopy (NEXAFS). This technique provides additional information about the geometrical arrangement of neighboring atoms surrounding an atom of interest [221]. To identify the Ca species present in nHz, we selected some reference samples representative of Ca in a variety of environments and performed linear combination fitting (**Methods 6.6.3.1**). Our reference samples included two calcium phosphates, *P. falciparum* parasites of the 3D7-H strain and calcium acetate ($\text{Ca}(\text{CH}_3\text{COO})_2$) as possible models for carboxylated calcium ions (**Methods 6.6.2.15**).

Figure S.6.6.6 shows the spectra obtained for native Hz, *P. falciparum* parasites of the strain 3D7-H and all the reference samples. All the samples showed a small pre-edge feature at around 4035 eV arising from the electronic transition from 1s to 3d orbitals [222]. The adsorption edge at around 4040 eV is assigned to the transitions associated to 1s to $4p_{1/2}$ and 1s to $4p_{3/2}$; the relative

intensities of the latter peaks are associated to the neighboring atoms surrounding the calcium [223].

The linear combination fitting results (**Table S.6.1**) showed that the Ca in nHz is mostly constituted by Ca acetate (around 90%), suggesting that Ca ions are present in an organic matrix, probably as calcium coordinated to carboxylate groups, again confirming both XPS and EDS map results. Conversely, the analysis of the parasites revealed that only a small proportion of Ca ions are present in the form of carboxylated calcium. This may be related to the calcium phosphate compounds stored inside the acidocalcisomes in the parasites [220] or due to the low concentration of Ca present in both samples that result in spectra with low signal-to-noise ratio.

Atomic environment of phosphorus

The XPS analysis of P_{2p} of nHz collected from *P. falciparum* 3D7-H cultured *in vitro* showed two peaks characteristic of the spin-orbit splitting of this element at 133.1 ± 0.1 eV (P_{2p3/2}) and at 133.9 ± 0.1 eV (P_{2p1/2}), as shown in **Figure 6.3.5.A**. As before, we analyzed the P_{2p} spectra of HA suspended in blood serum, RBC membranes and in the buffers used to lyse the parasites (**Methods 6.6.2.6**). Only phosphorus from RBC membranes adhered on Hz surface, producing a P_{2p3/2} signal at 133.5 ± 0.0 eV (**Figure 6.3.5.B**). The difference between this binding energy and that measured on nHz ($P=0.005$) suggests that despite the strong affinity of RBC membranes towards HA or Hz crystals [178], the P found on the organic coating of nHz may have a different origin; we hypothesized that it may be *Plasmodium*-derived. In fact, in the asexual stage of *Plasmodium*, P is found in the parasitic membranes in the form of phospholipids, especially phosphatidylcholine [224].

To test this hypothesis, we suspended HA crystals in solubilized phosphatidylcholine (**Methods 6.6.2.12**). The XPS P_{2p} spectrum of this sample (**Figure 6.3.5.C**) showed a $P_{2p_{3/2}}$ peak located at 132.9 ± 0.0 eV, very close to that in nHz ($P=0.07$), suggesting that phosphatidylcholine could adhere to the Hz surface when Hz is released from the parasite. These results suggest the presence of phospholipids or phosphorylated proteins derived from parasite structures in the organic layer of nHz, discriminating between possible P-containing contaminants in nHz.

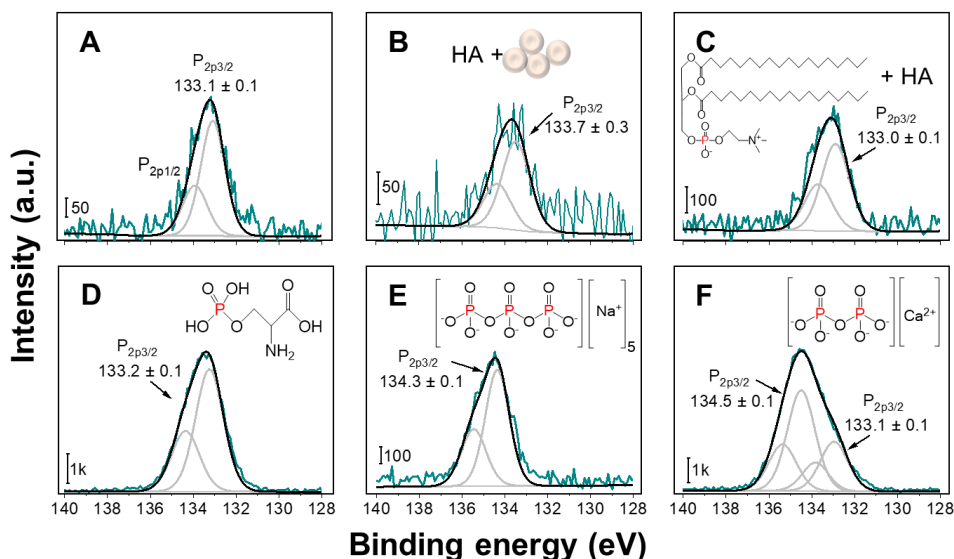


Figure 6.3.5. High-resolution P_{2p} XPS spectra collected for A) Hz extracted from *P. falciparum* of the strain 3D7-H, B) HA suspended in RBC membranes, C) HA mixed with PC, D) reference sample of ortho-DL-phosphoserine, E) sodium polyphosphate, and F) calcium pyrophosphate. Experimental data is shown in red, peaks fit in gray, and the overall fit in black.

In *Plasmodium*, phosphorus is also associated with the phosphorylation of some proteins [174]. We analyzed the $P_{2p_{3/2}}$ signal from ortho-DL-phosphoserine, as a compound representative of the chemical environment of P in an organic environment. The XPS spectrum (**Figure 6.3.5.D**) shows a $P_{2p_{3/2}}$ signal at 133.2 eV ± 0.1 eV, similar to that measured on nHz ($P=0.08$), showing that P in nHz could also originate from phosphorylated proteins.

Overall, the similar localization of the $P_{2p3/2}$ peaks of HA suspended in phosphatidylcholine and ortho-DL-phosphoserine suggests that the P associated to nHz might be present as an orthophosphate group (PO_4^{3-}) since this chemical environment is consistent among these samples and their energy is very close to that measured for nHz.

Another source of P in *Plasmodium* is acidocalcisomes [219]. We analyzed two P compounds formed inside acidocalcisomes: sodium polyphosphate (Na polyP), containing phosphoanhydride bonds $(PO_3)_n^{n-}$; and Ca pyroP, bearing $P_2O_7^{4-}$ ions [220]. Both high-resolution spectra of these compounds are different from that measured on nHz: on Na polyphosphate (**Figure 6.3.5.E**) the $P_{2p3/2}$ signal is at much higher binding energy (134.3 ± 0.1 eV, $P=1.2 \times 10^{-10}$), while on Ca pyroP we found two $P_{2p3/2}$ peaks at 133.1 ± 0.1 and 134.5 ± 0.1 eV (**Figure 6.3.5.F**). The signal at lower energy is identical to that in nHz ($P=0.6$) and calcium phosphate ($CaHPO_4$) (**Figure S.6.6.7.A**); however, the presence of an additional $P_{2p3/2}$ peak clearly indicates that this compound is not the one found in the organic coating of nHz. These results ruled out the presence of deposits from acidocalcisomes on the organic coating of nHz.

6.4. Conclusions and Outlook

In this work, we used XPS, NEXAFS, and EDS for the first time to study the elemental composition and speciation of the organic residues adhered to Hz collected from different models of *Plasmodium* and gently washed with organic solvents. We showed that the residues are not only constituted by C, O, and N, but they also contain a variety of inorganic elements, namely Na, Cl, Si, Ca and P. We found these inorganic elements in crystals both extracted from *Plasmodium* obtained from *in vitro* cultures and from macrophages derived from an *in vivo* model of rodents,

suggesting that their composition remains unaltered despite the interaction with a variety of cells or culture models. The fact that Ca was not found in some samples of nHz collected from *in vitro* cultures may be an indication that something is different in the Hz synthesis in the strains of *P. falciparum* used to collect the Hz. More studies should be pursued to explain this observation.

Biomolecules and inorganic elements may adhere to Hz during its biomineralization, its release from the DV or the parasite's egress from RBC. The observation that Ca and Si are strongly adsorbed on Hz suggests that these elements are related to Hz crystallization, whereas the weak adsorption of Na, Cl, and P on Hz surface may occur during the crystal's egress from the DV or RBC.

Even though XPS, EDS, and NEXAFS alone cannot determine the exact biomolecular composition of Hz's coating, our approach involving the use of controls as candidates for the adsorbed species in conjunction with high-resolution XPS spectra analysis has provided us with several crucial insights.

Possibly the most interesting finding from this work was the presence of two different Si species on nHz and on *Plasmodium* parasites of various strains, and its similarity with the Si-species found on Si-rich plants and possibly in mammals. To the best of our knowledge, there are no reports about the absorption of Si by *Plasmodium* or any other parasites; however, this element is essential for the development of plants and some algae with similar evolutionary lines of *Plasmodium* [225, 226], and is required for the normal growth and development of connective tissue and bones in mammals [227]. Several questions arise from these observations: first, what is the pathway, localization and function of Si in the parasite? Second, why is this element present on the surface of Hz? Finally, is it possible that the Si is associated with Hz biomineralization or implicated in the immune modulation of Hz in the host? Unlike Na, Cl, and P, we found Si on Hz surface even

after washes with high pH buffers and proteases [192]; this suggests that indeed Si may adsorb on Hz within the DV of *Plasmodium*. Our findings suggest that the parasites have reserves of solubilized hydrated silica, or Si bound to cell components, and some SiO₂. Further work is necessary to clarify this intriguing hypothesis and understand how/if it is related to Hz crystallization.

Both XPS and NEXAFS showed that Ca associated with nHz is most likely derived from Ca coordinated to carboxylate groups that may adhere to Hz during its release from the DV after schizogony. The carboxylate groups may derive from Hz surface or from proteins that may coordinate Ca in their structure, which is related to several vital functions for the development of the parasite and RBC invasion and egress [173]. Such proteins could be used as a target for the development of novel antimalarials [173].

As future work, the NEXAFS analysis could be extended to Si, Ca and P species in nHz using reference samples that best resemble their source and biological environment within the parasite. This analysis will help identify the inorganic species and their possible role in Hz biomineralization and in the immune modulation related to the crystals. A similar analysis could be also performed on Hz collected from other hematophagous parasites that produce Hz, such as *Schistosoma* or the bug of the triatomine species *Rhodnius prolixus*. This would determine if the inorganic species are preserved regardless of the parasite producing Hz, which in turn could provide further insights into their physiology and mechanism of survival.

6.5. Experimental

6.5.1. Materials

Reagent grade hexane, dichloromethane (DCM), sodium chloride, calcium chloride, sodium deoxycholate, and Igepal CA-630 were obtained from Sigma-Aldrich Canada. Sodium hydroxide

pellets and hydrochloric acid ACS grade were purchased from Fisher Scientific. RPMI 1640 and L-glutamine were acquired from Gibco (Life Technologies), Halt protease inhibitor (single use cocktail, 100x) was purchased from Thermofisher Scientific. Practical grade saponin from Quillaja Saponaria Molina and *N*-2-hydroxyethylpiperazine-*N'*-2-ethanesulfonic acid (HEPES) were obtained from Acros Organics MS and sorbitol from Sigma life sciences. Phosphate buffer saline (PBS) tablets were purchased from BioShop, Canada Inc. A+ blood was purchased from The Interstate Blood Bank, INC.

Stock solutions of 25 mM HEPES, 0.05% saponin in PBS (1x) and 5% sorbitol, PBS (1x, pH 7.4), 10 mM Tris-HCl (pH 8) were prepared in advance. 10 mM CHAPS buffer was prepared by mixing 150 mM NaCl, 1 mM CaCl₂ and the protease inhibitor in 50 mM Tris HCl, with the pH adjusted to 7.4. RIPA (radioimmunoprecipitation assay) buffer was prepared using 50mM Tris HCl (pH 7.4), 1% Igepal CA-630, 0.25% sodium deoxycholate and the protease inhibitor. The pH of the stock solutions was adjusted with 0.1 M HCl or 0.1 M NaOH. Milli-Q water from a Barnstead purification system (resistivity of 18.2 MΩ-cm) was used to prepare all the solutions and experiments unless specified. Protein LoBind tubes were purchased from Eppendorf.

6.5.2. Methods

6.5.2.1. *In vitro* cultivation of *P. falciparum* and H₂ extraction

Plasmodium falciparum of the CQ-sensitive strain 3D7-H and CQ-resistant strain 7G8 were cultivated in A+ human erythrocytes in a 2% hematocrit maintained in a synchronous culture with RPMI 1640 media supplemented with 10% (v/v) human plasma, L-Glutamine and 25 mM HEPES, as reported by Trager and Jensen's cultivation method [168]. The parasitic blood stages were synchronized using 5% sorbitol, and the parasites were collected at the late trophozoite stage,

followed by washes with PBS. Then, 0.05% saponin in PBS was added to lyse the red blood cell, followed by washes with PBS and extraction with 10 mM CHAPS or RIPA buffer. The lysates were centrifuged at 15k rpm for 10 min, with the temperature controlled at 4°C. The supernatant was removed, and the resulting Hz was resuspended in PBS and stored at 4°C for further treatment.

6.5.2.2. Mice infection and Hz extraction

Parasites and Animals

P. chabaudi AS was maintained in mice, by weekly passage, as described in the literature [136]. Female C57BL/6 (B6) mice 8-12 weeks old, purchased from Charles River Laboratories, were infected intraperitoneally with 1×10^6 parasitized RBCs (PRBCs). Infected B6 mice were sacrificed and spleens were harvested during peak parasitemia of >35% PRBC. Mice were maintained and handled according to the guidelines of the Canadian Council on Animal Care and the McGill University Animal Care Committee (ACC). All procedures performed on experimental mice were approved by the McGill University ACC (Protocol #2015-3750).

Preparation of splenic macrophages

Spleens from infected mice were perfused with complete RPMI 1640 medium (Life Technologies, Burlington, ON, Canada) supplemented with 10% heat-inactivated fetal calf serum (FCS), 25 mM HEPES (Life Technologies), 0.12% gentamicin (Life Technologies), and 2 mM glutamine (Life Technologies) and spleen tissues were pressed through a sterile steel mesh. Spleen cells were centrifuged, re-suspended in 0.175 M NH_4Cl to lyse red blood cells (Sigma-Aldrich), washed, counted and re-suspended in complete RPMI 1640 medium to 5×10^6 cells/ml and cultured in T-75 tissue culture flasks for macrophage adherence at 37°C for 4 hrs with 5% CO_2 . Non-adherent cells

were removed by washing the adherent cell layer with PBS. Adherent macrophages were lysed with 0.1% saponin, centrifuged, and the pellet collected.

Preparation of Hz from *P. chabaudi* AS infected splenic macrophages

Macrophage pellets obtained from steps described above washed in PBS and treated with 2% sodium dodecyl sulfate (SDS) in endotoxin-free PBS followed by sonication for 20 seconds. After centrifugation, the pellet was resuspended in proteinase K (2 mg/mL) and incubated overnight at 37°C. The digested product was washed 3 times with 2% SDS, resuspended in 6 M urea, and incubated on a shaker for 3 hours at room temperature. After 3 washes in 2% SDS and a PBS wash, the pellet was treated with DNase I (50 U/mL) for 1 hour at 37°C followed by heating to 95°C for 10 minutes to inactivate DNase I. Finally, Hz crystals were washed 2x with PBS and centrifuged at 15k rpm for 10 min. Hz was resuspended in PBS and stored at 4°C until further treatment.

6.5.2.3. Treatment of crude extracts of Hz with organic solvents

Crude pellets of Hz obtained from both *P. falciparum* and *P. chabaudi* AS were subjected to alternative washes with hexane and DCM. Briefly, Hz pellet was centrifuged at 9k rpm for 3 min and supernatants removed. Then, 1 mL of hexane was added to the mixture and sonicated for 30 seconds and centrifuged again at 9k rpm for 3 min. This procedure was repeated using dichloromethane, followed by centrifugation at 9k rpm for 5 min and the supernatant removed. Finally, Hz was treated again with hexane, centrifuged at 9k rpm, supernatant removed and dried at room temperature overnight and kept under vacuum until its analysis. The resulting material is referred to as native Hz (nHz).

6.5.2.4. Characterization techniques

The atomic composition of nHz and the control samples were studied by X-ray photoelectron spectrometry (XPS) using a Thermo Scientific K α spectrometer, equipped with a monochromated Al cathode with an incident K α X-ray source (1486.6 eV, 0.843 nm), and an ultrahigh vacuum chamber (10^{-9} Torr). A flood gun of low energy electrons was used to prevent surface charging during the measurement. The analyses were carried out with a pass energy of 1 eV for all survey scans, and 0.1 eV for elemental high-resolution scans. Six points were randomly selected along each sample and at least three samples were analyzed. Quantitative analysis of the survey spectra and high-resolution spectra were fitted using Advantage Software version 5.956, using Gaussian-Voigt curve functions, and background removal through the Smart method. High-resolution spectral energies were normalized by fixing the position of the C-C/C=C component of C_{1s} at 284.5 eV.

The surface morphology and the elemental distribution of nHz samples were characterized by combining scanning electron microscopy (SEM) and energy-dispersive X-ray spectroscopy (EDS). The samples were mounted on an aluminum sample holder with carbon tape, followed by 8.5 nm of carbon coating (carbon sputter coater, EMS150R ES, Electron Microscopy Sciences (EMS)). The images were obtained using an Inspect-50 field emission scanning electron microscope (SEM) (FEI, Japan), operated in low vacuum mode, at 5 kV operating voltage. EDS spectra and elemental maps were acquired in the regions of interest using an EDX spectrometer (EDX, Thermo Scientific, USA).

6.5.2.5. Statistical analysis

Three independent experiments were performed for each Hz sample and at least two different spots were randomly selected and characterized along the same sample. All the data are expressed as mean \pm standard deviation (SD). Means that are statistically different are indicated with a subscript asterisk (*). Microsoft Excel 2016 was used to perform statistical analysis. The unpaired *t*-test was performed to assess the statistic difference, where $P < 0.01$ was considered to be a significant difference.

6.6. Supporting Information

6.6.1. Materials

The following materials were obtained from Sigma-Aldrich Canada, ACS grade: hexane, dichloromethane (DCM), hematin, sodium bicarbonate, silicic acid, poly(dimethyl siloxane) -OH terminated (PDMS, average Mn~550, viscosity ~25 cst), ortho-DL-phosphoserine, calcium pyrophosphate, sodium polyphosphate, calcium phosphate (CaHPO_4), β -tricalcium phosphate (β -TCP), cholesterol (sheep wool-derived). Sodium hydroxide, propionic acid and monosodium phosphate (NaH_2PO_4), anhydrous ethanol ACS grade were purchased from Fisher Scientific. Phosphate buffer saline (PBS) (1x) tablets and sodium dodecyl sulfate (SDS) were purchased from BioShop, Canada Inc.

Stock solutions of PBS (1x) pH 7.4, 0.01 M sodium bicarbonate, 0.1 M NaOH and 5 mM NaH_2PO_4 pH 8, were prepared and used freshly. The pH of the stock solutions was adjusted with a solution of 0.1 M HCl or 0.1 M NaOH. Milli-Q water from a Barnstead purification system

(resistivity of 18.2 MΩ-cm) was used to prepare all the stock solutions and experiments, unless specified. Protein LoBind tubes were purchased from Eppendorf.

6.6.2. Methods

6.6.2.1. Preparation of *Plasmodium falciparum* parasites for XPS analysis

Around 100 µL of a suspension of dead parasites of *Plasmodium falciparum* of the strain 3D7-H (see **Methods Section 6.5.2.1** of the main manuscript) were centrifuged at 9k rpm for 3 min and the supernatant was removed. Then, hexane was added and the pellet was mixed by inverting upside down, followed by centrifugation at 9k rpm for 1 min and supernatant discarded. Dichloromethane was added, the pellet was mixed and centrifuged again at 9k rpm for 1 min, with supernatant removal. This procedure was repeated by adding a final wash with hexane, with centrifugation for 1 min at 9k rpm and supernatant removal. The resulting material was dried at room temperature to evaporate the residual solvents and was kept in vacuum until analysis.

6.6.2.2. Preparation of blood serum

Whole blood of type A+ was left undisturbed at room temperature for around 20 min to allow the clot to form. The clot was removed by centrifugation at 2 xg for 10 min, with the temperature kept at 4°C. The resulting supernatant is serum; it was carefully removed and transferred into a propylene tube using a Pasteur pipette. The serum was kept at 4°C and used right away.

6.6.2.3. Preparation of red blood cell (RBC) membranes

RBC membranes were obtained by following what Steck *et al.* reported [189], with minor modifications. First, to obtain packed RBCs, whole blood was centrifuged at 5,000 xg for 7 min to remove cells, followed by centrifugation at 12,500 xg for 5 min to remove acellular constituents. Then, 1 mL of the resulting packed RBCs were suspended in 6 mL of PBS (1x, pH 7.4) and mixed carefully by trituration. The mixture was spun down at 1000 xg for 10 min, and the supernatant was removed. The packed RBCs were resuspended in 35 mL of 5 mM NaH_2PO_4 (pH 8.0), and left in a bath ice for about 30 min. Then, the suspension was centrifuged at 12,000 xg for 10 min and the supernatant was discarded. The pellet obtained from this step was resuspended in 5 mM NaH_2PO_4 (pH 8.0) in a bath ice until the color of the pellet changed to translucent, i.e. hemoglobin was removed. Finally, the volume of the RBC membranes was adjusted with 5 mM NaH_2PO_4 (pH 8.0), the solution was kept at 4°C and used freshly.

6.6.2.4. Synthesis of hematin anhydride (HA)

HA was synthesized according to the method reported by Slater *et al.* [32], with minor modifications. 0.6 mmol of hematin were dissolved in 80 mL of 0.1 M NaOH for 30 min under stirring, with the temperature set at 70°C. Then, 49 mmol of propionic acid were added drop-wise to precipitate the crystals. Once all the acid was added and well mixed, the stirring was stopped, and the reaction proceeded overnight covered from light. After the reaction was complete, the flask was cooled down to room temperature, the suspension was decanted and washed twice with distilled water and centrifuged at 9k rpm for 30 min in between. Unreacted and poorly aggregated heme was removed by rinses with 0.01 M sodium bicarbonate and left in an orbital shaker for 3 h followed by centrifugation at 9k rpm for 30 min and the supernatant decanted; this step was

repeated twice. The resulting crystals were washed four times with distilled water with centrifugation in between at 9k rpm for 30 min. The sample was dried at room temperature and kept in vacuum.

6.6.2.5. Suspension of HA in compounds used as control

HA was suspended in several solutions used as control, and treated with the procedure used to obtain nHz, unless specified. The resulting crystals were dried at room temperature to evaporate residual solvents and left under vacuum until characterization.

6.6.2.6. Suspension of HA in blood serum, RBC membranes, and lysis buffer

3 mg of HA were added separately to 1 mL of blood serum, RBC membranes and the lysis buffer (CHAPS), and vortexed. The samples were incubated for 24 h at 37°C, followed by centrifugation at 9k rpm for 5 min and the supernatant removed. Then, the samples were rinsed with hexane and dichloromethane, dried at room temperature overnight and transferred to vacuum.

6.6.2.7. Suspension of HA in silicic acid

3 mg of HA were added to 10 mg/mL of silicic acid (pH 4) and mixed with sonication. The suspension was left for 24 h at 37°C, followed by centrifugation at 9k rpm for 5 min and supernatant discarded. Then, the resulting material was washed with alternate washes of hexane and dichloromethane.

6.6.2.8. Suspension of HA in poly(dimethylsiloxane) (PDMS)

1 mL of PDMS was dissolved in 3 mL of anhydrous ethanol, and 5 mg of HA were added and mixed in an ultrasonic bath. The suspension was left undisturbed for 6 h, followed by alternate rinses with hexane and dichloromethane, and drying at room temperature. Finally, the resulting sample was stored under vacuum.

6.6.2.9. Suspension of HA in calcium acetate

3 mg of HA were added to 1.5 mL of 0.15 M calcium acetate and mixed in an ultrasonic bath. The mixture was incubated at 37°C for 24 h, followed by centrifugation at 9k rpm for 5 min, with supernatant removal.

6.6.2.10. Suspension of HA in calcium pyrophosphate (Ca pyroP)

3 mg of HA and 2 mg of Ca pyroP were mixed in 1.5 mL of anhydrous ethanol with the aid of an ultrasonic bath. The samples were then kept under rotational stirring (Rotamix, ATR Biotech Inc, model RKDYNAL) for 6 h to ensure the thorough mixing between HA crystals and the insoluble Ca pyroP salt. Then, the sample was centrifuged at 9k rpm for 2 min, and the supernatant was decanted. Then, more ethanol was added, and the suspension was vortexed and centrifuged again. The supernatant was removed, and the sample was dried at room temperature and kept under vacuum.

6.6.2.11. Suspension of HA and Ca pyroP in cholesterol

A solution of 1 mg/mL of cholesterol was prepared in anhydrous ethanol. Then, 3 mg of HA and 2 mg of Ca pyroP were suspended in 1.5 mL the cholesterol solution, and mixed in an ultrasonic bath. The samples were kept in a rotational stirrer for 6 h, followed by centrifugation at 9k rpm for 2 min and supernatant decanting. More ethanol was added, and the suspension was vortexed and centrifuged again. Finally, the sample was dried at room temperature to evaporate residual ethanol and was transferred to vacuum until its analysis.

6.6.2.12. Suspension of HA in phosphatidylcholine

10 mg of PC were mixed with 5 mL of chloroform with vigorous vortexing. Then 4 mg of HA were suspended in 2 mL of the phosphatidylcholine solution in an ultrasonic bath. The suspension was left for 18 h covered from light, followed by alternate rinses with hexane and dichloromethane, with centrifugation in between for 2 min at 9k rpm and supernatant removal. The sample was dried at room temperature and kept in vacuum.

6.6.2.13. Preparation of reference samples

6.6.2.14. Washes of Hz with water for SEM/EDS analysis

Around 100 μ L of freshly extracted Hz kept in PBS were centrifuged at 9k rpm for 5 min, and the supernatant discarded. Then, 1 mL of milli-Q water was added, and the mixture was vortexed, followed by centrifugation at 9k rpm for 5 min and supernatant discarded. The sample was dried at room temperature overnight and kept under vacuum.

6.6.2.15. Preparation of ortho-DL-phosphoserine, CaHPO_4 , sodium polyphosphate and calcium pyrophosphate

All the materials were used as received from the supplier, dried under vacuum for several days and analyzed before the analysis.

6.6.2.16. Preparation of cucumber skin and horsetail for XPS analysis

Thin portions of the epidermis of cucumber fruit of the English variety (*Cucumis sativus*) were excised (around 1 cm^2) with a razor blade and placed on a glass petri dish. Similarly, horsetail (*Equisetum hyemale*) branches were cut in around 2 cm length pieces and the sheaths removed; a longitudinal cut was made to expose the inner layer of the branch to allow a uniform drying. All the samples were rinsed with 70% ethanol, followed by air drying at room temperature for 2 h, covered with aluminum foil to avoid possible contamination. Then, the samples were dried at 55°C overnight until they became brittle. The samples were transferred to vacuum after cooling down. The XPS was performed on the external area of both the horsetail and the cucumber skin since most of the silica content is found on the outer surface of the skin [225].

6.6.3. Characterization techniques

6.6.3.1. Ca K-edge Near Edge X-ray Absorption Fine Structure (Ca K-edge NEXAFS) spectroscopy and linear combination fitting

Ca K-edge NEXAFS spectra from nHz and reference samples were collected at the bulk XAFS end-station of the Soft X-ray Microcharacterization beamline (SXRMB) at the Canadian Light Source (CLS), Saskatoon, Saskatchewan. Powder samples of nHz obtained from *P. falciparum* strain 3D7-H, dead parasites of *P. falciparum* strain 3D7-H and calcium acetate ($\text{Ca}(\text{CH}_3\text{COO})_2$).

Two samples of nHz and *P. falciparum* parasites were analyzed. The spectra were acquired in fluorescence mode, with energies between 1.7 and 10 keV and a photon beam spot of 2 mm x 6 mm. Athena software (Demeter 0.9.20) was used to calibrate, align and normalized the data. Linear combination fitting (LFC) was carried out on the NEXAFS data using all the possible combinations of the reference samples. The quality of the fitting was assessed by the R-factor value (values below 0.02 are indicative of satisfactory fitting analysis); therefore, only the spectra with LCF with the lowest R factor were reported. LCF was carried out using Athena software.

6.6.3.2. X-ray diffraction (XRD) and Fourier Transform – Infrared (FT-IR) spectroscopy

The crystallinity of synthesized HA was evaluated with XRD. The sample was slightly ground and transferred to a metallic holder. The diffraction patterns (**Figure S.6.6.8**) were acquired using a Phillips W1700 diffractometer, equipped with a Cu K α radiation source ($K_{\alpha 1}$ $\lambda=1.54$ Å) and a curved graphite monochromator set at 40 kV and 40 mA within the 5° to 27° range in 2θ .

To ensure the chemical composition of synthesized HA, FT-IR spectroscopy was employed. FT-IR spectrum was collected for HA (**Figure S.6.6.8.B**) on a Bruker Tensor 27 spectrometer equipped with a diffuse reflectance (DRIFT) accessory and a DTGS detector. The spectrum was acquired from 400 to 2000 cm^{-1} , in transmittance mode, using 56 scans and a resolution of 4 cm^{-1} . The data collected was analyzed in OPUS software version 7.0.0, (Bruker, Karlsruhe, Germany).

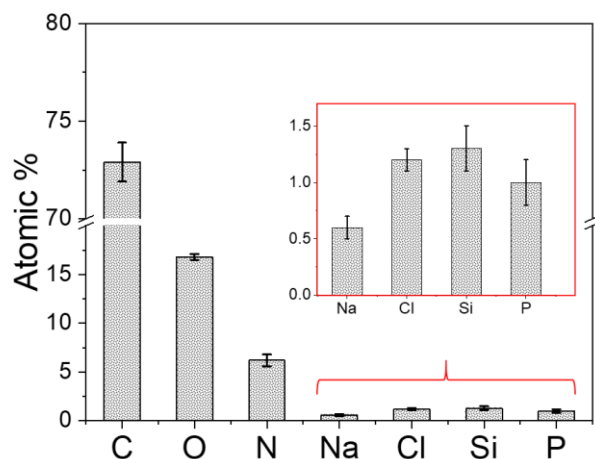


Figure S.6.6.1. XPS surveys measured on dead parasites of *P. falciparum* strain 3D7-H washed with hexane and dichloromethane.

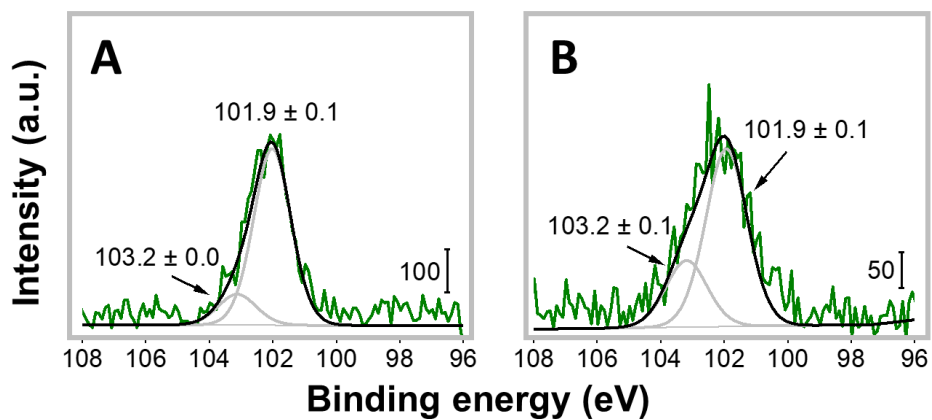


Figure S.6.6.2. XPS high-resolution Si_{2p} spectra collected on nHz isolated from A) *P. falciparum* strain 7G8 (CQ-resistant), and B) *P. chabaudi* AS (CQ-sensitive). Experimental data is presented in green, peak fitting in gray, and the overall fit in black.

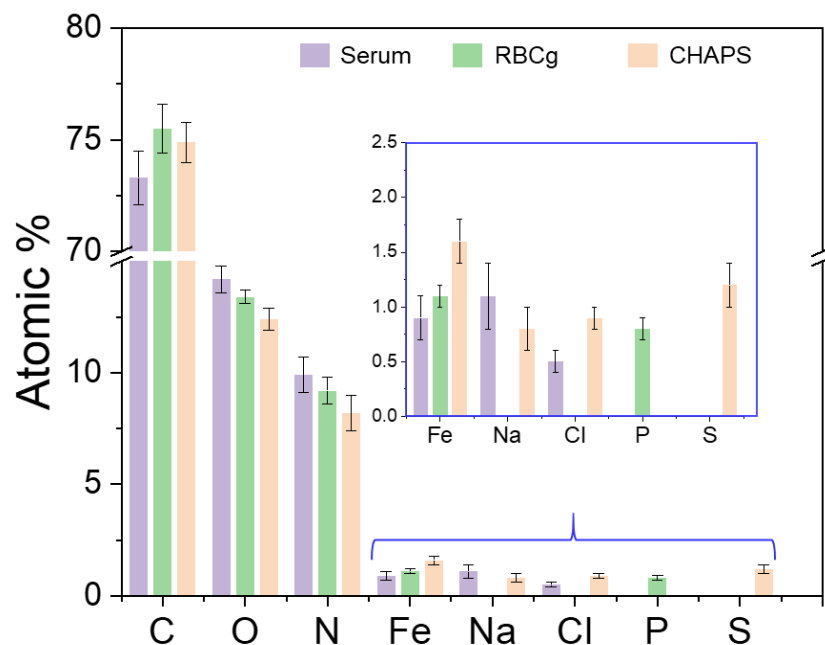


Figure S.6.6.3. Elemental composition obtained from XPS surveys collected from control samples consisting of HA suspended in blood serum (purple), red blood cell ghosts (RBCg, green) and the buffer used to extract Hz (CHAPS, orange).

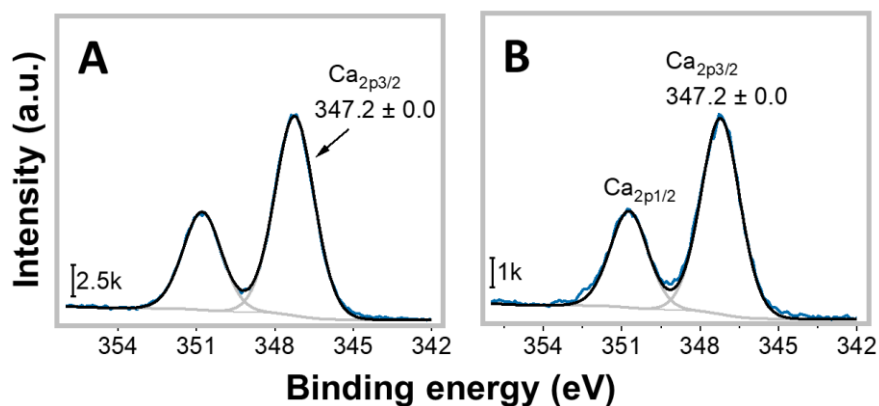


Figure S.6.6.4. XPS high-resolution Ca_{2p} spectra acquired on A) a reference sample of CaHPO_4 and B) nHz isolated from macrophages derived from *P. chabaudi* AS infected mice. Experimental data is presented in blue, peak fitting in gray, and the overall fit in black.

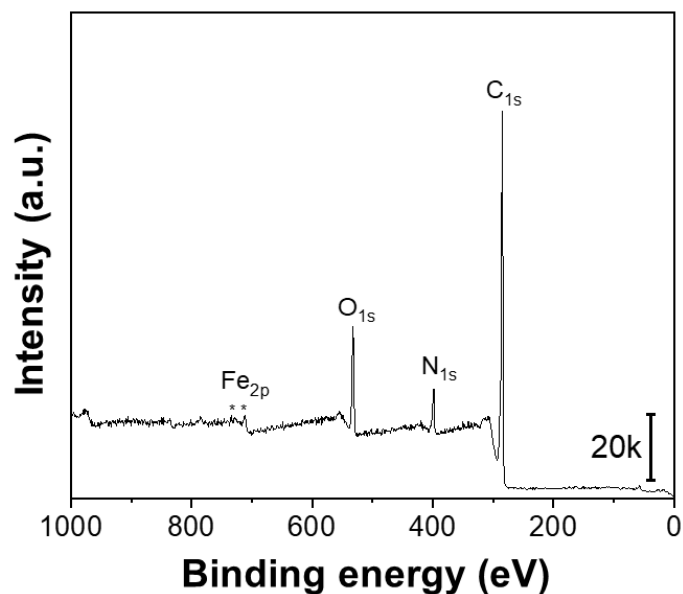


Figure S.6.6.5. XPS survey collected for HA suspended in a solution of Ca pyroP. The data show the signals of C_{1s}, O_{1s}, N_{1s}, and Fe_{2p}, characteristic of HA. The lack of a P_{2p} signal at 133 eV and Ca_{2p} at 348 eV indicates that Ca pyroP did not adsorb on HA crystals due to the absence of an adherent intermediate, e.g. lipids or proteins.

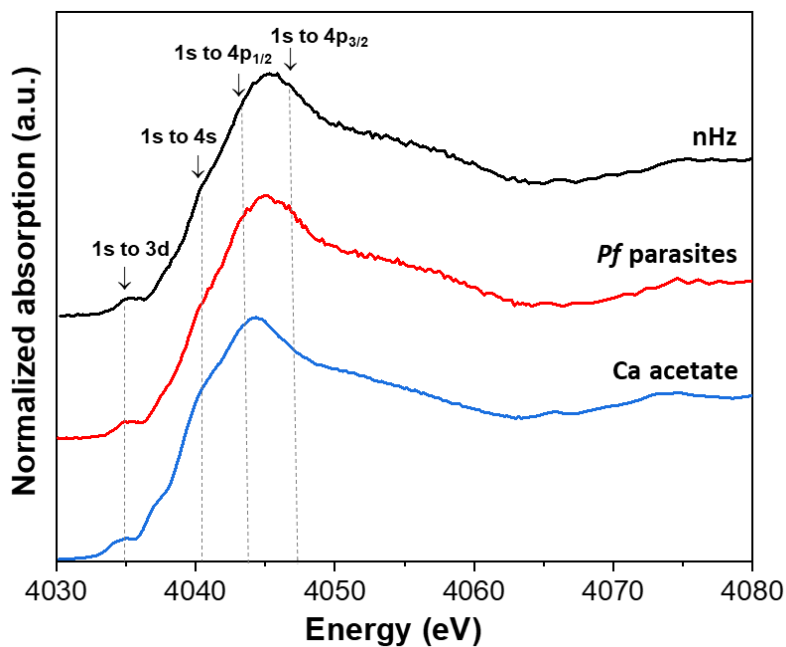


Figure S.6.6.6. Representative Ca K-edge NEXAFS reference spectra of nHz collected from *P. falciparum* strain 3D7-H, dead parasites *P. falciparum* strain 3D7-H and calcium acetate (Ca(CH₃COO)₂).

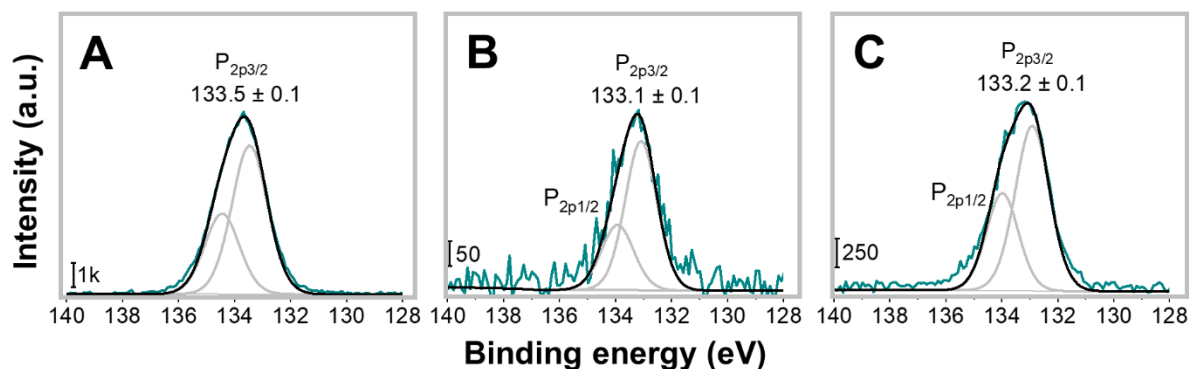


Figure S.6.6.7. XPS high resolution of P_{2p} collected for A) a reference sample of $CaHPO_4$, B) nHz isolated from *P. falciparum* strain 7G8 (CQ-resistant) and C) *P. chabaudi* AS (CQ-sensitive). Experimental data is presented in red, peak fitting in gray, and the overall fit in black.

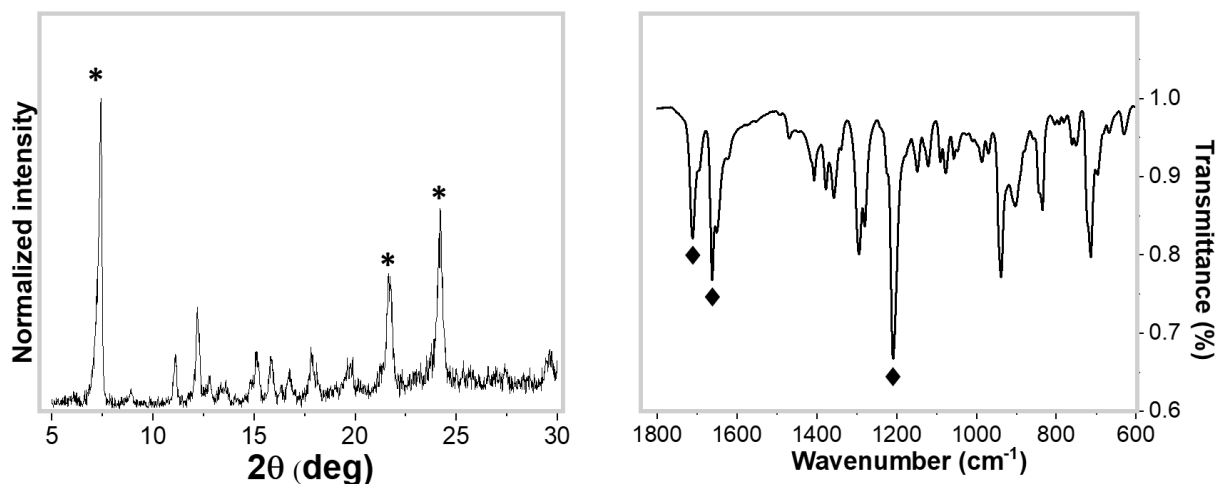


Figure S.6.6.8. A) XRD spectrum obtained for HA synthesized by slow acidification with propionic acid and used for all the control samples carried out in this work. The characteristic diffraction patterns of HA at 7.5° , 21° , and 24° are marked with an asterisk (*) [14]. B) The FT-IR spectrum of HA shows the peaks of at 1664 and 1209 cm^{-1} , representative of the coordination between the iron in heme and a propionate group. Whereas the peak located at 1712 cm^{-1} is characteristic of the hydrogen-bonded carboxylate group that links the heme dimers to extend the crystalline array [32, 190], these peaks are indicated with a diamond symbol (♦).

Table S.6.1. Percentages of $\text{Ca}(\text{CH}_3\text{COO})_2$, CHA and DCPD obtained from Hz cultured from *P. falciparum* of the strains 3D7-H, determined by LCF using NEXAFS spectra of reference samples, and R-factors of the LCF.

Samples	LCF results (%)			
	% Calcium acetate	% CHA	% DCPD	R-factor
Pf_3D7-1	24 ± 4	40 ± 6	36 ± 2	0.00942
Pf_3D7-2	21 ± 5	39 ± 7	4 ± 3	0.011549
Hz_3D7-1	89 ± 3	14 ± 3	0	0.01394
Hz_3D7-2	93 ± 4	12 ± 3	0	0.01643

Chapter 7. Original contributions

The main motivation of this doctoral project was to study the physicochemical properties of the surface of Hz and its isostructural synthetic phase, HA. This work produced original contributions presented to the scientific community for the first time, as highlighted below.

- We studied the surface properties of HA produced by two of the most widely used methods of synthesis, which are known to produce materials with remarkable differences in crystallinity, crystal size, and morphology. We correlated these features with the differences observed between the products of each synthesis in terms of specific surface area and porosity of the crystals, surface atomic chemistry and elemental composition. Additionally, we detected water despite extensive drying prior to the analysis. This new knowledge is relevant to understand the conflicting reports on how Hz and HA trigger the host's immune response, especially when different preparations of HA are used as representative models of Hz.
- We confirmed the presence of carboxylate groups on HA surface through a chemical labeling using fluorine. The information obtained from these studies can help determine adsorption sites on Hz during its biomineralization or in the presence of some antimalarials that inhibit its formation, such as quinolines and artemisinins. We reported that the amounts of active carboxylate groups on the crystals surface also vary according to the method of synthesis, which also clarifies the different immune responses observed when using HA for these tests, as mentioned earlier.
- We investigated the surface of Hz obtained from *in vitro* cultures of *Plasmodium falciparum*, the most lethal malaria species in humans. We studied the influence of the washing protocol on the surface of the crystals and found that the composition and amount

of the organic contaminants vary according to the cleaning protocol, which in fact introduces partial contamination. When the cleaning steps were shortened, the organic material adhered on Hz surface presented unexpected inorganic species, not previously reported. We also found that the residual biomolecules could be associated with protein fragments prevailing on Hz surface regardless of the washing protocol. We proposed that these biomolecules could derive from an organic matrix incorporated within the crystalline structure of Hz, which would act as nucleation sites to enhance Hz formation. This study proposes a mechanism of Hz biomineralization previously not investigated that could account for the several differences between Hz collected from parasites and Hz prepared in the lab as HA.

- We investigated the role of carboxylate groups on HA interactions and we established that they are the main sites of surface adsorption. This is of crucial importance to understand the mechanism of action of the most important antimalarials and to design new ones. This finding also helps to understand Hz biomineralization since carboxylate groups may mediate the adhesion of lipids and proteins that may promote crystal growth.
- We reported for the first time the presence of silicon, calcium, and phosphorus present in the organic residuals associated with Hz obtained from *in vivo* and *in vitro* models. We showed that the inorganic species are endogenous of the parasites and not a result of external contamination. Their presence on Hz collected from both *in vitro* and *in vivo* models prove that the composition of the components adsorbed on Hz is similar regardless of the model used to obtain the crystals.
- We proposed that silicon is present in two possible chemical states: as silicon complexed with cell components, in addition to SiO₂. We hypothesized that this inorganic element is

strongly adsorbed on Hz and the function of Si in the parasite could be related to a mechanism of defense or survival, as observed in plants and some algae.

- We proposed that calcium is present as calcium coordinated to carboxylate groups, such as in Ca^{2+} -dependent proteins, these proteins are involved in vital functions of the parasite, thus, they are a potential target for the development of novel antimalarials and possible participators in the pathogenesis of malaria. We propose that phosphorus is in the form of orthophosphate ions, possibly originating from phosphorylated proteins or phospholipids that could interact with Hz during its biomineralization or egress from the DV of *Plasmodium* or the RBC.
- Finally, we proposed XPS and MALDI-ToF as standard characterization tools to assess the surface of HA or Hz before using the crystals in immune modulation tests. In addition, these techniques demonstrate a potential use to obtain molecular information of HA or Hz surface after antimalarials screening during the formation of the crystal.

Chapter 8. Conclusions and future perspectives

The results and methods developed in this work can serve as a guideline for future investigations related to Hz. For this reason, foreseeable challenges and future directions to further expand this research are explained below.

- (i) In **Chapter 4** we used XPS and N₂ adsorption at 77 K as surface-sensitive techniques to study HA prepared by two different synthesis methods to gain insight on the crystal surface area, atomic environment and to identify surface carboxylate groups. The surface characterization of HA could be extended using inverse gas chromatography (IGC). This technique can provide information on the enthalpy and entropy of sorption, surface energy, work of co-adhesion, specific surface area, among others [228]. This information will help to predict the mechanism of molecular attachment, in relation to antimalarials or surface contaminants. A possible challenge related to this technique could be producing enough quantities of HA to perform the analysis.
- (ii) In **Chapter 5**, we masked the -COOH groups on HA surface to evaluate the crystal's ability to interact with some biomolecules. We found that carboxylate groups are essential for some crystal-molecule interactions. This approach can be extended to understand the interaction of HA surface with quinolines and artemisinins in two possible ways: with fluorinated HA crystals fully formed and with fluorinated heme or hematin; while the products from these assays can be characterized using XPS, MALDI-ToF, SEM, and AFM. This study has not been previously carried out and will help identify drug binding sites on Hz and HA. A milestone associated with this investigation is to avoid oxidation of heme to hematin when testing artemisinins.

- (iii) In **Chapter 5**, we stated that the use of an alkaline buffer could substitute the use of DNase and RNase in the extensive washing of Hz. This step certainly causes a decrease in Hz yield due to the dissolution of the outermost layers of the crystals by the action of the harsh buffer. Thus, this method could be used several times with centrifugation in between, keeping the supernatant for further characterization. In this way, the outermost layers of Hz will be dissolved, and its inner constituents and free heme will remain in solution. These analytes can be studied to determine the presence of components within the crystal configuration of Hz in terms of composition and amount in relation to heme concentration. One limitation of this process could be the possible denaturation of proteins or other constituents in the presence of the alkaline solution. In addition, it can be expected to obtain insufficient amounts of material if the sample of Hz processed is not large enough.
- (iv) In **Chapter 6**, we reported the presence of inorganic species associated with Hz. Although the analysis of the chemical environment of these compounds provides important clues about their possible structure and source, further work is necessary to determine the exact composition of these molecules. We propose the use of NEXAFS since this technique requires small amounts of samples and provides crucial information to identify the compounds of interest. This knowledge is critical to clarify the function, biochemical pathway and the possible role of these species in the role of Hz as immune modulator. Other techniques that can provide separation and

identification of these compounds include gas chromatography-mass spectrometry (GC-MS) and high-performance liquid chromatography (HPLC).

- (v) We have not explored the surface properties of Hz isolated from other parasites. While the diffraction patterns of Hz obtained from *Schistosoma* or the bug *Rhodnius prolixus* show identical patterns to Hz from *Plasmodium*, their arrangement and morphology differ, as demonstrated in a previous work [29]. Therefore, further characterization of the surface of these crystals can be done following the methods reported in this work to determine possible similarities or discrepancies between Hz from *Plasmodium* and *Schistosoma*, for example. These differences or similarities could provide clues on the process of Hz crystallization or parasite's physiology and survival.

References

1. Salas, P.F., C. Herrmann, and C. Orvig, *Metalloantimalarials*. Chemical Reviews, 2013. **113**(5): p. 3450-3492.
2. World Health Organization, *World malaria report 2018*. 2018.
3. Patz, J.A. and S.H. Olson, *Malaria risk and temperature: influences from global climate change and local land use practices*. Proceedings of the National Academy of Sciences, 2006. **103**(15): p. 5635-5636.
4. Hay, S.I., et al., *Climate change and the resurgence of malaria in the East African highlands*. Nature, 2002. **415**(6874): p. 905.
5. Egan, T.J., *Haemozoin formation*. Mol Biochem Parasitol, 2008. **157**(2): p. 127-36.
6. Toh, S.Q., et al., *Heme and blood-feeding parasites: friends or foes?* Parasites & vectors, 2010. **3**(1): p. 108.
7. Pagola, S., et al., *The structure of malaria pigment β -haematin*. Nature, 2000. **404**(6775): p. 307-310.
8. Boura, M., et al., *The hemozoin conundrum: is malaria pigment immune-activating, inhibiting, or simply a bystander?* Trends in parasitology, 2013. **29**(10): p. 469-476.
9. Bohle, D.S., E.L. Dodd, and P.W. Stephens, *Structure of Malaria Pigment and Related Propanoate-Linked Metalloporphyrin Dimers*. Chemistry & Biodiversity, 2012. **9**(9): p. 1891-1902.
10. Olafson, K.N., et al., *Antimalarials inhibit hemozoin crystallization by unique drug-surface site interactions*. Proceedings of the National Academy of Sciences, 2017: p. 201700125.
11. Coronado, L.M., C.T. Nadovich, and C. Spadafora, *Malarial hemozoin: from target to tool*. Biochimica et Biophysica Acta (BBA)-General Subjects, 2014. **1840**(6): p. 2032-2041.
12. Wongsrichanalai, C., et al., *A review of malaria diagnostic tools: microscopy and rapid diagnostic test (RDT)*. The American journal of tropical medicine and hygiene, 2007. **77**(6_Suppl): p. 119-127.
13. Carney, C.K., et al., *The basis of the immunomodulatory activity of malaria pigment (hemozoin)*. JBIC Journal of Biological Inorganic Chemistry, 2006. **11**(7): p. 917-929.
14. Jaramillo, M., et al., *Synthetic Plasmodium-like hemozoin activates the immune response: a morphology-function study*. PloS one, 2009. **4**(9): p. e6957.

15. Shio, M.T., et al., *Innate inflammatory response to the malarial pigment hemozoin*. Microbes and Infection, 2010. **12**(12): p. 889-899.
16. Aditya, N.P., et al., *Advances in nanomedicines for malaria treatment*. Advances in Colloid and Interface Science, 2013. **201–202**(0): p. 1-17.
17. Patz, J.A., et al., *Impact of regional climate change on human health*. Nature, 2005. **438**(7066): p. 310.
18. Nosten, F. and N.J. White, *Artemisinin-based combination treatment of falciparum malaria*. The American journal of tropical medicine and hygiene, 2007. **77**(6_Suppl): p. 181-192.
19. CDC. *Malaria and travelers*,. (accessed December 26, 2018); Available from: <https://www.cdc.gov/malaria/travelers/index.html>.
20. World Health Organization, *Global malaria control and elimination: report of a technical review*. 2008.
21. World Health Organization, *Malaria vaccine: WHO position paper–January 2016*. Weekly Epidemiological Record= Relevé épidémiologique hebdomadaire, 2016. **91**(4): p. 33-52.
22. Klein, S.L., et al., *RTS, S malaria vaccine and increased mortality in girls*. MBio, 2016. **7**(2): p. e00514-16.
23. World Health Organization, *Malaria fact sheet no. 94*. WHO, Geneva, 2010.
24. Kokwaro, G., *Ongoing challenges in the management of malaria*. Malaria Journal, 2009. **8**(1): p. S2.
25. Michalakis, Y. and F. Renaud, *Malaria: Evolution in vector control*. Nature, 2009. **462**(7271): p. 298-300.
26. Fujiwara, T. and H. Harigae, *Biology of heme in mammalian erythroid cells and related disorders*. BioMed research international, 2015. **2015**.
27. Kumar, S. and U. Bandyopadhyay, *Free heme toxicity and its detoxification systems in human*. Toxicology Letters, 2005. **157**(3): p. 175-188.
28. Portela, C., et al., *Definition of an electronic profile of compounds with inhibitory activity against hematin aggregation in malaria parasite*. Bioorganic & medicinal chemistry, 2004. **12**(12): p. 3313-21.

29. Noland, G.S., N. Briones, and D.J. Sullivan, *The shape and size of hemozoin crystals distinguishes diverse Plasmodium species*. Molecular and Biochemical Parasitology, 2003. **130**(2): p. 91-99.
30. Pisciotta, J.M., et al., *Hemozoin formation in Echinostoma trivolvis rediae*. International Journal for Parasitology, 2005. **35**(10): p. 1037-1042.
31. Lvova, M., et al., *Hemozoin is a product of heme detoxification in the gut of the most medically important species of the family Opisthorchiidae*. International journal for parasitology, 2016. **46**(3): p. 147-156.
32. Slater, A., et al., *An iron-carboxylate bond links the heme units of malaria pigment*. Proceedings of the National Academy of Sciences, 1991. **88**(2): p. 325-329.
33. Martiney, J.A., A. Cerami, and A. Slater, *Inhibition of hemozoin formation in Plasmodium falciparum trophozoite extracts by heme analogs: possible implication in the resistance to malaria conferred by the beta-thalassemia trait*. Molecular Medicine, 1996. **2**(2): p. 236.
34. Carter, M.D., et al., *Hemozoin: A Paradigm for Biominerals in Disease*, in *Wiley Encyclopedia of Chemical Biology*. 2007, John Wiley & Sons, Inc.
35. Egan, T.J., W.W. Mavuso, and K.K. Ncokazi, *The mechanism of β -hematin formation in acetate solution. Parallels between hemozoin formation and biomineralization processes*. Biochemistry, 2001. **40**(1): p. 204-213.
36. Weissbuch, I. and L. Leiserowitz, *Interplay between malaria, crystalline hemozoin formation, and antimalarial drug action and design*. Chemical reviews, 2008. **108**(11): p. 4899-4914.
37. Ketchum, M.A., et al., *Hematin crystallization from aqueous and organic solvents*. J Chem Phys, 2013. **139**(12): p. 121911.
38. Egan, T.J., *Physico-chemical aspects of hemozoin (malaria pigment) structure and formation*. Journal of Inorganic Biochemistry, 2002. **91**(1): p. 19-26.
39. Bohle, D.S., A.D. Kosar, and P.W. Stephens, *Phase homogeneity and crystal morphology of the malaria pigment-hematin*. Acta Crystallographica Section D: Biological Crystallography, 2002. **58**(10): p. 1752-1756.
40. Tekwani, B.L. and L.A. Walker, *Targeting the hemozoin synthesis pathway for new antimalarial drug discovery: technologies for in vitro beta-hematin formation assay*. Combinatorial chemistry & high throughput screening, 2005. **8**(1): p. 63-79.

41. Egan, T.J., *Recent advances in understanding the mechanism of hemozoin (malaria pigment) formation*. J Inorg Biochem, 2008. **102**(5-6): p. 1288-99.
42. Sandlin, R.D., et al., *Detergent-mediated formation of β -hematin: heme crystallization promoted by detergents implicates nanostructure formation for use as a biological mimic*. Crystal growth & design, 2016. **16**(5): p. 2542-2551.
43. Ncokazi, K.K. and T.J. Egan, *A colorimetric high-throughput β -hematin inhibition screening assay for use in the search for antimalarial compounds*. Analytical Biochemistry, 2005. **338**(2): p. 306-319.
44. Bohle, D.S. and J.B. Helms, *Synthesis of β -hematin by dehydrohalogenation of hemin*. Biochemical and biophysical research communications, 1993. **193**(2): p. 504-508.
45. Carter, M.D., et al., *Lipophilic mediated assays for β -hematin inhibitors*. Combinatorial chemistry & high throughput screening, 2010. **13**(3): p. 285-292.
46. Olafson, K.N., et al., *Mechanisms of hematin crystallization and inhibition by the antimalarial drug chloroquine*. Proceedings of the National Academy of Sciences, 2015. **112**(16): p. 4946-4951.
47. Buller, R., et al., *Quinoline binding site on malaria pigment crystal: a rational pathway for antimalaria drug design*. Crystal growth & design, 2002. **2**(6): p. 553-562.
48. Sullivan, D.J., I.Y. Gluzman, and D.E. Goldberg, *Plasmodium hemozoin formation mediated by histidine-rich proteins*. Science, 1996. **271**(5246): p. 219-222.
49. Bergström, L., et al., *Mesocrystals in biominerals and colloidal arrays*. Accounts of chemical research, 2015. **48**(5): p. 1391-1402.
50. Fitch, C.D., et al., *Involvement of lipids in ferriprotoporphyrin IX polymerization in malaria*. Biochimica et Biophysica Acta (BBA) - Molecular Basis of Disease, 1999. **1454**(1): p. 31-37.
51. Jackson, K.E., et al., *Food vacuole-associated lipid bodies and heterogeneous lipid environments in the malaria parasite, Plasmodium falciparum*. Molecular microbiology, 2004. **54**(1): p. 109-122.
52. Oliveira, M.F., et al., *Structural and morphological characterization of hemozoin produced by Schistosoma mansoni and Rhodnius prolixus*. FEBS letters, 2005. **579**(27): p. 6010-6016.

53. Bendrat, K., B.J. Berger, and A. Cerami, *Haem polymerization in malaria*. Nature, 1995. **378**(6553): p. 138-139.
54. Huy, N.T., et al., *Phospholipid Membrane-Mediated Hemozoin Formation: The Effects of Physical Properties and Evidence of Membrane Surrounding Hemozoin*. PloS one, 2013. **8**(7): p. e70025.
55. Pisciotta, J.M., et al., *The role of neutral lipid nanospheres in Plasmodium falciparum haem crystallization*. Biochem J, 2007. **402**(1): p. 197-204.
56. Kapishnikov, S., et al., *Oriented nucleation of hemozoin at the digestive vacuole membrane in Plasmodium falciparum*. Proceedings of the National Academy of Sciences, 2012. **109**(28): p. 11188-11193.
57. Weissbuch, I., M. Lahav, and L. Leiserowitz, *Toward Stereochemical Control, Monitoring, and Understanding of Crystal Nucleation*. Crystal Growth & Design, 2003. **3**(2): p. 125-150.
58. Ziegler, J., R.T. Chang, and D.W. Wright, *Multiple-Antigenic Peptides of Histidine-Rich Protein II of Plasmodium falciparum: Dendrimeric Biomineralization Templates*. Journal of the American Chemical Society, 1999. **121**(11): p. 2395-2400.
59. Pandey, A.V., et al., *Hemozoin formation in malaria: a two-step process involving histidine-rich proteins and lipids*. Biochemical and Biophysical Research Communications, 2003. **308**(4): p. 736-743.
60. Schneider, E.L. and M.A. Marletta, *Heme binding to the histidine-rich protein II from Plasmodium falciparum*. Biochemistry, 2005. **44**(3): p. 979-986.
61. Pandey, A.V. and V.S. Chauhan, *Heme polymerization by malarial parasite: a potential target for antimalarial drug development*. Current Science, 1998. **75**(9): p. 911-918.
62. Jani, D., et al., *HDP-a novel heme detoxification protein from the malaria parasite*. PLoS Pathog, 2008. **4**(4): p. e1000053.
63. Nakatani, K., et al., *Identification of essential histidine residues involved in heme binding and Hemozoin formation in heme detoxification protein from Plasmodium falciparum*. Scientific reports, 2014. **4**: p. 6137.
64. Chugh, M., et al., *Protein complex directs hemoglobin-to-hemozoin formation in Plasmodium falciparum*. Proceedings of the National Academy of Sciences, 2013. **110**(14): p. 5392-5397.

65. Goldberg, D.E., *Complex nature of malaria parasite hemoglobin degradation*. Proceedings of the National Academy of Sciences, 2013. **110**(14): p. 5283-5284.
66. Kasemo, B. and J. Lausmaa, *Material-tissue interfaces: the role of surface properties and processes*. Environmental health perspectives, 1994. **102**(suppl 5): p. 41-45.
67. Wood, B.R., et al., *Tip-enhanced Raman scattering (TERS) from hemozoin crystals within a sectioned erythrocyte*. Nano letters, 2011. **11**(5): p. 1868-1873.
68. Olafson, K.N., J.D. Rimer, and P.G. Vekilov, *Growth of large hematin crystals in biomimetic solutions*. Crystal growth & design, 2014. **14**(5): p. 2123-2127.
69. Pisciotto, J.M. and D. Sullivan, *Hemozoin: Oil versus water*. Parasitology International, 2008. **57**(2): p. 89-96.
70. Thomas, V., et al., *A novel way to grow hemozoin-like crystals in vitro and its use to screen for hemozoin inhibiting antimalarial compounds*. PloS one, 2012. **7**(7): p. e41006.
71. Dandapani, S., et al., *Hits, leads and drugs against malaria through diversity-oriented synthesis*. Future Medicinal Chemistry, 2012. **4**(18): p. 2279-2294.
72. Achan, J., et al., *Quinine, an old anti-malarial drug in a modern world: Role in the treatment of malaria*. Malaria Journal, 2011. **10**.
73. O'Neill, P.M., et al., *4-Aminoquinolines: Chloroquine, Amodiaquine and Next-Generation Analogues*, in *Treatment and Prevention of Malaria*. 2012, Springer. p. 19-44.
74. Kaur, K., et al., *Quinolines and structurally related heterocycles as antimalarials*. European Journal of Medicinal Chemistry, 2010. **45**(8): p. 3245-3264.
75. Bachhawat, K., et al., *Interaction of Chloroquine and Its Analogues with Heme: An Isothermal Titration Calorimetric Study*. Biochemical and Biophysical Research Communications, 2000. **276**(3): p. 1075-1079.
76. Vippagunta, S.R., et al., *Characterization of chloroquine-hematin μ -oxo dimer binding by isothermal titration calorimetry*. Biochimica et Biophysica Acta (BBA) - General Subjects, 2000. **1475**(2): p. 133-140.
77. Soares, J.B.C., et al., *Interference with hemozoin formation represents an important mechanism of schistosomicidal action of antimalarial quinoline methanols*. PLoS neglected tropical diseases, 2009. **3**(7): p. e477.

78. Egan, T.J., et al., *Structure-function relationships in aminoquinolines: effect of amino and chloro groups on quinoline-hematin complex formation, inhibition of β -hematin formation, and antiparasmodial activity*. Journal of medicinal chemistry, 2000. **43**(2): p. 283-291.
79. Fitch, C.D., *Ferriprotoporphyrin IX, phospholipids, and the antimalarial actions of quinoline drugs*. Life sciences, 2004. **74**(16): p. 1957-1972.
80. Vangapandu, S., et al., *Recent advances in antimalarial drug development*. Medicinal Research Reviews, 2007. **27**(1): p. 65-107.
81. Sullivan, D.J., et al., *On the molecular mechanism of chloroquine's antimalarial action*. Proceedings of the National Academy of Sciences, 1996. **93**(21): p. 11865-11870.
82. Daniel, W.A., M.H. Bickel, and U.E. Honegger, *The Contribution of Lysosomal Trapping in the Uptake of Desipramine and Chloroquine by Different Tissues*. Pharmacology & Toxicology, 1995. **77**(6): p. 402-406.
83. Egan, T.J., *Interactions of quinoline antimalarials with hematin in solution*. Journal of Inorganic Biochemistry, 2006. **100**(5–6): p. 916-926.
84. O'Neill, P.M., et al., *4-Aminoquinolines—Past, present, and future; A chemical perspective*. Pharmacology & Therapeutics, 1998. **77**(1): p. 29-58.
85. Kuter, D., S.J. Benjamin, and T.J. Egan, *Multiple spectroscopic and magnetic techniques show that chloroquine induces formation of the μ -oxo dimer of ferriprotoporphyrin IX*. Journal of Inorganic Biochemistry, 2014. **133**(0): p. 40-49.
86. Kuter, D., et al., *Solution structures of chloroquine–ferriheme complexes modeled using MD simulation and investigated by EXAFS spectroscopy*. Journal of inorganic biochemistry, 2016. **154**: p. 114-125.
87. Trape, J.-F., *The public health impact of chloroquine resistance in Africa*. The American journal of tropical medicine and hygiene, 2001. **64**(1 suppl): p. 12-17.
88. Patzewitz, E.-M., et al., *Glutathione transport: a new role for PfCRT in chloroquine resistance*. Antioxidants & redox signaling, 2013.
89. Fidock, D.A., et al., *Mutations in the P. falciparum Digestive Vacuole Transmembrane Protein PfCRT and Evidence for Their Role in Chloroquine Resistance*. Molecular Cell, 2000. **6**(4): p. 861-871.
90. Krogstad, D.J., et al., *Efflux of Chloroquine from Plasmodium falciparum: Mechanism of Chloroquine Resistance*. Science, 1987. **238**(4831): p. 1283-1285.

91. Tu, Y., *The discovery of artemisinin (qinghaosu) and gifts from Chinese medicine*. Nat Med, 2011. **17**(10): p. 1217-1220.
92. Klayman, D.L., *Qinghaosu (artemisinin): an antimalarial drug from China*. Science, 1985. **228**(4703): p. 1049-1055.
93. Eastman, R.T. and D.A. Fidock, *Artemisinin-based combination therapies: a vital tool in efforts to eliminate malaria*. Nat Rev Microbiol, 2009. **7**(12): p. 864-74.
94. Weinberg, E.D. and J. Moon, *Malaria and iron: history and review*. Drug metabolism reviews, 2009. **41**(4): p. 644-662.
95. World Health Organization, *Guidelines for the treatment of malaria*. 2006: World Health Organization.
96. Krishna, S., A.-C. Uhlemann, and R.K. Haynes, *Artemisinins: mechanisms of action and potential for resistance*. Drug Resistance Updates, 2004. **7**(4): p. 233-244.
97. O'Neill, P.M., V.E. Barton, and S.A. Ward, *The Molecular Mechanism of Action of Artemisinin—The Debate Continues*. Molecules, 2010. **15**(3): p. 1705-1721.
98. Meshnick, S.R., T. Taylor, and S. Kamchonwongpaisan, *Artemisinin and the antimalarial endoperoxides: from herbal remedy to targeted chemotherapy*. Microbiological reviews, 1996. **60**(2): p. 301-315.
99. Pandey, A.V., et al., *Artemisinin, an endoperoxide antimalarial, disrupts the hemoglobin catabolism and heme detoxification systems in malarial parasite*. Journal of biological chemistry, 1999. **274**(27): p. 19383-19388.
100. Eckstein-Ludwig, U., et al., *Artemisinins target the SERCA of Plasmodium falciparum*. Nature, 2003. **424**(6951): p. 957-961.
101. del Pilar Crespo, M., et al., *Artemisinin and a Series of Novel Endoperoxide Antimalarials Exert Early Effects on Digestive Vacuole Morphology*. Antimicrobial Agents and Chemotherapy, 2008. **52**(1): p. 98-109.
102. Arie, F., et al., *A molecular marker of artemisinin-resistant Plasmodium falciparum malaria*. Nature, 2014. **505**(7481): p. 50-55.
103. Robert, A. and B. Meunier, *Characterization of the first covalent adduct between artemisinin and a heme model*. Journal of the American Chemical Society, 1997. **119**(25): p. 5968-5969.

104. Meshnick, S.R., *Artemisinin: mechanisms of action, resistance and toxicity*. International Journal for Parasitology, 2002. **32**(13): p. 1655-1660.
105. Loup, C., et al., *Trioxaquines and heme-artemisinin adducts inhibit the in vitro formation of hemozoin better than chloroquine*. Antimicrobial agents and chemotherapy, 2007. **51**(10): p. 3768-3770.
106. Noedl, H., D. Socheat, and W. Satimai, *Artemisinin-Resistant Malaria in Asia*. New England Journal of Medicine, 2009. **361**(5): p. 540-541.
107. Dondorp, A.M., et al., *Artemisinin resistance: current status and scenarios for containment*. Nat Rev Micro, 2010. **8**(4): p. 272-280.
108. Noedl, H., et al., *Evidence of Artemisinin-Resistant Malaria in Western Cambodia*. New England Journal of Medicine, 2008. **359**(24): p. 2619-2620.
109. Jambou, R., et al., *Resistance of Plasmodium falciparum field isolates to in-vitro artemether and point mutations of the SERCA-type PfATPase6*. The Lancet. **366**(9501): p. 1960-1963.
110. Macreadie, I., et al., *Antimalarial drug development and new targets*. Parasitology Today, 2000. **16**(10): p. 438-444.
111. World Health Organization. *Malaria: Microscopy*. 2018 14-January-2018; Available from: <https://www.who.int/malaria/areas/diagnosis/microscopy/en/>.
112. Joanny, F., et al., *Limit of blank and limit of detection of Plasmodium falciparum thick blood smear microscopy in a routine setting in Central Africa*. Malaria Journal, 2014. **13**(1): p. 234.
113. Newman, D.M., et al., *A magneto-optic route toward the in Vivo diagnosis of malaria: preliminary results and preclinical trial data*. Biophysical Journal, 2008. **95**(2): p. 994-1000.
114. Wilson, B.K., et al., *Detection of malarial byproduct hemozoin utilizing its unique scattering properties*. Optics express, 2011. **19**(13): p. 12190-12196.
115. Giacometti, M., et al., *Electrical and magnetic properties of hemozoin nanocrystals*. Applied Physics Letters, 2018. **113**(20): p. 203703.
116. Parroche, P., et al., *Malaria hemozoin is immunologically inert but radically enhances innate responses by presenting malaria DNA to Toll-like receptor 9*. Proceedings of the National Academy of Sciences, 2007. **104**(6): p. 1919-1924.

117. McBirney, S.E., et al., *Rapid Diagnostic for Point-of-Care Malaria Screening*. ACS Sensors, 2018. **3**(7): p. 1264-1270.
118. Butykai, A., et al., *Malaria pigment crystals as magnetic micro-rotors: key for high-sensitivity diagnosis*. Sci Rep, 2013. **3**: p. 1431.
119. Hillenkamp, F. *Laser Desorption Mass Spectrometry. A Review*. 1986. Berlin, Heidelberg: Springer Berlin Heidelberg.
120. Scholl, P.F., et al., *Rapid detection of malaria infection in vivo by laser desorption mass spectrometry*. The American journal of tropical medicine and hygiene, 2004. **71**(5): p. 546-551.
121. Hobro, A.J., et al., *Raman spectroscopic analysis of malaria disease progression via blood and plasma samples*. Analyst, 2013. **138**(14): p. 3927-3933.
122. Yuen, C. and Q. Liu, *Magnetic field enriched surface enhanced resonance Raman spectroscopy for early malaria diagnosis*. Journal of Biomedical Optics, 2012. **17**(1): p. 017005.
123. Wood, B.R., et al., *Resonance Raman microscopy in combination with partial dark-field microscopy lights up a new path in malaria diagnostics*. Analyst, 2009. **134**(6): p. 1119-1125.
124. Lukianova-Hleb, E.Y., et al., *Hemozoin-generated vapor nanobubbles for transdermal reagent-and needle-free detection of malaria*. Proceedings of the National Academy of Sciences, 2014. **111**(3): p. 900-905.
125. Burnett, J.L., J.L. Carns, and R. Richards-Kortum, *In vivo microscopy of hemozoin: towards a needle free diagnostic for malaria*. Biomedical optics express, 2015. **6**(9): p. 3462-3474.
126. Frita, R., et al., *In vivo hemozoin kinetics after clearance of Plasmodium berghei infection in mice*. Malaria research and treatment, 2012. **2012**.
127. Lemaitre, M., et al., *Coinfection with Plasmodium falciparum and Schistosoma haematobium: additional evidence of the protective effect of Schistosomiasis on malaria in Senegalese children*. The American journal of tropical medicine and hygiene, 2014. **90**(2): p. 329-334.
128. Jaramillo, M., et al., *Hemozoin-Inducible Proinflammatory Events In Vivo: Potential Role in Malaria Infection*. The Journal of Immunology, 2004. **172**(5): p. 3101-3110.

129. Coban, C., et al., *Purified malaria pigment (hemozoin) enhances dendritic cell maturation and modulates the isotype of antibodies induced by a DNA vaccine*. Infection and immunity, 2002. **70**(7): p. 3939-3943.
130. Skorokhod, O.A., et al., *Hemozoin (malarial pigment) inhibits differentiation and maturation of human monocyte-derived dendritic cells: a peroxisome proliferator-activated receptor- γ -mediated effect*. The Journal of Immunology, 2004. **173**(6): p. 4066-4074.
131. Basilico, N., et al., *Malaria pigment stimulates chemokine production by human microvascular endothelium*. Acta Tropica, 2017. **172**: p. 125-131.
132. Deroost, K., et al., *Hemozoin Induces Lung Inflammation and Correlates with Malaria-Associated Acute Respiratory Distress Syndrome*. 2013. **48**(5): p. 589-600.
133. Deroost, K., et al., *Hemozoin Induces Hepatic Inflammation in Mice and Is Differentially Associated with Liver Pathology Depending on the Plasmodium Strain*. PLOS ONE, 2014. **9**(11): p. e113519.
134. Olivier, M., et al., *Malarial Pigment Hemozoin and the Innate Inflammatory Response*. Frontiers in Immunology, 2014. **5**: p. 25.
135. Olivier, M. and M. Jaramillo, *Modulation of positive signaling and proinflammatory responses by hemozoin, a plasmodium metabolic waste*. Protozoans in macrophages. Austin, Texas, USA, 2007: p. 67-72.
136. Thawani, N., et al., *Plasmodium products contribute to severe malarial anemia by inhibiting erythropoietin-induced proliferation of erythroid precursors*. Journal of Infectious Diseases, 2013: p. 140-149.
137. Lee, M.S., et al., *Plasmodium products persist in the bone marrow and promote chronic bone loss*. Science immunology, 2017. **2**(12): p. eaam8093.
138. Sun, J., et al., *Can hemozoin alone cause host anaemia?* Parasitology Research, 2016. **115**(12): p. 4611-4616.
139. Murray, C.J.L., et al., *Global malaria mortality between 1980 and 2010: a systematic analysis*. The Lancet, 2012. **379**(9814): p. 413-431.
140. Francis, S.E., et al., *Hemoglobin metabolism in the malaria parasite Plasmodium falciparum*. Annual Reviews in Microbiology, 1997. **51**(1): p. 97-123.

141. Stiebler, R., et al., *On the mechanisms involved in biological heme crystallization*. Journal of bioenergetics and biomembranes, 2011. **43**(1): p. 93-99.
142. Giglio, E.D., et al., *Surface (XPS, SIMS) chemical investigation on poly (pyrrole-3-acetic acid) films electrosynthesized on Ti and TiAlV substrates for the development of new bioactive substrates*. Surface and interface analysis, 2005. **37**(6): p. 580-586.
143. Sing, K.S., *Reporting physisorption data for gas/solid systems with special reference to the determination of surface area and porosity (Recommendations 1984)*. Pure and applied chemistry, 1985. **57**(4): p. 603-619.
144. Bohle, D.S., A.D. Kosar, and P.W. Stephens, *The reversible hydration of the malaria pigment β -hematin*. Canadian Journal of Chemistry, 2003. **81**(11): p. 1285-1291.
145. Rienzo, A., et al., *X-ray absorption and photoemission spectroscopy of zinc protoporphyrin adsorbed on rutile TiO₂ (110) prepared by in situ electrospray deposition*. The Journal of chemical physics, 2010. **132**(8): p. 084703.
146. Moulder, J.F., J. Chastain, and R.C. King, *Handbook of X-ray photoelectron spectroscopy: a reference book of standard spectra for identification and interpretation of XPS data*. 1992: Perkin-Elmer Eden Prairie, MN.
147. Dementjev, A.P., et al., *X-Ray photoelectron spectroscopy reference data for identification of the C₃N₄ phase in carbon–nitrogen films*. Diamond and Related Materials, 2000. **9**(11): p. 1904-1907.
148. Gulino, A., et al., *Similarities and differences among monolayers of a free base porphyrin and its copper complex: synthesis and characterization of a luminescent copper (II) porphyrin monolayer*. The Journal of Physical Chemistry C, 2007. **111**(38): p. 14125-14130.
149. Plecenik, T., et al., *Surface transport properties of Fe-based superconductors: The influence of degradation and inhomogeneity*. Applied Physics Letters, 2013. **103**(5): p. 052601.
150. Pauleau, Y., *Materials surface processing by directed energy techniques*. 2006: Elsevier.
151. Sarno, D.M., L.J. Matienzo, and W.E. Jones, *X-ray photoelectron spectroscopy as a probe of intermolecular interactions in porphyrin polymer thin films*. Inorganic Chemistry, 2001. **40**(24): p. 6308-6315.

152. Yamashita, T. and P. Hayes, *Analysis of XPS spectra of Fe²⁺ and Fe³⁺ ions in oxide materials*. Applied Surface Science, 2008. **254**(8): p. 2441-2449.
153. Kapishnikov, S., et al., *Aligned hemozoin crystals in curved clusters in malarial red blood cells revealed by nanoprobe X-ray Fe fluorescence and diffraction*. Proceedings of the National Academy of Sciences, 2012. **109**(28): p. 11184-11187.
154. Hutt, D.A. and G.J. Leggett, *Functionalization of hydroxyl and carboxylic acid terminated self-assembled monolayers*. Langmuir, 1997. **13**(10): p. 2740-2748.
155. Chilkoti, A., B.D. Ratner, and D. Briggs, *Plasma-deposited polymeric films prepared from carbonyl-containing volatile precursors: XPS chemical derivatization and static SIMS surface characterization*. Chemistry of Materials, 1991. **3**(1): p. 51-61.
156. Alexander, M.R., et al., *Plasma polymer chemical gradients for evaluation of surface reactivity: epoxide reaction with carboxylic acid surface groups*. Journal of Materials Chemistry, 2004. **14**(3): p. 408-412.
157. Wang, X., et al., *Self-Assembled Monolayers as Templates for Heme Crystallization*. Crystal Growth & Design, 2010. **10**(2): p. 798-805.
158. Tempera, C., et al., *Characterization and optimization of the haemozoin-like crystal (HLC) assay to determine Hz inhibiting effects of anti-malarial compounds*. Malaria Journal, 2015. **14**(1).
159. World Health Organization, *World malaria report 2017*. 2017.
160. Griffith, J.W., et al., *Pure hemozoin is inflammatory in vivo and activates the NALP3 inflammasome via release of uric acid*. Journal of immunology (Baltimore, Md. : 1950), 2009. **183**(8): p. 5208-5220.
161. Taramelli, D., et al., *Macrophage preconditioning with synthetic malaria pigment reduces cytokine production via heme iron-dependent oxidative stress*. Laboratory Investigation, 2000. **80**(12): p. 1781.
162. Casals-Pascual, C., et al., *Suppression of erythropoiesis in malarial anemia is associated with hemozoin in vitro and in vivo*. Blood, 2006. **108**(8): p. 2569-2577.
163. Skorokhod, O.A., et al., *Inhibition of erythropoiesis in malaria anemia: role of hemozoin and hemozoin-generated 4-hydroxynonenal*. Blood, 2010.

164. Guerra, E.D., D.S. Bohle, and M. Cerruti, *Surface characterization of hematin anhydride: A comparison between two different synthesis methods*. Langmuir, 2016. **32**(18): p. 4479-4484.
165. Bulmer, J.N., et al., *Placental malaria. I. Pathological classification*. Histopathology, 1993. **22**(3): p. 211-218.
166. Schwarzer, E., et al., *Malaria-parasitized erythrocytes and hemozoin nonenzymatically generate large amounts of hydroxy fatty acids that inhibit monocyte functions*. Blood, 2003. **101**(2): p. 722-728.
167. Wessel, D. and U. Flügge, *A method for the quantitative recovery of protein in dilute solution in the presence of detergents and lipids*. Analytical biochemistry, 1984. **138**(1): p. 141-143.
168. Trager, W. and J.B. Jensen, *Cultivation of Erythrocytic and Exoerythrocytic Stages of Plasmodia*, in *Pathology, Vector Studies, and Culture*, J.P. Kreier, Editor. 1980, Academic Press. p. 271-319.
169. Klug, A. and D. Rhodes, *'Zinc fingers': a novel protein motif for nucleic acid recognition*. Trends in Biochemical Sciences, 1987. **12**: p. 464-469.
170. Shard, A.G., *Detection limits in XPS for more than 6000 binary systems using Al and Mg K α X-rays*. Surface and Interface Analysis, 2014. **46**(3): p. 175-185.
171. Jugdaohsingh, R., *Silicon and bone health*. The journal of nutrition, health & aging, 2007. **11**(2): p. 99-110.
172. Guntzer, F., C. Keller, and J.-D. Meunier, *Benefits of plant silicon for crops: a review*. Agronomy for Sustainable Development, 2012. **32**(1): p. 201-213.
173. Moreno, S.N.J., L. Ayong, and D.A. Pace, *Calcium storage and function in apicomplexan parasites*. Essays in biochemistry, 2011. **51**: p. 97-110.
174. Green, J.L., et al., *The motor complex of Plasmodium falciparum phosphorylation by a calcium-dependent protein kinase*. Journal of Biological Chemistry, 2008. **283**(45): p. 30980-30989.
175. Lourido, S. and S.N.J. Moreno, *The calcium signaling toolkit of the Apicomplexan parasites Toxoplasma gondii and Plasmodium spp.* Cell Calcium, 2015. **57**(3): p. 186-193.
176. MacDonald, R.G. and W.G. Chaney, *Biochemistry*. 2007.

177. Stevens, J.S., et al., *Quantitative analysis of complex amino acids and RGD peptides by X-ray photoelectron spectroscopy (XPS)*. Surface and Interface Analysis, 2013. **45**(8): p. 1238-1246.
178. Goldie, P., et al., *Biochemical Characterization of Plasmodium falciparum Hemozoin*. The American Journal of Tropical Medicine and Hygiene, 1990. **43**(6): p. 584-596.
179. Kalantari, P., et al., *Dual Engagement of the NLRP3 and AIM2 Inflammasomes by Plasmodium-Derived Hemozoin and DNA during Malaria*. Cell Reports, 2014. **6**(1): p. 196-210.
180. Ebeling, W., et al., *Proteinase K from Tritirachium album limber*. The FEBS Journal, 1974. **47**(1): p. 91-97.
181. Apte, J.S., et al., *XPS and ToF-SIMS Investigation of α -Helical and β -Strand Peptide Adsorption onto SAMs*. Langmuir, 2010. **26**(5): p. 3423-3432.
182. Briggs, T. and A.M. Chandler, *Biochemistry*. 1995.
183. Jakubke, H.D., P. Kuhl, and A. Könnicke, *Basic principles of protease-catalyzed peptide bond formation*. Angewandte Chemie International Edition in English, 1985. **24**(2): p. 85-93.
184. Goswami, A. and S.G. Van Lanen, *Enzymatic Strategies and Biocatalysts for Amide Bond Formation: Tricks of the Trade Outside of the Ribosome*. Molecular bioSystems, 2015. **11**(2): p. 338-353.
185. Demirev, P.A., et al., *Detection of Malaria Parasites in Blood by Laser Desorption Mass Spectrometry*. Analytical Chemistry, 2002. **74**(14): p. 3262-3266.
186. Matthiesen, R., *Mass spectrometry data analysis in proteomics*. 2013, Humana Press: New York.
187. Perry, C.C. and T. Keeling-Tucker, *Biosilicification: the role of the organic matrix in structure control*. JBIC Journal of Biological Inorganic Chemistry, 2000. **5**(5): p. 537-550.
188. LeGeros, R.Z., *Properties of Osteoconductive Biomaterials: Calcium Phosphates*. Clinical Orthopaedics and Related Research®, 2002. **395**: p. 81-98.
189. Steck, T.L. and J.A. Kant, *Preparation of impermeable ghosts and inside-out vesicles from human erythrocyte membranes*, in *Methods in enzymology*. 1974, Elsevier. p. 172-180.
190. Egan, T.J., *Discovering antimalarials: A new strategy*. Chemistry and Biology, 2002. **9**(8): p. 852-853.

191. de Villiers, K.A., et al., *Oriented Nucleation of β -Hematin Crystals Induced at Various Interfaces: Relevance to Hemozoin Formation*. Crystal Growth & Design, 2009. **9**(1): p. 626-632.
192. Guerra, E.D., et al., *What is pure hemozoin? A close look at the surface of the malaria pigment*. Journal of Inorganic Biochemistry, 2019. **194**: p. 214-222.
193. Ashong, J., I. Blench, and D. Warhurst, *The composition of haemozoin from Plasmodium falciparum*. Transactions of the Royal Society of Tropical Medicine and Hygiene, 1989. **83**(2): p. 167-172.
194. Guerra, E.D., et al., *What is pure hemozoin? A close look at the surface of the malaria pigment*. Journal of Inorganic Biochemistry, in press.
195. Vernon, W.B., *The role of magnesium in nucleic-acid and protein metabolism*. Magnesium, 1988. **7**(5-6): p. 234-248.
196. Goldstein, J.I., et al., *Scanning electron microscopy and X-ray microanalysis*. 2017: Springer.
197. Gilbert, J.B., M.F. Rubner, and R.E. Cohen, *Depth-profiling X-ray photoelectron spectroscopy (XPS) analysis of interlayer diffusion in polyelectrolyte multilayers*. Proceedings of the National Academy of Sciences, 2013: p. 201222325.
198. Tanabe, K., A. Izumo, and K. Kageyama, *Growth of Plasmodium Falciparum in Sodium-Enriched Human Erythrocytes*. The American Journal of Tropical Medicine and Hygiene, 1986. **35**(3): p. 476-478.
199. Dunham, P.B., G.W. Stewart, and J.C. Ellory, *Chloride-activated passive potassium transport in human erythrocytes*. Proceedings of the National Academy of Sciences, 1980. **77**(3): p. 1711-1715.
200. Dietrich, P.M., et al., *Quantification of silane molecules on oxidized silicon: are there options for a traceable and absolute determination?* Analytical chemistry, 2015. **87**(19): p. 10117-10124.
201. Guo, X., et al., *Synthesis and characterization of carbon sphere-silica core-shell structure and hollow silica spheres*. Colloids and Surfaces A: Physicochemical and Engineering Aspects, 2009. **345**(1): p. 141-146.
202. Carlisle, E.M., *The Nutritional Essentiality of Silicon*. Nutrition Reviews, 1982. **40**(7): p. 193-198.

203. Birchall, J.D., *The essentiality of silicon in biology*. Chemical Society Reviews, 1995. **24**(5): p. 351-357.
204. Balas, F., J. Pérez-Pariente, and M. Vallet-Regí, *In vitro bioactivity of silicon-substituted hydroxyapatites*. Journal of Biomedical Materials Research Part A, 2003. **66A**(2): p. 364-375.
205. Tanizawa, Y. and T. Suzuki, *Effects of silicate ions on the formation and transformation of calcium phosphates in neutral aqueous solutions*. Journal of the Chemical Society, Faraday Transactions, 1995. **91**(19): p. 3499-3503.
206. Li, H.-f., et al., *Investigation of nitric oxide and Ar annealed SiO₂/SiC interfaces by x-ray photoelectron spectroscopy*. Journal of applied Physics, 1999. **86**(8): p. 4316-4321.
207. Debona, D., F.A. Rodrigues, and L.E. Datnoff, *Silicon's Role in Abiotic and Biotic Plant Stresses*. Annual Review of Phytopathology, 2017. **55**(1): p. 85-107.
208. Alzahrani, Y., et al., *The defensive role of silicon in wheat against stress conditions induced by drought, salinity or cadmium*. Ecotoxicology and environmental safety, 2018. **154**: p. 187-196.
209. Ma, J.F. and N. Yamaji, *Silicon uptake and accumulation in higher plants*. Trends in Plant Science, 2006. **11**(8): p. 392-397.
210. Martin-Jézéquel, V., M. Hildebrand, and M.A. Brzezinski, *Silicon metabolism in diatoms: implications for growth*. Journal of phycology, 2000. **36**(5): p. 821-840.
211. Azam, F. and S. Chisholm, *Silicic acid uptake and incorporation by natural marine phytoplankton populations*. Limnology and Oceanography, 1976. **21**(3): p. 427-435.
212. Schwarz, K., *A bound form of silicon in glycosaminoglycans and polyuronides*. Proceedings of the National Academy of Sciences of the United States of America, 1973. **70**(5): p. 1608-1612.
213. Becker, C.H. and A.G.S. Jánossy, *Silicon in the blood vessel wall: A biological entity?* Micron (1969), 1979. **10**(4): p. 267-272.
214. Jurkić, L.M., et al., *Biological and therapeutic effects of ortho-silicic acid and some ortho-silicic acid-releasing compounds: New perspectives for therapy*. Nutrition & metabolism, 2013. **10**(1): p. 2-2.

215. Antonini, J.M., et al., *Subschronic Silica Exposure Enhances Respiratory Defense Mechanisms and the Pulmonary Clearance of Listeria Monocytogenes in Rats*. Inhalation toxicology, 2000. **12**(11): p. 1017-1036.
216. Biagini, G.A., et al., *The digestive food vacuole of the malaria parasite is a dynamic intracellular Ca²⁺ store*. Journal of Biological Chemistry, 2003. **278**(30): p. 27910-27915.
217. Feng, B., et al., *Carbonate apatite coating on titanium induced rapidly by precalcification*. Biomaterials, 2002. **23**(1): p. 173-179.
218. Harper, J.F. and A. Harmon, *Plants, symbiosis and parasites: a calcium signalling connection*. Nature Reviews Molecular Cell Biology, 2005. **6**: p. 555.
219. Docampo, R., et al., *Acidocalcisomes ? conserved from bacteria to man*. Nature Reviews Microbiology, 2005. **3**: p. 251.
220. Docampo, R. and S.N.J. Moreno, *Acidocalcisomes*. Cell Calcium, 2011. **50**(2): p. 113-119.
221. Hofmann, S., *Surface and Interface Analysis*, in *Kirk-Othmer Encyclopedia of Chemical Technology*. 2000, John Wiley & Sons, Inc.
222. Gourgas, O., et al., *Multidisciplinary approach to understand medial arterial calcification*. Arteriosclerosis, thrombosis, and vascular biology, 2017: p. ATVBAHA. 117.309808.
223. Eichert, D., et al., *Preliminary characterization of calcium chemical environment in apatitic and non-apatitic calcium phosphates of biological interest by X-ray absorption spectroscopy*. Spectrochimica Acta Part B: Atomic Spectroscopy, 2005. **60**(6): p. 850-858.
224. Pessi, G., G. Kociubinski, and C.B. Mamoun, *A pathway for phosphatidylcholine biosynthesis in Plasmodium falciparum involving phosphoethanolamine methylation*. Proceedings of the National Academy of Sciences, 2004. **101**(16): p. 6206-6211.
225. Samuels, A., et al., *The effects of silicon supplementation on cucumber fruit: changes in surface characteristics*. Annals of Botany, 1993. **72**(5): p. 433-440.
226. Andrabi, S.B.A., et al., *Plant hormone cytokinins control cell cycle progression and plastid replication in apicomplexan parasites*. Parasitology international, 2018. **67**(1): p. 47-58.
227. Jugdaohsingh, R., et al., *The decrease in silicon concentration of the connective tissues with age in rats is a marker of connective tissue turnover*. Bone, 2015. **75**: p. 40-48.
228. Mohammadi-Jam, S. and K. Waters, *Inverse gas chromatography applications: A review*. Advances in colloid and interface science, 2014. **212**: p. 21-44.

Appendix: Copyright waivers

Guerra, E.D., D.S. Bohle, and M. Cerruti, *Surface characterization of hematin anhydride: A comparison between two different synthesis methods*. Langmuir, 2016. **32**(18): p. 4479-4484.

Lightslink® by Copyright Clearance Center

<https://s100.copyright.com/AppDispatchServlet>



RightsLink®

Home

Account
Info

Help



ACS Publications
Most Trusted. Most Cited. Most Read.

Title:

Surface Characterization of
Hematin Anhydride: A
Comparison between Two
Different Synthesis Methods

Logged in as:

Elizabeth Guerra
McGill University

LOGOUT

Author:

E. Danae Guerra, D. Scott Bohle,
Marta Cerruti

Publication: Langmuir

Publisher: American Chemical Society

Date: May 1, 2016

Copyright © 2016, American Chemical Society

PERMISSION/LICENSE IS GRANTED FOR YOUR ORDER AT NO CHARGE

This type of permission/license, instead of the standard Terms & Conditions, is sent to you because no fee is being charged for your order. Please note the following:

- Permission is granted for your request in both print and electronic formats, and translations.
- If figures and/or tables were requested, they may be adapted or used in part.
- Please print this page for your records and send a copy of it to your publisher/graduate school.
- Appropriate credit for the requested material should be given as follows: "Reprinted (adapted) with permission from (COMPLETE REFERENCE CITATION). Copyright (YEAR) American Chemical Society." Insert appropriate information in place of the capitalized words.
- One-time permission is granted only for the use specified in your request. No additional uses are granted (such as derivative works or other editions). For any other uses, please submit a new request.

BACK

CLOSE WINDOW

Copyright © 2019 Copyright Clearance Center, Inc. All Rights Reserved. [Privacy statement](#). [Terms and Conditions](#).
Comments? We would like to hear from you. E-mail us at customercare@copyright.com

Guerra, E. D., Baakdah, F., Georges, E., Bohle, D. S., & Cerruti, M. *What is pure hemozoin? A close look at the surface of the malaria pigment*. Journal of inorganic biochemistry, 2019. **194**, 214-222.

Confirmation Number: 11805946
Order Date: 04/09/2019

If you paid by credit card, your order will be finalized and your card will be charged within 24 hours. If you choose to be invoiced, you can change or cancel your order until the invoice is generated.


Payment Information

Elizabeth Guerra
McGill University
elizabeth.guerralopez@mail.mcgill.ca
+1 (438) 832-4808
Payment Method: n/a

Order Details

Journal of inorganic biochemistry

Order detail ID: 71872786
Order License Id: 4564850592587
ISSN: 0162-0134
Publication Type: Journal
Volume:
Issue:
Start page:
Publisher: ELSEVIER INC.

Permission Status:  **Granted**

Permission type: Republish or display content
Type of use: Thesis/Dissertation

 [View details](#)

Note: This item will be invoiced or charged separately through CCC's **RightsLink** service. [More info](#)

\$ 0.00

Total order items: 1

This is not an invoice.

Order Total: 0.00 USD

Figure 3.2.1

SPRINGER NATURE LICENSE TERMS AND CONDITIONS	
Feb 02, 2019	
<hr/>	
This Agreement between McGill University -- Elizabeth Guerra ("You") and Springer Nature ("Springer Nature") consists of your license details and the terms and conditions provided by Springer Nature and Copyright Clearance Center.	
License Number	4521080215534
License date	Feb 02, 2019
Licensed Content Publisher	Springer Nature
Licensed Content Publication	Nature
Licensed Content Title	Malaria: Evolution in vector control
Licensed Content Author	Yannis Michalakis, François Renaud
Licensed Content Date	Nov 18, 2009
Licensed Content Volume	462
Licensed Content Issue	7271
Type of Use	Thesis/Dissertation
Requestor type	academic/university or research institute
Format	electronic
Portion	figures/tables/illustrations
Number of figures/tables /illustrations	1
High-res required	no
Will you be translating?	no
Circulation/distribution	< 501
Author of this Springer Nature content	no
Title	Miss
Institution name	McGill University
Expected presentation date	Feb 2019
Portions	Figure 1
Requestor Location	McGill University 3610 University Street

Figure 3.4.2

Rightslink® by Copyright Clearance Center

<https://s100.copyright.com/AppDispatchServlet#formTop>



RightsLink®

Home

Account
Info

Help



SPRINGER NATURE

Title: Identification of Essential
Histidine Residues Involved in
Heme Binding and Hemozoin
Formation in Heme
Detoxification Protein from
Plasmodium falciparum

Author: Keisuke Nakatani, Haruto
Ishikawa, Shigetoshi Aono,
Yasuhisa Mizutani

Publication: Scientific Reports

Publisher: Springer Nature

Date: Aug 20, 2014

Copyright © 2014, Springer Nature

Logged in as:

Elizabeth Guerra
McGill University

LOGOUT

Creative Commons

The request you have made is considered to be non-commercial/educational. As the article you have requested has been distributed under a Creative Commons license (Attribution-Noncommercial), you may reuse this material for non-commercial/educational purposes without obtaining additional permission from Springer Nature, providing that the author and the original source of publication are fully acknowledged (please see the article itself for the license version number). You may reuse this material without obtaining permission from Springer Nature, providing that the author and the original source of publication are fully acknowledged, as per the terms of the license. For license terms, please see <http://creativecommons.org/>

Figure 3.6.1

Mail - elizabeth.guerralopez@mail.mcgill.ca

https://outlook.office.com/owa/?realm=mail.mcgill.ca&exsvurl=1&ll-cc

Regarding Incident 2533720 Permission for copyright of figure in a paper

support@services.acs.org

Mon 2019-02-04 10:37 AM

To: Elizabeth Guerra López <elizabeth.guerralopez@mail.mcgill.ca>;



Hi,

Thank you for contacting ACS Publications Support.

Your permission request is granted and there is no fee for this reuse. In your planned reuse, you must cite the ACS article as the source, add this direct <https://pubs.acs.org/doi/10.1021/cg5002682> and include a notice to readers that further permissions related to the material excerpted should be directed to the ACS.

I hope this is helpful and if you need further assistance, please feel free to contact me.
Sincerely,

Ashley Gibson
ACS Publications
Customer Services & Information
Website: <https://help.acs.org>

Incident Information:

Incident #: 2533720
Date Created: 2019-02-02T21:39:38
Priority: 3
Customer: elizabeth.guerralopez@mail.mcgill.ca
Title: Permission for copyright of figure in a paper
Description: Hello,

My name is Elizabeth Guerra, I write to you because I'd like to reuse figures 2 and 3 for a paper published in ACS. The title is "Growth of large hematin crystals in biomimetic solutions", by Olafson, Katy N. et al. The figures are meant to be used in a thesis.

Information:
<https://pubs.acs.org/doi/10.1021/cg5002682>
Figure 2 and 3
To be reused in a thesis/dissertation

Thank you.

1 of 2

2019-02-04, 11:17 a.m.

Mail - elizabeth.guerralopez@mail.mcgill.ca

https://outlook.office.com/owa/?realm=mail.mcgill.ca&exsvurl=1&ll-cc

Kind regards,
Elizabeth

Figure 3.7.4

ightslink® by Copyright Clearance Center

https://s100.copyright.com/AppDispatchServie



RightsLink®

Home

Account
Info

Help



AMERICAN
SOCIETY FOR
MICROBIOLOGY

Title: Trioxaquinones and Heme-
Artemisinin Adducts Inhibit the
In Vitro Formation of Hemozoin
Better than Chloroquine

Author: Christophe Loup, Joël
Lelièvre, Françoise Benoit-
Vical, Bernard Meunier

Publication: Antimicrobial Agents and
Chemotherapy

Publisher: American Society for
Microbiology

Date: Sep 21, 2007

Copyright © 2007, American Society for Microbiology

Logged in as:

Elizabeth Guerra
McGill University

LOGOUT

Permissions Request

ASM authorizes an advanced degree candidate to republish the requested material in his/her doctoral thesis or dissertation. If your thesis, or dissertation, is to be published commercially, then you must reapply for permission.

Figure 3.8.1

Requesting Permission

Anyone may, without requesting permission, use original figures or tables published in PNAS for noncommercial and educational use (i.e., in a review article, in a book that is not for sale), provided that the full journal reference is cited and, for articles published in volumes 90–105 (1993–2008), "Copyright (copyright year) National Academy of Sciences." Commercial reuse of figures and tables (i.e., in promotional materials, in a textbook for sale) requires permission from PNAS.

Text and data mining are permitted for noncommercial institutions with an active institutional site license to PNAS for internal noncommercial research purposes. Other requests should be sent to PNASpermissions@nas.edu.

Figure 3.8.2

pubscopyright <copyright@osa.org>

Mon 2019-02-04 1:59 PM

To: Elizabeth Guerra López <elizabeth.guerralopez@mail.mcgill.ca>; pubscopyright <copyright@osa.org>;

Dear Elizabeth Guerra,

Thank you for contacting The Optical Society.

For the use of figure 1 from Jennifer L. Burnett, Jennifer L. Carns, and Rebecca Richards-Kortum, "In vivo microscopy of hemozoin: towards a needle free diagnostic for malaria," Biomed. Opt. Express 6, 3462-3474 (2015):

OSA considers your requested use of its copyrighted material to be Fair Use under United States Copyright Law. It is requested that a complete citation of the original material be included in any publication.

While your publisher should be able to provide additional guidance, OSA prefers the below citation formats:

For citations in figure captions:

[Reprinted/Adapted] with permission from ref [x], [Publisher]. (with full citation in reference list)

For images without captions:

Journal Vol. #, first page (year published) An example: Biomed. Opt. Express 6, 3462 (2015)

Please let me know if you have any questions.

Kind Regards,

Rebecca Robinson

Rebecca Robinson
February 4, 2019
Authorized Agent, The Optical Society

The Optical Society (OSA)
[2010 Massachusetts Ave., NW](https://www.osa.org)
[Washington, DC 20036 USA](https://www.osa.org)
[\[www.osa.org\]](https://www.osa.org)www.osa.org

Reflecting a Century of Innovation

